

2017

Ex-companions of Supernovae Progenitors

Zhichao Xue

Louisiana State University and Agricultural and Mechanical College, zcxueastro@gmail.com

Follow this and additional works at: https://digitalcommons.lsu.edu/gradschool_dissertations



Part of the [Physical Sciences and Mathematics Commons](#)

Recommended Citation

Xue, Zhichao, "Ex-companions of Supernovae Progenitors" (2017). *LSU Doctoral Dissertations*. 4456.
https://digitalcommons.lsu.edu/gradschool_dissertations/4456

This Dissertation is brought to you for free and open access by the Graduate School at LSU Digital Commons. It has been accepted for inclusion in LSU Doctoral Dissertations by an authorized graduate school editor of LSU Digital Commons. For more information, please contact gradetd@lsu.edu.

EX-COMPANIONS OF SUPERNOVAE PROGENITORS

A Dissertation

Submitted to the Graduate Faculty
of the Louisiana State University and
Agricultural and Mechanical College
in partial fulfillment of the
requirements for the degree of
Doctor of Philosophy

in

The Department of Physics and Astronomy

by
Zhichao Xue (薛志超)
B.S., Shandong University, P.R.China, 2012
July 2017

For Mom and Dad

Acknowledgements

I have been extremely fortunate to gain help, mentorship, encourage and support from many incredible people during my pursuit of my Ph.D. I would like to start by thanking my parents for backing up my decision to study abroad alone in the first place despite that I am their only child. Their combined love and support carried me through all the low and high in this process. On an equal level, I would like to express my gratitude to my advisor, Bradley Schaefer. I remembered the first time we met on the day of Christmas eve, 2012 and we talked about astronomy for a straight 6 hours. I knew at that moment, it would be a wonderful adventure ahead of me. There is no way for me to finish this process without your unconditional support when I feel discouraged and low. You gave me enough independence and treat me as a collaborator and friend. Your broad interests and work in many fields of astronomy continues to surprise me since day one. Your passionate keeps driving me to explore many aspects of astronomy. I would also like to thank my collaborator Andy Howell, Frederick Walter and Barbara McArthur for all the insightful suggestions and discussions. To Iair Arcavi, Curtis McCully and Griffin Hosseinzadeh, I had a wonderful time in Las Cumbres Observatory and it was pleasure working with you all.

I would like to acknowledge all of the exceptional research mentors I have had the privilege of working with over my very short career: Xiaofeng Wang, Hongxing Yin, Manos Chatzopoulos, Ed Nelan, Jose Prieto, Joseph Lyman, Janet Chen, Melissa Graham, Stefano Valenti, Peter Brown and David Armstrong. Further, I would like to say to Weidong Li, who passed away much too soon, I cherish all the help you provided me in the very early stage of my career.

I would like to thank all the members in my thesis committee. Especially, nearly all of you have taught me in the past five years and occasionally sought help from for my research. I very much enjoyed all the classes and I appreciate all the support and encourage.

I would also like to thank the numerous friends that I have made over the years. You

are simply too many to list and I hope that you will not take any omission as a slight. To Shiqing Duan, Ruzhou Yang, Zinan Wang, Haoyu Qi, Xinji Zhu, Yuli Liang, Gaoming Wang, Xiaotian Gong, Jiesi Luo, Xin Zhou, Edward Montiel, Chris Johnson, Zach Edwards, Alison Dreyfuss, Kelsie Krafon, Jon Cripe, Aaron Grocholski, Anton Joe, Kundan Kadam, Amber Lauer, Ishita Maity, Noah Morris, Jonny Olson. Terra Hardwick, Sahil Saini, Tyler Elis, Azadeh Keivani, Sarah Eve Roberts, Yupeng Gao, You Chenglong, Julia Yarbrough, Kaushik P. Seshadreesan, David Guevel, Ashkan Balouchi, Christopher Britt, Kavindi De Silva, Stephanie Haakenson Rachford, Erica Wu Insler, Sarah Morvant, Arunn Pisharody, Haggai D. Davis, Tabettha Boyajian, Christina Davis, Khan Mojammel, Spencer Aertker, Steven Dorsher. Thanks for all the wonderful experiences with you guys in my first years in the states.

Table of Contents

Acknowledgements	iii
List of Tables	vii
List of Figures	viii
Abstract	ix
1. Introduction	1
1.1 Supernovae	1
1.2 Type Ia Progenitor Problem	2
1.3 Core-collapse Supernovae and Their Companions	6
2. Searching for an Ex-companion within a SNR of a SNIa	11
2.1 The Intriguing Case of Tycho’s SN	11
2.2 Explosion Position From a SNR Expansion Model	13
2.3 The Ex-companion Candidates	30
2.4 Conclusions	30
3. Probing SNIa Progenitor Systems Through the Rare Case of ASASSN-14dc	33
3.1 Observations and Data Reduction	33
3.2 Analysis	41
3.3 Discussion	53
3.4 Summary	58
4. Ex-companion of a Core-Collapse Supernova’s Progenitor?	60
4.1 Is Muzzio 10 the Ex-companion Star of the PSR B1509-58’s Progenitor?	60
4.2 Observations and Data Analysis	64
4.3 Astrometry	67
4.4 Conclusion and Discussion	77
5. Discussion and Conclusions	81
Bibliography	86
APPENDIX A. Permission to Reproduce Copyrighted Material	93
APPENDIX B. Testing DA White Dwarf Variability using the <i>Kepler</i> and K2 mission	94

B.1	Introduction	94
B.2	Target Selection and Data Reduction	98
B.3	Discussion and Summary	105
B.4	References	111
Vita	114

List of Tables

2.1	Geometric center of Tycho's SNR	17
2.2	Observed radii and velocities, and their best fit model values	23
3.1	LT u'g'r'i'z' photometry of ASASSN-14dc	37
3.2	LCO Bg'Vr'i' photometry of ASASSN-14dc	38
4.1	All the available <i>Chandra</i> ACIS-I images	66
4.2	Reference stars used for the FGS astrometry solution	69
4.3	Reference stars used for the <i>Chandra</i> astrometry solution	74
B.1	Parameters of the 15 DA WDs	100
B.2	Summary of Result	105
B.3	Parameters of the DA WDs in the extended sample	107
B.4	Statistical Results of the 16 WDs in the extended sample	108

List of Figures

2.1	The two new and independent measured positions for the site of SN1572. . .	14
2.2	Geometric center of Tycho's SNR	19
2.3	The 19 observed radii and best fit model radii from SNR expansion model . .	24
2.4	The 19 observed SNR expansion velocity and the model expansion velocities	31
3.1	ASASSN-14dc	34
3.2	ASASSN-14dc multi-wavelength light curves	39
3.3	ASASSN-14dc light curve in r' compared to other SNe Ia-CSM	42
3.4	ASASSN-14dc light curve in r' compared to SNe IIn	43
3.5	ASASSN-14dc spectra evolution	45
3.6	ASASSN-14dc spectra comparison	48
3.7	ASASSN-14dc spectra decomposition	50
3.8	ASASSN-14dc Balmer lines evolution	51
4.1	Muzzio 10 and PSR B1509-58 region	63
4.2	HST FGS 1r field and Muzzio 10 and reference stars	70
4.3	Proper Motion of Muzzio 10 measured from HST FGS	72
4.4	Common sources detected in Chandra ACIS-I images from different epochs .	74
4.5	Bootstrap result from Chandra data (2005-2000)	75
4.6	Bootstrap result from Chandra data (2017-2000)	76
4.7	Muzzio 10 proper motion extrapolated a few thousands years ago	79
B.1	15 DA WDs in the T_{eff} - $\log g$ space	97
B.2	Example of the <i>Kepler</i> light curve 1	102
B.3	Example of the <i>Kepler</i> light curve 2	103
B.4	16 DA WDs from the extended sample in the T_{eff} - $\log g$ space	107
B.5	Newly found DA WD with high variability	112

Abstract

Supernovae (SNe) are titanic explosions that end the life of stars. Fast expanding ejecta can create brightness that is comparable to the entire luminosity of the host galaxy for weeks. Eventually, the ejecta run into the ambient medium, creating the so-called supernova remnant (SNR) that fades away in $\sim 10,000$ years. SNe come from two completely different mechanisms. The Type Ia SNe (SNIa) are powered by thermonuclear runaway when a white dwarf (WD) in a binary system accretes enough mass from a companion star. The Core Collapse supernovae (CCSNe) are massive stars that run out of fuel at the end of their lives and collapse. The basic scenario for SNIa is well established, but the type of the binary system containing the WD is the long-debated ‘Type Ia Progenitor Problem’. (1) Searching for an ex-companion within a SNIa SNR would directly solve this problem as a binary system including two WDs should leave nothing behind, while others should leave a non-degenerate star near the site of the explosion. One of the results from this thesis is the determination of the explosion site of Tycho’s SN (SN 1572). From this, I reject popular ex-companion candidates, e.g. Tycho star ‘G’ and a few other ones as they are too far away from the explosion site I determined. (2) Another attempt to address this problem is carried out by studying a rare kind of Type Ia SNe. Detailed photometric and spectral analysis indicates that ASASSN-14dc resembles features from the so-called SN Ia-CSM, in which, a SNIa explodes inside of dense Hydrogen-rich Circumstellar Material (CSM). The origin of the CSM brings serious questions to the traditional views of SNIa formation as none of them can comfortably explain the derived mass and distribution of the CSM. A recent realization of a particular model might solve a lot of puzzles around this rare class of SNIa. (3) CCSNe are known to be massive stars that rapidly evolve off the main sequence and soon explode. Nearly 80% of such stars have one or more massive companion stars, and these companions will survive the SN event with nearly the same luminosity in most cases. Interestingly, there is a runaway O-type star, Muzzio 10, that sits just $18''$ to the north of PSR B1509-58 in SNR

G320.4-01.2. This makes Muzzio 10 a remarkable object for an ex-companion candidate. I will present the result from using *HST* and *Chandra* to measure both the O star and the pulsar's proper motion and to see whether they came from the same spot.

1. Introduction

1.1 Supernovae

Supernovae (SNe) are spectacular outbursts caused by the explosive disruption of stars, marking the ends of their lives. At the time of the explosion, materials are ejected at a speed around 10,000 km/s. Normally, a supernova reaches its peak brightness in ~ 15 days. Around peak brightness for a few weeks, a supernova outshines all the other stars in its host galaxies. Then it fades rapidly as the ejecta cools adiabatically and becomes optically thin. Eventually, as the SN ejecta expand into the ambient interstellar medium, it creates a hot and tenuous gas shell, visible as a supernova remnant (SNR).

Supernovae are classified into two major types, I and II, according to the absence or presence of hydrogen emission lines in their spectra. They can also be distinguished by different physical mechanisms: Type Ia SNe (SNIa) and core-collapse SNe (CCSNe). When a carbon/oxygen white dwarf (CO WD) collects enough material from a companion star to reach near the Chandrasekhar limit ($\sim 1.4M_{\odot}$), it ignites thermonuclear runaway burning, which produces the SNIa. The explosion destroys the WD leaving nothing behind. Core-Collapse Supernovae come from stars with main sequence mass >8 solar mass, with their cores going through successive cycles of running out of nuclear fuel, contraction of the core, and ignition of a fuel composed of the ash from the previous cycle. This cycle continues until the central ash of iron is created as fusing iron into heavier elements would require additional energy instead of producing energy to support the star from collapsing. With iron being unable to ignite, the core will collapse, and then rebound, creating shocks that sweep through the whole star and blow it up. This explosion will leave behind a neutron star or a black hole depends on the star's main-sequence mass.

1.2 Type Ia Progenitor Problem

The basic scenario of SNIa coming from a binary system containing a carbon/oxygen white dwarf is well-established. However, the identity of the companion star is unknown. This is the long-standing important and controversial Type Ia Progenitor Problem.

The nature of the progenitor system for a supernova (SN) of Type Ia (SNIa) is among the most important questions in astrophysics (Ruiz-Lapuente 2014). This progenitor problem has been controversial for decades. While the empirical application of SNIa as a cosmological indicator has successfully led to the discovery of the the accelerating Universe (Perlmutter et al. 1999; Riess et al. 1998), we still need to close the gap in our theoretical understanding of them. A SNIa is known to be the product of a close binary system where one of the stars is a carbon/oxygen white dwarf. The companion could be a main-sequence star, sub-giant star, red giant star or another CO WD. SNIa are produced by one of two channels: the single-degenerate (SD) channel (Whelan & Iben 1973; Iben & Tutukov 1984) and the double-degenerate (DD) channel (Webbink 1984). The SD scenario has an ordinary companion star spilling matter onto the WD, accumulating material until the WD gets near the Chandrasekhar mass, thus initiating a thermonuclear explosion. Within the SD scenario, the companion star might have been a red-giant, a sub-giant, an AGB star, a main-sequence star, or a helium star etc. In all cases, SD progenitors will leave behind a luminous ex-companion star, now orbiting nothing, that has been battered by the supernova blast. The DD scenario has two CO WDs in close orbit, in-spiraling until the two stars merge, with a combined mass near the Chandrasekhar limit, thus triggering a thermonuclear explosion that leaves nothing but a beautiful expanding remnant.

1.2.1 Searching for an Ex-companions of SN Ia

One of the most direct and effective ways to distinguish between progenitor models is to search for a possible ex-companion within a supernova remnant (SNR), as first proposed by Ruiz-Lapuente (1997). Her idea is that the different models predict different surviving

companion stars, for example, a symbiotic progenitor would leave behind a red giant star, a recurrent nova would likely leave behind a red giant or a sub-giant star, a super-soft source would leave behind a sub-giant or a massive main sequence star, while a DD progenitor would leave behind no companion. This method can starkly distinguish between the SD and DD scenarios simply by looking for whether there is a luminous ex-companion star or not.

This method was first turned towards Tycho’s supernova of 1572, which is now confidently known to have been a SNIa event from observed light echoes (Rest et al. 2008; Krause et al. 2008). Ruiz-Lapuente et al. (2004, RL04) searched deep within the central area of Tycho’s SNR and found a G-type sub-giant (labeled star ‘G’) with high proper motion and probably the right distance to be an ex-companion. RL04 noted that the ex-companion is like the secondary star in the recurrent nova U Sco, thus pointing to recurrent nova as being the SNIa progenitor.

Our group at the Louisiana State University applied the Ruiz-Lapuente method by using the *Hubble Space Telescope* (*HST*) to look deep in the center of SNRs in the Large Magellanic Cloud known to be SNIa by the spectrum of their light echoes. The most startling case was for SNR 0509-67.5, where the 3-sigma uncertainty circle in the center was completely empty of any point source to $V=26.9$ (corresponding to $M_V = 8.4$), pointing to the DD model because all published SD models were strongly rejected (Schaefer & Pagnotta 2012). (There is a background $z=0.031$ galaxy in the central error circle; Pagnotta et al. 2014.) Edwards et al. (2012) applied the same method to SNR 0519-69.0, and demonstrated that there are no giant or sub-giant ex-companions, ruling out most SD models. Pagnotta & Schaefer (2015) have looked in the centers of SNR 0505-67.9 and SNR 0509-68.7 to find many red giants and sub-giants, so these two SNRs are not useful. Further work has demonstrated that SN 1006 has no ex-companions going deep (Gonzalez Hernandez et al. 2012; Kerzendorf et al. 2012), and that Kepler’s SN (SN 1604) has no red-giant ex-companions, nor any sub-giant ex-companions down to $10 L_{\odot}$ (Kerzendorf et al. 2014). In all, we have a stark case that five SNIa SNRs do not have the SD-predicted ex-companions, with one to very deep limits.

The one possible exception is star G in Tycho's SNR.

One of the tasks in this thesis is to determine whether Tycho star G is the ex-companion by figuring out the explosion site of Tycho's SN. The method and result will be discussed in Chapter 2.

1.2.2 Probing SNIa Progenitor System Through SNe Ia-CSM

Another way to tackle the SNIa progenitor problem is to study the Type Ia supernova itself. There is a peculiar kind of supernovae which were originally classified as Type IIIn supernovae but have a SNIa origin. SN 1997cy (e.g., Germany et al. 2000) was the first of this kind. Its spectra showed strong narrow and intermediate components in the Hydrogen lines, which is a sign of strong H-rich circumstellar material (CSM) interaction. Later, SN 2002ic was discovered which showed similarity with SN 1997cy (e.g. Hamuy et al. 2003; Wood-Vasey et al. 2004). However, the pre-peak spectrum was not dominated by CSM interaction, instead it resembled the peculiar bright/broad Type Ia supernova like SN 1991T and SN 1999aa. Hence, a thermonuclear origin was suggested for this supernova. By the standard supernova classification scheme, the presence of Hydrogen will put the supernova into the Type II category, further, Type IIIn if narrow Hydrogen can be seen. Hence, this rare kind of supernovae were started to be labeled as 'SN Ia-CSM'. SN 2005gj (Aldering et al. 2006; Prieto et al. 2007) was another Ia-CSM candidate but brighter. Not all authors are convinced that these objects have thermonuclear origins. For example, a core-collapse origin was favored by some authors for SN 2002ic and SN 2005gj (e.g. Benetti et al. 2006; Trundle et al. 2008). The arrival of PTF 11kx partially settled doubts about whether such a Ia-CSM object even exists or not. PTF 11kx showed clear Type Ia SN evidence in the pre-peak and early spectrum and followed with CSM interaction dominated spectra. It is suggested that origin of the CSM is from the material expelled by a companion red giant star (Dilday et al. 2012). About a dozen these kind of objects were found in the last two decades, although most of them were classified as SN IIIn initially (Silverman et al. 2013a).

The sample gathered in Silverman et al. (2013a) is largely based on the similarity in the spectral features. Most of them except PTF 11kx are ambiguous due to the lack of early time spectra to validate their SNIa origins. These SNe Ia-CSM have rather slow-declining light curves, peaking at absolute magnitudes brighter than about -19 mag. Their spectra can be interpreted as strong multi-components Hydrogen lines (the cause of all the SN II classification initially) superimposed on CSM interaction ‘diluted’ Type Ia spectra.

So we know that we can have a SN Ia explode inside of dense CSM, but is this possible to achieve through any SN Ia models we know and how often we can have these events? Traditionally, these dense environments suggest that a Single-Degenerate scenario is responsible for these explosion, since the Double-Degenerate (DD) model cannot explain the Hydrogen rich CSM. In the DD scenario it is the spiraling-in due to gravitational waves that lead to the eventual merger and supernova explosion with a time-scale of billions of years. The lost hydrogen envelope would be long gone before the merger. However, the mass of the CSM estimated from these objects are on the order of one solar mass or more and they must be lost from the progenitor only decades prior to the supernova explosion (e.g. Inserra et al. 2016; Silverman et al. 2013a). This is hard to achieve through normal wind mass loss from stars during the Asymptotic Giant Branch (AGB) or Red Giant (RG) phase (typical mass loss rate of $\sim 10^{-7} M_{\odot}/\text{yr}$). Even invoking asymmetry and clumpiness in the CSM geometry cannot solve this dilemma. So the SD channel does not work for SNe Ia-CSM either. Discussion of whether normal SN Ia formation could produce such events can be found in Livio & Riess (2003) upon the discovery of SN 2002ic and further, a series of paper (Soker et al., 2013; Soker et al., 2014) describing a ‘core-degenerate’ (CD) scenario attempted to explain the PTF 11kx and other SNe Ia-CSM. In this model, instead of two white dwarfs in the DD model, the merger happens between a CO white dwarf and the CO core of an Asymptotic Giant Branch star in the late stages of common envelope. The rapid spiraling in of the CO WD and the CO core already in a tight orbit releases large amount of gravitational energy to eject most of its common envelope. A prompt violent merger forms a super-Chandrasekhar

WD that ignites the Type Ia supernova explosion. For the obvious reason, the $\sim 1 M_{\odot}$ CSM required for SNe Ia-CSM is originated from the complete or most of common envelope ejection just before the SN. This model can potentially solve a lot of problems at once. Solar mass of hydrogen can be account for and the merger between a CO white dwarf and a degenerate CO core can explain the Ia feature in the spectra. This certainly could offer an away out for these mystery SN Ia-CSM.

ASASSN-14dc is a Ia-CSM candidate discovered by the All-Sky Automated Survey for SuperNovae (ASAS-SN). Photometry and spectroscopic follow up have been carried out by a variety of telescopes. It is among the brightest SNe Ia-CSM ever found and its peak luminosity is in the super-luminous supernova regime. Its high brightness and slow light curve decline rate has suggested interaction with a higher mass of CSM compared to previously known cases. This is even more challenging for traditional Type Ia supernova mechanism. In this project, I will present the multi-band follow up and spectroscopic observation for this supernova and the potential implication for its progenitor system in Chapter 3.

1.3 Core-collapse Supernovae and Their Companions

The reported O-star binary frequency for spectroscopic companions out to 3000 day periods is $69\% \pm 9\%$ (Sana et al. 2012). If the high-mass exploding star originally had any companion star in orbit, then this star will be battered and likely unbound from its orbit (becoming an ‘ex-companion’ star) to leave the explosion site at its original orbital velocity. The fast expanding material will eventually become a large shell called a supernova remnant (SNR), near the middle of which will be the neutron star or black hole, plus any ex-companion star.

As the more massive star evolves off the main sequence (on its way to exploding as a SN), many companions will be too far away to have significant interaction, but an important fraction of the companions will be close enough that the more massive star will start spilling matter onto the companion by Roche lobe overflow. This case is one likely means for producing the Type IIb, Ib, and Ic SNe arising from stars with their outer envelopes

stripped away (e.g. Iben & Tutukov 1985; Yoon et al. 2010; Claeys et al. 2011; Dessart et al. 2012). In the cases where the progenitor system goes through an interacting binary stage, the companion star will be made more massive and hence more luminous, and it will survive. Thus, we expect that most companions will survive from the main sequence stage up until the time of the explosion (e.g. Kochanek 2009; Koo et al. 2011, Marietta et al. 2000). Detailed calculations demonstrate that the companion will survive the SN explosion largely intact, losing only a small fraction of its mass, and with nearly its original luminosity or a somewhat higher luminosity (Marietta et al. 2000; Pan et al. 2014). Based on the Virial theorem, the star in orbit around the exploding star could become unbound when the massive star suddenly loses more than half of the system mass. When the companion becomes unbound, it will be traveling at its pre-SN orbital velocity, and in the absence of other forces will just keep traveling with this same velocity, getting farther and farther away from the original explosion site (Hoogerwerf et al. 2000; Zinnecker & Yorke 2007),. In all cases, we expect that the companions will remain within the central few percent of the SNR radius.

1.3.1 Searching for Ex-companions of CCSNe

The most direct way to identify such companion stars would be looking for massive stars right at the site of a core-collapse supernova event soon before and after the explosion. This method is limited by the fact that the supernova must be either galactic or in a nearby galaxy and the field would have been looked at before and after the SN event with deep high-resolution images, which is often achieved by the *Hubble Space Telescope (HST)*. A B-supergiant star has been observed at the location of SN 1993J, while the supernova's progenitor, a K-supergiant star could not be seen in the post-explosion *HST* images (Maund & Smartt 2009). Folatelli et al. 2014 claimed that they found a point source in the *HST* near-UV filters and it is compatible with the interacting binary model that has a yellow supergiant as the progenitor of SN 2011dh in M51.

Another approach would be trying to connect runaway OB stars with supernova remnants, as one of the hypotheses to produce massive runaway stars is from core-collapse SNe in binary systems. The violent mass loss from the SN explosion would release the gravitational attraction on the companion star, which will survive the SN explosion and fly away with its original orbital speed. Dinel et al. (2015) found a B0.5V type star (HD 37424) with a peculiar velocity ~ 75 km/s (derived from UCAC4 plus radial velocity measurements from spectra) and combined with previously measured pulsar (PSR J0538+2817) proper motion via the Very Long Baseline Array, they conclude that they can be traced back to a location close to the center of the SNR S147. A runaway G0 super-giant star HIP 13962 is suggested to be the ex-companion of the progenitor of PSR J0826+2637, however, the lack of underlying supernova remnant could question the reliability of this claim (Tetzlaff et al. 2014). A systematic search using the Tycho-*Gaia* astrometric solution (TGAS) found three new runaway candidates for HB 21, the Cygnus Loop and the Monoceros Loop, respectively, with the best candidate being a Be star BD+50 3188 in HB 21 (Boubert et al. 2017).

Also, Dufton et al. (2011) discovered an extremely rapidly rotating late O-type star, VFTS102, from a spectroscopic survey of 30 Doradus and they suggested that the O star's rapid rotational velocity could be resulting from mass transfer from the progenitor of PSR J0537-691, thus, VFTS102 could be the ex-companion star.

The discovery of a CCSN ex-companion would be exciting news and good for several topics in astrophysics:

(1) I can measure the effects on a star being blasted by a SN and this can be compared to models. The stellar parameters of the post-SN companion can help constraint the final stage of binary interaction.

(2) Runaway stars themselves are dynamically interesting objects in their own right. I can measure the space velocity and directions for comparison with the pulsar velocity and pole orientation. The asymmetry in supernova explosions might be responsible for the very high velocities observed in pulsars (e.g. Wongwathanarat et al. 2013). Since I will be measuring

the velocity of both the companion star and the pulsar, if I find the pulsar's velocity is as high as several hundred km/s, this could point to the SN asymmetric explosion or any asymmetric effects during the explosion.

(3) I am excited by the possibility of seeing r-processed elements infused into the companion star's atmosphere. The default idea in textbooks for over fifty years is that slow neutron-capture process (s-process) and rapid neutron-capture process (r-process) are the two major mechanisms for explaining the production of the stable (and some long-lived radioactive) neutron-rich nuclides heavier than iron in our universe (Burbidge et al. 1957). Roughly half of the isotopes above the iron group can be accounted by the r-process, in which heavy nuclei are produced by capturing neutrons on a timescale shorter than their beta-decay lifetime. However, the origin of the r-process remains one of the widely discussed topics in nuclear astrophysics (Arnould et al. 2007). Core collapse supernovae and neutron star binary mergers are likely r-process sites (Meyer et al. 1992; Woosley et al. 1994; Qian et al. 1998; Qian 2012; Freiburghaus et al.1999; Korobkin et al. 2012), but little evidence yet exists for their in situ formation in such environments. However, in fact, current calculation and simulation fail to produce enough $A > 130$ heavy r-processed elements in the nucleosynthesis in proto-neutron star winds (e.g. Thompson et al. 2001; Arnould et al. 2007; Wanajo 2013). Qian et al. (1998) suggested using gamma-rays from decaying r-process nuclei in young SN remnants to test the core-collapse supernova origin for the r-process site. However, it will face the challenge of significant low abundances of r-processed material and the high expansion velocity spreading weak gamma-ray lines (Ripley et al. 2014). It is obvious to think that if CCSNe are one of the r-process sites, a surviving companion star's atmosphere would have large chance of being contaminated with material above the iron group. Thus, examining the spectra of such surviving companion star would be a perfect way to test this long-standing puzzle. To achieve that, we need to find such a system and this is the main driving force for one of the projects I am reporting.

(4) I can measure the SN age both by the intersecting proper motions (PM) of the pulsar

and the ex-companion as well as by the SNR filament expansion age, and these can be compared to the spin-down age of the pulsar.

I found that a run-away O-type star, Muzzio 10 (2MASS J15135520-5907516) (Muzzio 1979) sits ~ 18 arc-second to the north of PSR B1509-58 in SNR G320.4-01.2 with comparable distance. This makes Muzzio 10 an interesting object for an ex-companion candidate. I will describe the work to determine whether Muzzio 10 is the ex-companion Star of the PSR B1509-58's Progenitor in Chapter 4.

2. Searching for an Ex-companion within a SNR of a SNIa ¹

2.1 The Intriguing Case of Tycho's SN

If Tycho star G is indeed the ex-companion, then we have immediately eliminated the DD scenario and the symbiotic model, forcing ourselves into a SD answer, at least for this one supernova. Following the publication of Ruiz-Lapuente et al. (2004, RL04), our community expressed substantial amounts of skepticism that Tycho Star G is the ex-companion star. Based on many comments heard and read at the time, most of the initial skepticism had poor bases; either the reaction was that the progenitor systems are DD so star G is not the ex-companion (assuming that which is trying to be proven) or that the proper motion of star G is perpendicular to the center of the SNR (but the position of star G in 1572 was still inside the RL04 error circle for the site of the explosion, so all is OK). Despite these early reactions, various follow-up investigations of star G have turned up good reasons to be critical of the claim that it is an ex-companion star. A surviving companion of a SNIa should show some distinctive features. First, it should show up close to the explosion site of the supernova. Second, it might show peculiar high velocity compared to the average motion of other local stars, due to the now-unbounded orbital velocity of the previous binary system. Third, the stellar atmosphere should be contaminated by accreted SN ejecta, which mainly consists of heavy elements like iron and nickel. Thus, heavy metal lines should show up in the spectrum of the proposed ex-companion star. Each feature has been extensively debated, with papers and arguments going several levels deep. For the issue of the high proper motion, Kerzendorf et al. (2009) first challenged the claim of high proper motion in RL04, but later Kerzendorf et al. (2013) and Bedin et al. (2014) confirmed the RL04 detection of high velocity of star G with high precision. Kerzendorf et al. (2009) raised the issue that a tidally synchronized

¹This chapter previously appeared in the *The Astrophysical Journal* as Xue & Schaefer. 2015, ApJ, 809, 183. Part of the introduction has been omitted due to the overlap with the information presented in Chapter 1 of my thesis. My advisor Dr. Bradley Schaefer is the collaborator on this work. It is reprinted by permission of the American Astronomical Society (see Appendix A).

companion star would lead to a fast rotating ex-companion star, while they measured that star G is slow rotating. Gonzalez-Hernandez et al. (2009) pointed out this can be well explained in part by the SN explosion blasting away the outer layers of the companion, hence carrying away angular momentum, and in part by the expansion of the ex-companion back to an equilibrium state and slowing its rotation as it expands. Further, Pan et al. (2012) and Liu et al. (2013) suggested that the rotational velocity would be reduced due to the impact of SN ejecta. Gonzalez Hernandez et al. (2009) have claimed that star G has an anomalously high nickel abundance, with this being disputed by Kerzendorf et al. (2012), while Bedin et al. (2014) re-evaluated the nickel abundance to be anomalously high. The argument that Star G is a giant star with distance ~ 10 kpc is brought up by Schmidt et al. (2007). But the high resolution spectra obtained with Keck again confirmed Star G is a sub-giant with distance that is compatible with being inside the SNR (~ 3 kpc). In the absence of any decisive argument, workers have proposed that Tycho star ‘B’ or Tycho star ‘E’ might be the long-sought ex-companion of SN 1572 (Kerzendorf et al. 2013; Ihara et al. 2007). My judgment of all this contradictory evidence is that no persuasive case has been made that any star either is or is-not an ex-companion.

I have realized that there is one critical question that no group has seriously addressed, and that is to the position in the sky of the original supernova explosion. Various groups had reported geometric centers for the SNR, all apparently with only casual care. RL04 took some sort of an average without explanation, then selected a reasonable error circle radius ($39''$) as the central 15% of the SNR radius. I further realized that the position of the original supernova explosion can be greatly improved. My collaborator, Dr. Bradley Schaefer, and I have two completely independent methods to do this. The first method is to use the original astrometry from 1572, where Tycho Brahe himself and six other observers reported 42 angular distances between nearby bright stars and the supernova itself, with accuracies measured to be as good as $84''$. A chi-square fit to all these observations produces a position of the supernova with a $1-\sigma$ error ellipse $28''$ by $35''$, see Figure 2.1, all with no

uncertainties from expansion, distance, proper motion, or extinction. (For the explosion position from astrometry in 1572, please see Xue & Schaefer (2015)).

The second method is to construct an analytic expansion model for the SNR, where I reproduce the observed expansion velocities and angular sizes for 19 positions around the edge of the SNR shell for which the densities of the swept up material have been measured previously. My chi-square fit reproduces the slightly out-of-round shape of the SNR, and shows that the relatively high density of swept up material to the northeast and northwest have made the apparent geometric center of the SNR offset to the south-southeast of the original explosion site. My position of the explosion site has a $1\text{-}\sigma$ accuracy of $7.5''$. In this project, I will present in detail of the second measure and this will provide a simple and convincing resolution of the conflict as to whether Tycho star G can be the ex-companion or not.

2.2 Explosion Position From a SNR Expansion Model

Simplistically, the position of the supernova explosion should be at the geometric center of the SNR. But no SNR is perfectly round, or even symmetric in shape, so it is unclear how to measure the center. Further, it is unclear how to define the positions around the edge, and the center might depend on the wavelength of light used for the image. Prior workers have reported central positions in the radio and X-ray (Duin & Strom 1975; Henbest 1980; Reynoso et al. 1997; Reynoso & Goss 1999; Hughes 2000; Katsuda et al. 2010), but they reported little details of their derivation, they gave no error bars, and indeed it appears that their reported centers were made with only approximate care. To derive an accurate geometric center (and its error circle), I used a systematic centroid method to measure the centers from 8 images, all at different photon energies, each with a quantified error bar, and then combined these together, where my final geometric center uses the scatter of all 8 individual centers to define a final error circle. The position of star G can then be compared

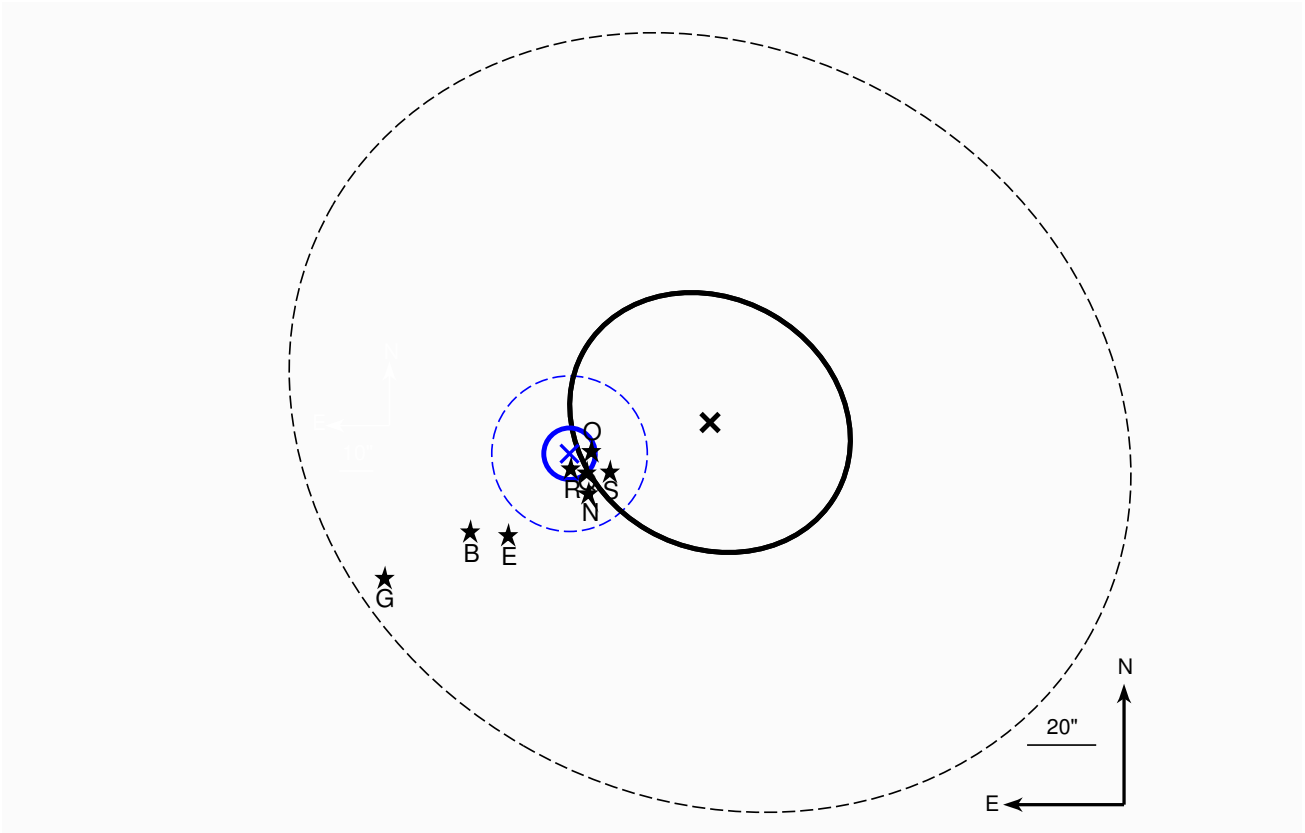


Figure 2.1: The two new and independent measured positions for the site of the 1572 supernova. My first method is to use the 42 astrometric measures of the supernova itself as observed by Tycho himself, plus six other observers, in 1572. My best fit position is shown with the black X, the thick tilted ellipse is my one-sigma error region, while the large thin-dashed ellipse is the three-sigma error region. No prior workers had made a serious attempt to use the original astrometry to get the position of SN 1572, and it turns out to be surprisingly good. My second method is to use a realistic expansion model, as applied to 19 points on the outer edge of Tycho's SNR with measured radii, expansion velocities, and post-shock ISM densities. My best fit position for this second method is marked with a blue X, the thick-lined blue circle represents the one-sigma error region (with a 7.5 arc-second radius), and the thin-dashed blue circle encloses the three-sigma error region. A variety of points can be seen from this Figure: (1) The two greatly-different methods are in good agreement with each other, with their one-sigma regions having much overlap, and in good agreement that SN 1572 exploded to the NW of the modern SNR geometric center (see Figure 2.2.). This provides good confidence that both methods are free from any substantial systematic error. (2) Star G is rejected at the 2.6-sigma level and the 8.2-sigma level for the two methods. This provides a simple and sure resolution to the long-standing controversy as to whether this star is the ex-companion. (3) Star B and E, other proposed ex-companion candidates, are also rejected at the 5.1-sigma and 4.1-sigma levels, respectively. (4) The real site of SN 1572 is a small region around stars O and R.

to my final geometric center.

The position of the geometric center is actually not what is relevant for knowing the explosion position of the supernova, because there will inevitably be some offset between the two positions. To see this, I can imagine an idealized case where the SNR is expanding into the ISM with a density gradient, so that one side is running into a higher gas/dust density than the other side. The expansion towards the high density side will be slowed, while the expansion away from it will be relatively fast. The SNR shape as seen from the side will have its geometric center at the point halfway from the slow edge and its fast edge. In this case, the geometric center will be offset significantly from the explosion center in the direction away from the dense side.

Schaefer & Pagnotta (2012) reported an infrared bright edge seen in SNR 0509-67.5, caused by differing amounts of swept up dust and mass in different directions, and this made for a flattened oval. By fitting an ellipse, they determined the offset from the real SNe explosion site. In general, relatively dense clouds around the edges will limit the expansion along those edges, making for complicated offsets. Kaplan et al. (2008) reported the explosion location of the Crab SNR through fitting a ‘divergent point’ of the proper motion of many filaments in the remnant field. In the case of Tycho’s SNR, the remnant edges are roughly circular with relatively large deviations, while the swept up matter (as judged by the infrared brightness around the edge) is highly asymmetric. The southern quarter has little swept-up mass, while relatively dense clouds are towards the northeast and towards the northwest. With this, the 1572 explosion site must have an offset towards the north from the geometric center.

A realistic model for the SNR should match the observed radii and expansion velocities in all directions from the center as a function of the mass of swept-up matter. Fortunately, around the rim, Tycho’s SNR has well measured expansion velocities (Katsuda et al. 2010 in X-ray; Reynoso et al. 1997 in radio), well measured densities for the swept-up material (Williams et al. 2013), and a realistic one-dimensional expansion model (Dwarkadas &

Chevalier 1998; Carlton et al. 2011). My work on the geometric center has measured the radii around the rim from the geometric center which can be easily converted into radii from the explosion center. With this, I can compare the observed and modeled radii and velocities as a function of the explosion position on the sky. The best position will be the position with the lowest chi-square for this comparison, while the $1\text{-}\sigma$ error region will be for places on the sky with a chi-square within 1.0 of this minimum.

2.2.1 Geometric Center

To determine the geometric center of the remnant, I have used public domain images in X-rays, infrared, and radio wavelengths. Tycho's SNR is faint and ill-defined in optical light. In X-rays, the *Chandra X-ray Observatory* provided images from 0.95-1.26 keV, 1.63-2.26 keV, and 4.1-6.1 keV. In the far infrared, the *Wide-field Infrared Survey Explorer* (WISE) provided a 22 micron image, while the *Herschel Space Observatory* provided a 70 micron image. In the radio, the Cambridge One-mile Telescope Radio provided images at 1.4 GHz in 1980, 2.7 GHz in 1972, and 5 GHz in 1972 (Henbest 1980, Tan & Gull 1985). The X-ray, radio, and infrared emission is all from different physical mechanisms within the remnant. The reason for using all eight independent images is partly to beat down the error, but is mainly so that the my geometric center will not be dependent on the vagaries of the remnant's shape due to varying brightnesses changing with the emission mechanism.

In each image, I took the edge of the SNR to be the radial position at which the flux had fallen to a fiducial value of 25% of the peak flux in the nearby rim. For each image, I started by constructing a set of nine baselines, with each baseline passing through a preliminary center and each with position angles at 10° intervals. Along each baseline, I determined the two edges of the SNR, bisected the resultant line segment, drew a perpendicular line through this middle point, determined the edge positions along this perpendicular line, and took the indicated center to be the middle position of the line segment on the perpendicular line. This results in nine positions sampling different parts of the edge of the SNR. I combined these

Table 2.1: Geometric center of Tycho's SNR

ID	α (J2000)	δ (J2000)
RL04 geometric center	0h 25m 19.9s	64 08' 18.2"
WISE (22 μm)	0h 25m 19.63s \pm 0.33s	64 08' 13.1" \pm 2.6"
Herschel (70 μm)	0h 25m 18.85s \pm 0.45s	64 08' 9.3" \pm 1.1"
Chandra X-ray (950-1260 eV)	0h 25m 19.35s \pm 0.42s	64 08' 13.3" \pm 1.9"
Chandra X-ray (1630-2260 eV)	0h 25m 19.42s \pm 0.41s	64 08' 12.9" \pm 2.2"
Chandra X-ray (4100-6100 eV)	0h 25m 19.33s \pm 0.39s	64 08' 12.7" \pm 2.3"
Radio (1.4 GHz)	0h 25m 18.54s \pm 0.29s	64 08' 18.7" \pm 2.2"
Radio (2.7 GHz)	0h 25m 19.10s \pm 0.36s	64 08' 17.9" \pm 2.6"
Radio (5 GHz)	0h 25m 19.58s \pm 0.32s	64 08' 17.5" \pm 2.3"
Combined geometric center	0h 25m 19.23s \pm 0.12s	64 08' 14.4" \pm 1.2"

nine points as a simple average to get the geometric center for this image. (I iterated with this center in place of my preliminary center, but this made no difference in the resultant center.) For a different analysis method, I fit circles to my 36 edge positions with a χ^2 fit procedure, and these are in perfect agreement with the results I got from my first method.

The uncertainty in the geometric centers for each image (from the nine baselines) is simply the RMS of the nine coordinates in both right ascension and declination, divided by the square root of 9 (for the number of independent centers averaged together). All of the centers derived for the nine baselines produce positions consistent with a scatter of around 6", and so the resultant geometric center for each image has an uncertainty of around 2". This is a smaller uncertainty than might be expected, but it is based on 36 measured edge positions for each image, and the small scatter in the nine independent centers for each baseline demonstrates that the geometric center can be determined to high accuracy for my given definition.

The eight images result in eight geometric centers (see Table 2.1 and Figure 2.2). My final geometric center is simply the straight average of all eight centers. (A weighted average gives the same final center and its error bar to within 0.3".) The RMS scatter of these eight positions (2.5 arc-seconds in right ascension and 2.6 arc-seconds in declination) is dominated by the measurement errors. Again, I see that the observed scatter in my 8 independent centers is smaller than might be expected, demonstrating that the geometric center has been

measured to good accuracy for my given definition. With this, the uncertainties in each coordinate are just the RMS scatter divided by the square-root of 8. So my final geometric center is J2000 00h 25m 19.23s \pm 0.12s and +64 08' 14.4 " \pm 1.2".

The uncertainty in my geometric center is greatly smaller than the search region in RL04. Tycho star G is far to the east and the south of the geometric center (see Figure 2.2), being far outside the three-sigma error circle. The proper motion of star G (Bedin et al. 2014) from 1572 to now is 2.1 arc-seconds, and is completely negligible in this context.

The geometric center is offset by some amount from the real explosion site of 1572. The direction of this offset can be seen by looking at infrared images (e.g. in Williams et al. 2013), with the brightness around the SNR rim being dominated by swept-up ISM dust, so the infrared bright portions of the rim indicate a lot of swept-up ISM material and a small expansion radius. Tycho's SNR is infrared bright to the northeast and to the northwest, indicating that the 1572 explosion site must be somewhere north of the geometric center. Similarly, the entire southern quadrant of the SNR is infrared faint, indicating little swept-up material, so that the expansion is relatively free and fast in that direction, again pointing to the true expansion center being somewhere to the north of the geometric center. With star G being to the southeast of my small geometric center error circle and with the explosion site being shifted in some amount to the north, there is no way that star G can be inside any error region for the explosion site. Thus, the answer is already apparent from just my geometric center analysis plus the infrared image, and this is that star G cannot have been anywhere near the explosion site in 1572.

2.2.2 Expansion Model

To create a chi-square model for the radii and velocities around the edge of the SNR, I need a realistic physical model of the radius of the leading edge of the ejecta as a function of time and the density of swept-up material. Fortunately, I can adopt an analytic expansion

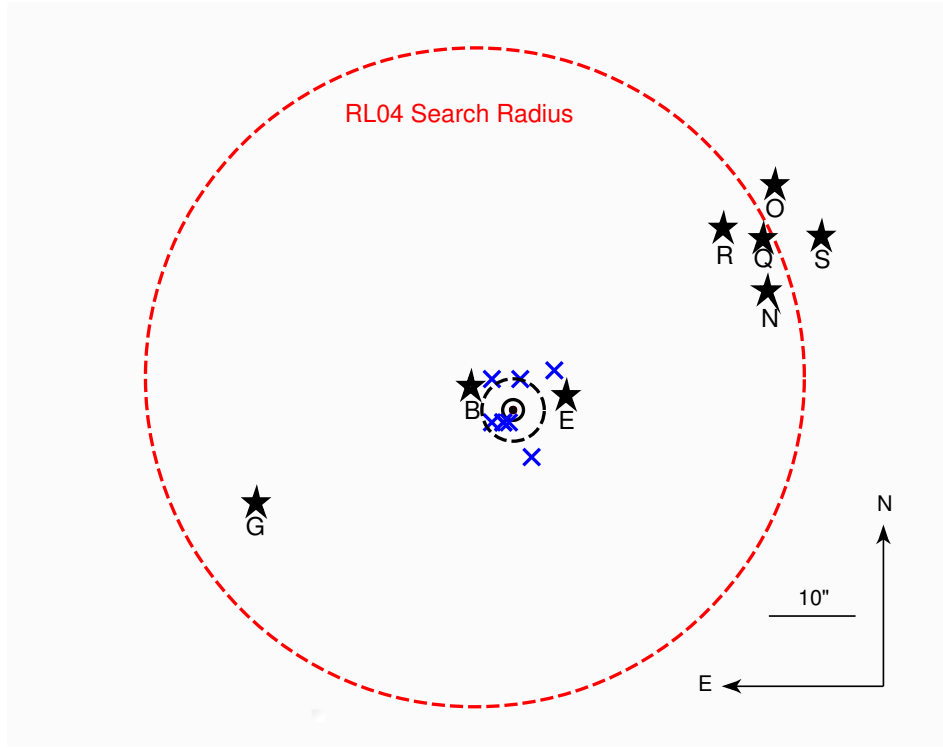


Figure 2.2: Geometric center of Tycho's SNR. The dashed red circle is the original search radius in RL04 for ex-companion candidates with a 0.65 arc-min radius. Previously proposed ex-companion stars, Tycho stars G, B, and E, are within that original search region. The eight blue Xs are the eight geometric center derived from infrared, X-ray and radio images. The black dot is the combined geometric center, while the solid circle is the one-sigma error region for this geometric center (with 1.2 arc-second radius), and the black thin dashed circle shows the three-sigma error region. I know from the infrared image that the SNR has little swept-up material towards the south, so the explosion site must be northwards from the geometric center. But star G is to the south and east of the geometric center, so putting in the offset to get to the explosion site will certainly have star G too far away too be the ex-companion.

model, as used by other workers on Tycho's SNR (Dwarkadas & Chevalier 1998; Carlton et al. 2011). This is a one-dimensional model that assumes a constant density of swept-up ISM. The model assumes that the SN ejecta have an exponential density profile given by

$$\rho \propto t^{-3} \exp(-v/v_e), \quad (2.2.1)$$

where t is the time since the start of the explosion, v is the expansion velocity, and v_e is the velocity scale for the supernova ejecta. Carlton et al. (2011) justified the applicability of thin shell approximation in a young supernova remnant, such as Tycho's SNR with an age of approximately 450 yrs. They reached an analytic solution for the dimensionless blast wave radius as

$$r' \equiv \frac{R}{R'} = \left(1 + 4\frac{v_e}{v} + 6\left(\frac{v_e}{v}\right)^2\right)^{\frac{1}{3}} \left(\frac{2v}{v_e}\right)^{\frac{1}{3}} \exp\left(\frac{-v}{3v_e}\right), \quad (2.2.2)$$

$$R' = 2.19 \left(\frac{M_e}{M_{ch}}\right)^{\frac{1}{3}} n_0^{-\frac{1}{3}} \text{ pc} \quad (2.2.3)$$

$$v/v_e = 8.03 \left(\frac{R}{2\text{pc}}\right) \left(\frac{t}{100\text{yr}}\right)^{-1} (E_{51})^{-\frac{1}{2}} \left(\frac{M_e}{M_{ch}}\right)^{\frac{1}{2}}. \quad (2.2.4)$$

Here, E_{51} is the ejecta kinetic energy (in units of 10^{51} erg), M_e/M_{ch} is the ejecta mass in units of the Chandrasekhar mass M_{ch} , and n_0 is the pre-shock ISM density in cm^{-3} , pc is parsec. Then, with given values of t , E_{51} , M_e , and n_0 , I can solve for the radius R and velocity v .

With this expansion model, I adopt $M_e = M_{ch}$, which is true for almost all models, and is approximately true even for the sub-Chandrasekhar models. For the age of the SNR, I take $t = 431$ years, as appropriate for the date of the measured expansion velocities. My measured radii are all revised to the year 2003, which correspond to the SNR age of 431 yr. Based on prior published models, I expect that E_{51} is somewhere between 0.3 and 1.75, with Hughes (2000) pointing to 0.4-0.5, but I treat this as a free parameter.

The swept-up material has a density that varies substantially around the edge of Tycho’s SNR. Badenes et al. (2006) and Hayato et al. (2010) found that ejecta towards the northeast and towards the northwest are brighter than those towards the south in X-rays, while similar brightenings are seen in the radio and infrared. The directions towards the northwest and the northeast show a factor of 2-to-3 slower expansion rate compared to other directions (Fig. 5 in Katsuda et al. 2010; Fig. 4 in Tan & Gull 1985; Fig. 6 in Reynoso et al. 1997). Observational evidence show that Tycho’s SNR might be interacting with a dense molecular cloud on the eastern and northeastern sides, which gives bright emission and low expansion velocity (Decourchelle et al. 2001; Reynoso & Goss 1999; Lee et al. 2004). By tracing the outer edge of the cloud from photoionizing radiation, Ghavamian et al. (2000) found that Tycho might be interacting with a warm ISM cloud. Simulations by Chiotellis et al. (2013) show models with a pre-existing stellar wind bubble would not only solve the discrepancy in ISM estimate but also match very well with the morphology, dynamics, and x-ray spectrum of the current Tycho’s SNR. However they have trouble explaining the origin of the wind bubble. It’s clear that Tycho’s SNR shows evidence of asymmetric features that are apparently caused by the interaction with ambient ISM. Williams et al. (2013) performed a model fit for the observed $70 \mu\text{m}$ to $24 \mu\text{m}$ flux ratio from *Spitzer* to get the post-shock ISM density (n_{post}) distribution for 19 positions around the edge of the shell. I adopted their values.

Williams et al. (2013) gives the post-shock density of the swept-up ISM, whereas n_0 (in equation 2.2.3) is the pre-shock density. With the usual shock jump conditions for an adiabatic index of $5/3$, the density will increase by a factor of 4 across the shock, so $n_{post}/n_0 = 4$. For Tycho’s SNR, the value might be somewhat different, for example from effects of cosmic ray acceleration and Rayleigh-Taylor instabilities (Vink et al. 2010; Williams et al. 2011; Warren et al. 2005; Warren & Blondin 2013). Efficient cosmic ray acceleration would increase the shock compression ratio and bring the contact discontinuity closer to the forward shock. Rayleigh-Taylor instabilities tend to smooth out high densities at the contact

discontinuity that would affect the estimate of ISM density as well. Both mechanisms have little or no impact on the expansion parameter (Warren & Blondin 2013). Since I do not know the exact shock jump density ratio, I take $n_{post}/n_0 = Q$, where Q is a free parameter.

2.2.3 Chi-square Model Fit

I now have a realistic expansion model for Tycho's SNR, where the radius and velocity can be predicted with adjustable parameters of E_{51} and Q . (Recall that I have set $t=431$ years, $M_e=1$, and take n_{post} from Williams et al. (2013).) To convert the radii and velocities into angular radii and angular velocities, I further need the parameter of the distance to the SNR, D . (This distance is a number that I will fit for, and I expect it to come out near the usual value of 2.3 kpc or so.) My expansion model must also specify the exact position of the supernova explosion, which I will label as α_{SN} and δ_{SN} for the right ascension and declination in J2000 coordinates. Thus, my expansion model has five free parameters.

My model can be compared to the observed radii and velocities. The velocities for each position angle around the rim of the SNR are taken from Williams et al. (2013), as shown in Table 2.2. The radii at each position around the edge depends on the center, α_{SN} and δ_{SN} . For this, I have taken the positions of the edge (as in Section 2.2.1) and calculated their angular distances from the center for comparison with the model radii. For my final best fit center, the observed radii of the SNR edge from this center for each position angle are also presented in Table 2.2.

I now have a complete expansion model that can be compared to a complete set of measured radii and velocities at 19 positions around the edge of Tycho's SNR. For each set of five input model parameters, I can compare the model with the observations in the usual chi-square manner. I can then vary the five model parameters until a minimum chi-square (χ^2_{min}) is reached. This set of five best parameters will then be my best fit, including my best fit position for the explosion site in 1572. The $1-\sigma$ uncertainty will be the ranges of the parameters for which $\chi^2 \leq \chi^2_{min} + 1$, while the $3-\sigma$ uncertainty will be the ranges of the

Table 2.2: Observed radii and velocities, and their best fit model values

Θ^a	$n_0^b(cm^{-3})$	$R^c(arcsec)$	$v^d(arcsec/yr)$	Model $R^e(arcsec)$	Model $v^f(arcsec/yr)$
13	0.22	227.2	0.335	246.2	0.307
32	0.25	217.0	0.303	240.7	0.297
47	0.40	223.9	0.216	224.3	0.269
63	0.82	212.4	0.176	199.0	0.226
81	1.44	209.9	0.203	180.8	0.197
105	0.29	247.9	0.285	236.0	0.289
121	0.27	260.5	0.322	237.8	0.292
138	0.21	246.0	0.305	247.4	0.309
155	0.17	251.8	0.319	255.5	0.324
172	0.17	265.9	0.297	255.5	0.324
192	0.08	285.7	0.346	284.4	0.377
213	0.08	283.9	0.372	288.0	0.383
233	0.08	291.9	0.365	288.0	0.383
252	0.08	285.4	0.359	284.4	0.377
272	0.09	276.2	0.353	281.2	0.371
290	0.13	267.3	0.339	266.2	0.343
308	0.37	252.9	0.328	226.9	0.273
331	1.10	225.7	0.293	189.5	0.211
353	0.45	236.1	0.218	220.2	0.262

- a: Position angle around the edge of the remnant, measured from north towards the east
b: Pre-shock ISM density, taken from the Williams et al. (2013) measured post-shock density divided by my best fit $Q=1.5$.
c: Radius measured from remnant edge to the best fit explosion position, see Figure 2.3
d: Remnant expansion velocity measured from X-ray and radio observations, from Williams et al. (2013), with my best fit distance of 2.3 kpc, see Figure 2.4
e: Radius from the best fit model, see Figure 2.3
f: Remnant expansion velocity from the best fit model, converted to units of arcsec/yr with my best fit distance of 2.3 kpc, see Figure 2.4}

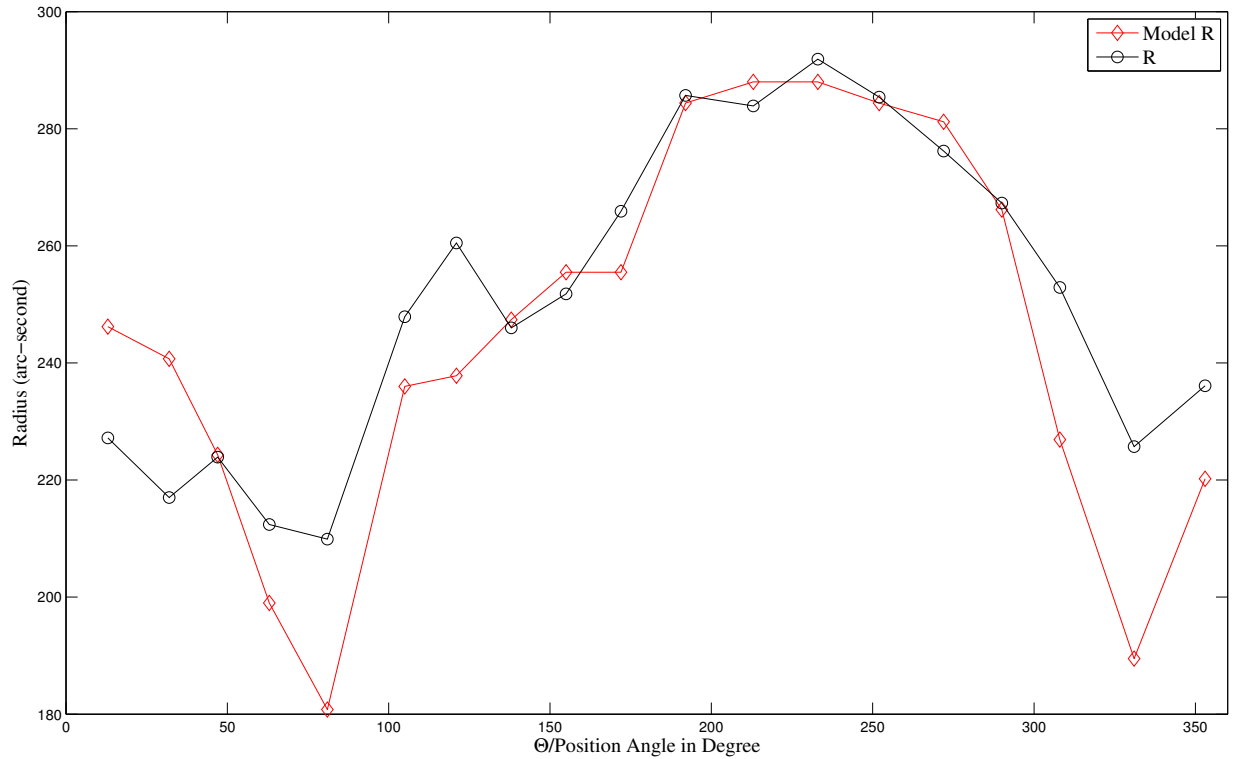


Figure 2.3: The 19 observed radii and best fit model radii from SNR expansion model. All values are measured or calculated with respect to the best fit explosion site. The point of this figure is that the observed radii vary substantially around the edge of Tycho’s SNR, and my modeled radii match these variations reasonably well. I do not expect arc-second agreement, because the outer edge of the remnant is partly determined by turbulent features not perfectly represented or resolved by the measures of the density of the swept-up material.

parameters for which $\chi^2 \leq \chi_{min}^2 + 9$.

For my chi-square fit, I am comparing the observations with my model for 19 radii and 19 velocities. My model has 5 adjustable parameters; E_{51} , Q , D , α_{SN} , and δ_{SN} . So my number of degrees of freedom is 33.

My measurement error for the radii are just a few arc-seconds, and in all models this leads to a large chi-square. What is going on is that there is some systematic error that must be added in quadrature, and I think that this is due to natural variations in the SNR radii that cannot now be modeled. In looking at the *Chandra* images, I see a very mottled surface with bumps and knobs on small and middling angular size scales, and these will make for intrinsic bumps as are seen around the edges. Such bumpiness might arise from early instabilities in the ejecta outflow, and they are at smaller scales than I can get far-infrared measures of the swept-up gas density. To avoid problems arising from an unrealistically large chi-square and to recognize the reality that there are un-modeled natural systematic variations in the SNR profile, I have added in quadrature a systematic uncertainty. The exact size of this added error is unknown, but I have set it such that the reduced chi-square associated with the measured radii is near unity. Thus, my measured errors in the radii (as reported in Table 2.2) have been added in quadrature with 23 arc-seconds for use in my chi-square fit. With this, the quality of my fit to the radii cannot be judged by my χ_{min}^2 . My procedure will not change the best fit parameters, but it will change the size of the error contours, making them reasonable for the reality of the bumps in the profile.

My best fit has $\chi_{min}^2=35.5$. This is for a distance $D=2.30\pm 0.04$ kpc, $E_{51}=0.46\pm 0.04$, $Q=1.5\pm 0.1$; all reasonable values. My derived center is at J2000 coordinates of $\alpha_{SN}=0^h 25^m 15.58^s$, $\delta_{SN}=64^\circ 8' 39.8''$. This newly determined supernova explosion site is 34.9 arc-seconds northwest of the geometric center. The $1-\sigma$ error region has a radius of 7.5 arc-seconds. The $3-\sigma$ error region has a 22.5 arc-second radius. The relative sizes and positions of my expansion-model error regions are shown in Figure 2.1.

The basic idea of my expansion model is to account for the variations in SNR radius,

expansion velocity, and density of swept-up material in all the directions around the edge of the remnant. All these quantities vary substantially with the position angle around the remnant. Figure 2.3 and Figure 2.4 plot the radius and the expansion velocity for both the observed values as well as for the best fit model values. The point of these figures is that the observed variations are reasonably well modeled, which is to say that my model is indeed catching the essence of the variations. I see that the reason for the observed variations is largely due to the variations in the amounts of swept-up ISM material in different directions.

The ISM density around Tycho's SNR is not perfectly uniform. Williams et al. (2013) found that the northeast and northwest sides have over ten times higher densities than those to the south, which might indicate a density gradient in the pre-supernova ISM. Any such overall gradient would require that any parcel of SN ejecta sweep up ISM material with density changes over the centuries since 1572. The origin of the density gradient is unknown. Chiotellis et al. (2013) found the best model of the ambient ISM distribution to reproduce the observed morphology, dynamics and X-ray emission spectrum of Tycho's SNR, which is that the supernova shock evolved into a pre-existing stellar wind bubble but is now expanding into a uniform ISM with lower density. This would reconcile the discrepancy between two ISM density determinations, where the current high shell expansion velocity and lack of thermal X-ray emission in the shell put a upper limit on the ISM density of $\sim 0.6 \text{ cm}^{-3}$ (Cassam-Chena et al. 2007; Katsuda et al. 2010), while the high ionization age of Tycho's SNR derived from the X-ray spectrum requires a high ambient ISM density. The resulting density of the wind and homogenous ISM is well below the upper limit. However the origin of the wind bubble remains a mystery. A proposed origin of stellar wind from low or intermediate mass giant stars is implausible given the non-detection of any giant stars within the centroid of Tycho's SNR that have the required properties. Also, the derived duration for the mass outflow is $\sim 5 \times 10^4$ years, and this is greatly shorter than the life time of giant stars, so fine tuning would be needed. A recurrent nova could generate a sequence of explosions that eject its shells and the collision among them might produce the density

structure seen in their model. On the other hand, for a DD channel, whether the ejection of common envelope could recreate the same feature remains unclear (Chiotellis et al. 2013). Figure 4 in Chiotellis et al. (2013) shows that around ~ 500 yr, the remnant evolves into a wind bubble that resembles the same features (morphology and dynamics) produced by one with a uniform ISM. Nonuniform ISM near to the SN will have negligible effect on the model expansion results, because there is little material swept up when compared to the mass of the ejecta. The effects of the progenitor (from wind bubbles, recurrent nova shells) will generally provide substantial density variations only close to the progenitor.

To compensate for these potential variations in the ISM density, I allow the parameter Q to vary freely, instead of fixing it to some specific value (such as a standard shock jump ratio) in my calculation. My best fit value of Q is below the standard value of 4, which might be telling me that Williams et al. (2013) has underestimated the post-shock density or that Rayleigh-Taylor instabilities are important. More fundamentally, my analysis is assuming that the relative densities around the shell are fixed and all the physical mechanisms affect the dynamics of the SNR in the same way in all directions. I am fitting the remnant in a relative way, with the shift between centroid of the SNR and real explosion site being independent of this assumption.

2.2.4 Explosion Site From a Simple Model

I can make a test for the sensitivity of my derived center position to my adopted expansion model. For this, I have adopted a rather simple expansion model, in this case simply requiring the conservation of momentum of the ejecta, all in a thin shell, as it sweeps up ISM material. As a simple numerical integral, I get the model shell radius and velocity as a function of the distance, the ejecta mass, the ejecta velocity, and the ISM density. I substituted this simple model for the expansion model from equations 2.2.2-2.2.4, I calculated the model radius and shell velocity along the same 19 azimuthal angles, and I compared those with the observed radii and velocities as discussed in the previous section. For this chi-square comparison, the

position of the explosion site on the sky provides two further free parameters, and indeed are the two parameters of interest here. By varying all the input parameters, I get a minimum χ^2 with $\alpha_{SN}=0\text{h } 25\text{m } 15.34\text{s}$, $\delta_{SN}=64^\circ 8' 40.9''$ which is just $2.1''$ away from the location I got from a more complex model. I take the independence in the derived supernova centers with a greatly different expansion model to be a good argument that my method is robust with respect to the details of the expansion model.

2.2.5 Effects of an Inhomogeneous ISM

For the previous calculations, in both the simple and the realistic models, I have assumed the density of the swept-up ISM to be a constant in the expansion history. While this is reasonable as an approximation, it is fully possible that any fragment of the expanding shell can encounter a significantly inhomogeneous ISM, for example as the supernova might blow up inside some sort of a bubble from the progenitor or the ejecta might encounter a relatively dense cloud in some direction. So I should calculate the sensitivity of the derived explosion site to plausible inhomogeneous ISM distributions. For this, I make the calculations within both the realistic model (cf. Section 2.2.2) and the simple model (c.f. Section 2.2.4).

Considering the ISM in each direction to have a density that is a step function, where its density is n_I out to some inner radius R_I , while outside that radius it has a density of n_0 . The total swept up ISM mass will be $(4\pi/3)(n_0(R_s^3 - R_I^3) + n_I R_I^3)$, where R_s is the shell radius. By introducing η as the ratio between n_I and n_0 and γ as the ratio between R_I and R_s , the swept-up ISM mass can now be written as $(4\pi/3)(1 - \gamma^3 + \eta\gamma^3)n_0 R_s^3$. This simple model is not the same as complex situations that can be envisioned (e.g., see Chiotellis et al. 2013), but nevertheless, a wide range in choices of γ and η can demonstrate the level of sensitivity in the derived explosion site to the inhomogeneities of the ISM. Following a similar notations described in Carlton et al. (2011), I derived an analytic, parametric solution for

the SNR shell radius. This analytic solution has

$$R' = 2.19(1 - \gamma^3 + \eta\gamma^3) \left(\frac{M_e}{M_{ch}} \right)^{\frac{1}{3}} n_0^{-\frac{1}{3}} pc, \quad (2.2.5)$$

along with equations 2.2.2 and 2.2.4. Note that when $\gamma = 0$ or $\eta = 1$, the solution will reduce to that of the homogenous ISM density profile.

With this, I can then repeat my χ^2 calculations of the position of the explosion site for a variety of ISM distributions. When $\gamma=0.5$, $\eta=0$, which means the SN was expanding into a bubble, I get a minimum χ^2 with $\alpha_{SN}=0h\ 25m\ 15.10s$, $\delta_{SN}=64^\circ\ 8'\ 42.36''$. For $\gamma=0.5$, $\eta=0.5$, I get a minimum χ^2 with $\alpha_{SN}=0h\ 25m\ 15.20s$, $\delta_{SN}=64^\circ\ 8'\ 42.00''$. For $\gamma=0.5$, $\eta=2$, the SN ejecta was sweeping through a dense ISM then encountered less dense material, I get a minimum χ^2 with $\alpha_{SN}=0h\ 25m\ 15.60s$, $\delta_{SN}=64^\circ\ 8'\ 38.76''$. In all these cases, the reduced χ^2 is close to unity. All these positions are within a few arc-seconds from my final position (Section 2.2.3) and are within the one-sigma error circle of 7.5 arc-seconds. However, for an extreme case with $\gamma=0.8$, $\eta=0$, which resembles the idea that Tycho's SN ejecta only went into some ISM very recently, I get $\alpha_{SN}=0h\ 25m\ 14.35s$, $\delta_{SN}=64^\circ\ 8'\ 48.12''$. This is 10 arc-seconds to the north-west of the position from Section 2.3.3, which is even further away from Star G. But in this case, I obtain a much larger minimum χ^2 . All this is saying that the position of the derived center has a small sensitivity on the radial distribution of the ISM material being swept-up, where the change of position is comparable and less than the one-sigma uncertainty. This conclusion is similar to the result in Figure 4 in Chiotellis et al. (2013), where the complex wind-driven bubble makes for little change from a homogenous ISM case in terms of the observed shell radius.

I have also examined the case of ISM inhomogeneities within the simple model of section 2.2.4. By adding different ISM density profiles, for example, a bubble or changing density along radius, I am still getting expansion centers within a few arc-seconds of the site given in section 2.2.3.

I conclude that substantial density inhomogeneities along the radii of expansion lead to shifts in the derived explosion site that are insensitive to the expansion model. The results from both models shows that the derived center is insensitive to even substantial inhomogeneities in the ISM. With this, I adopt the best position from expansion models as that from section 2.2.3.

2.3 The Ex-companion Candidates

For the position of Tycho star G in 1572, the best chi-square is 102.9, with $D=2.33\pm 0.04$ kpc, $E_{51}=0.45\pm 0.03$, $Q=1.55\pm 0.14$. The position of star G has $\chi^2 - \chi_{min}^2=67.4=8.2^2$. Thus star G is rejected at the $8.2\text{-}\sigma$ confidence level. Similarly, ex-companion candidate star B is rejected at the $5.1\text{-}\sigma$ level, and star E is rejected at the $4.1\text{-}\sigma$ level. See Figure 2.1 for the relative placement of these stars and my two independent error regions.

2.4 Conclusions

I have answered the question of the position of the 1572 supernova, and I have answered it with two positions. Both positions are significantly offset from the geometric center. The good agreement between my two positions, with radically different input, provides substantial confidence that *both* methods are accurate to within the stated error bars. That is, it is very unlikely that both methods would suffer significant unknown systematic errors that moved both positions by a similar amount in a similar direction.

With two valid methods to measure the position of the explosion site in 1572, my best measure will be the weighted average of the two positions. With this, my final position is $\alpha=0\text{h } 25\text{m } 15.36\text{s}$, $\delta=64^\circ 8' 40.2''$, and the $1\text{-}\sigma$ error radius is 7.3 arc-seconds. Star G is rejected at the $8.2\text{-}\sigma$ level. This proves a final and confident resolution for the controversy of whether this star is the ex-companion. Further, star B is rejected at the $5.1\text{-}\sigma$ level, while star E is rejected at the $4.1\text{-}\sigma$ level.

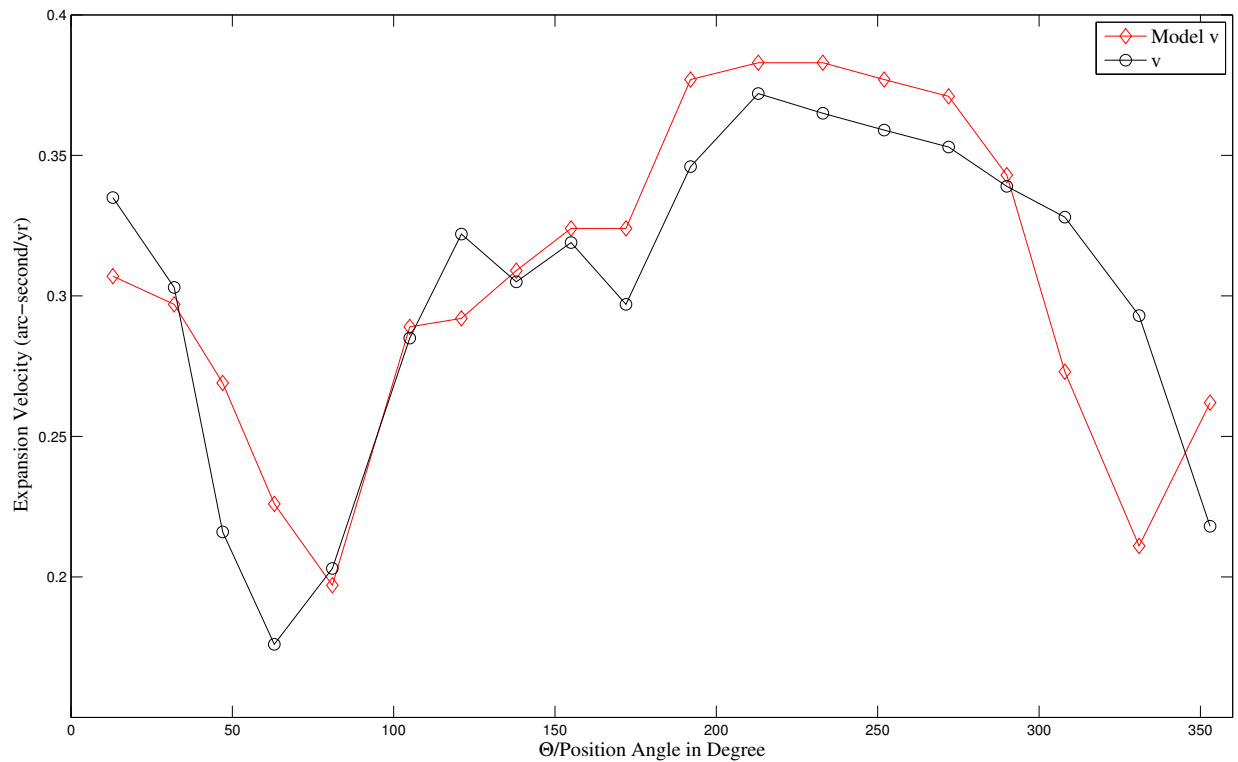


Figure 2.4: The 19 observed SNR expansion velocity and the model expansion velocities. Again, the expansion velocities vary greatly around the edges of the SNR, corresponding closely with the amount of swept up ISM material, and my model closely follows the observations. In comparing Figures 2.3 and 2.4 with Table 2.2, I see that the SNR has low expansion velocities in the same directions that it has small radii, and these are the same directions with dense ISM material. With the detailed expansion models of Carlton et al. (2011) allowing me to work backwards in time to determine the original center of expansion. Figures 2.3 and 2.4 are displays that my model is indeed matching the observed expansion history of the SNR, and hence that I can derive an accurate SNR expansion center.

I now have a confident and small error circle (see Figure 2.5). This is the region in which any ex-companion must be sought. Unfortunately, prior work has been exclusively inside the RL04 error circle, shown in Figure 2.2. I see that a large part of the new error circle has not been examined for ex-companions. That is, all prior searches have largely been looking in the wrong place. A new search is required to answer the question whether Tycho's SNR has any ex-companion star.

Prior work has provided photometry of some stars inside my final error circle (Bedin et al. 2014). These are labeled stars N, O, P, Q, R, and S (see Figure 2.2). Both stars O and P are given as being early-G spectral type, and both were rejected as ex-companions because their distances would be much closer than the SNR if they are main sequence stars, while their distances would be much farther than the SNR if they are typical red giants (Bedin et al. 2014). But this analysis ignores the possibility that either star O or P is a sub-giant, in which case their distance would match that of the SNR. (This is the exact same idea used to put star G at the distance to the SNR. Indeed, stars G, O, and P have identical colors and similar magnitudes, so any effort to put star G inside the remnant must also work for stars O and P.) I note that Bedin et al. (2014) measured star O to have a proper motion only a bit smaller than star G, so star O appears to be about as good an ex-companion candidate as star G originally was. And who knows what other candidates lie within my new error circle?

3. Probing SNIa Progenitor Systems Through the Rare Case of ASASSN-14dc

3.1 Observations and Data Reduction

ASASSN-14dc was discovered by the All-Sky Automated Survey for SuperNovae (ASAS-SN) on June 24.61, 2014 (UT) (MJD¹=56832.61) with a discovery magnitude of 15.8 in the V band and coordinates of α : 02:18:38.05, δ : +33:36:58.3 (J2000). The supernova was also detected in the images five days prior to the discovery date. A non-detection limit ($V > 16.6$) was placed on Feb. 12.28, 2014 (UT) and before (Holoien et al. 2014). The supernova was probably already past the peak when discovered (see the discussion in the light curve section). The host galaxy, probably a dwarf galaxy, 2MASX J02183825+3336556 has no redshift via the NASA/IPAC Extragalactic Database (NED)², nor any entry in the Sloan Digital Sky Survey (SDSS). Spectral confirmation has been made with an optical spectrum taken with the 4.2-m William Herschel Telescope + ISIS double-armed spectrograph 3 days after the discovery (Chen et al. 2014). Narrow emission lines from the host galaxy were detected, which implied a redshift ~ 0.044 . This is confirmed by the Asiago Transient Classification Program ~ 5 month later with a redshift of 0.043 (Ochner et al. 2014). Both teams suggested that ASASSN-14dc can be matched with the SNIIn/SNIa-CSM type, for example, SN 1997cy (Turatto et al. 2000, Silverman et al. 2013), or SN 2005gj (Aldering et al. 2006; Prieto et al. 2007) using GELATO (Harutyunyan et al. 2008) and SNID (Blondin and Tonry 2007). Figure 3.1 shows the relative position of the supernova and its host galaxy. I adopt cosmological parameters with $H_0 = 73 \text{ km s}^{-1} \text{ Mpc}^{-1}$, $\Omega_M = 0.3$, and $\Omega_\Lambda = 0.7$ throughout the paper, which yields a distance modulus of 36.35 mag to the host of ASASSN-14dc.

Intensive multi-wavelength follow-ups were carried out by the *Swift* in the UV, the Las Cumbres Observatory (LCO) 1-meter telescopes in B, V, g', r', i' and the 2-meter Liverpool Telescope (LT) in u', g', r', i', z'. The spectroscopic observations of ASASSN 14dc were

¹MJD=JD-2400000.5

²<https://ned.ipac.caltech.edu/>

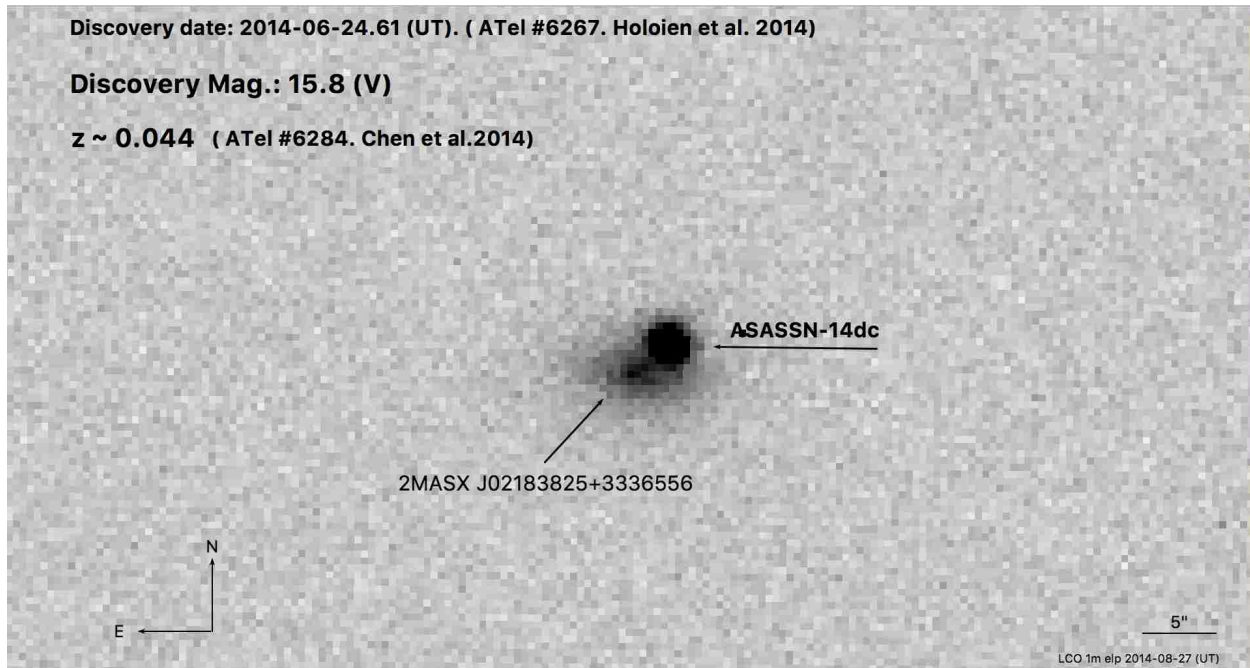


Figure 3.1: ASASSN-14dc and its host galaxy. The image showing is from the 1-m telescope of LCO taken on 2014-08-27(UT)

obtained mainly from the FLOYDS low resolution spectrograph on one of the LCO 2-meter telescopes. Additionally, I have an early time (relative to the discovery) ISIS spectrum from the WHT and a late time LRIS spectrum from the Keck telescope. I will present the detail of the photometry and spectroscopy in Section 3.1.1 and Section 3.1.2.

3.1.1 Photometry

Las Cumbres Observatory

LCO is a worldwide network of robotic 0.4-m, 1-m and 2-m telescopes designed for high-cadence rapid response to transient events (Brown et al. 2013). ASASSN-14dc was observed by LCO 1-m telescopes at the South African Astronomical Observatory, the McDonald Observatory in Texas, and Siding Spring observatory in Australia using SBIG cameras with B, V, g' , r' , and i' filters from June 28, 2014 to March 3, 2015. A custom Python-based *BANZAI* pipeline was used to perform the initial image processing when data comes in every

night.

Before photometry was extracted, I checked that the supernova is not visible any more by taking a series of deep images with the LCO 2-m Faulkes Telescope North on Haleakala in Hawaii. This site is also the host of the ASAS-SN telescopes, which made the discovery of the SN in the first place. Then the host galaxy templates were taken on July 26, 2016 in g' , r' , and i' and additional templates were taken the day after on July 27, 2016 in B and V. At the time, only a few 1-meter telescopes in the network still had the SBIG cameras and the network was replacing all the SBIG cameras by the Sinistro cameras. To avoid future transformation between different instruments, the galaxy templates were taken by the 1-m telescope in the Cerro-Tololo Inter-American Observatory in Chile with the SBIG camera.

Host galaxy images were subtracted using the algorithm of Alard (2000), implemented in HOTPANTS³. I extracted the photometry with the help of a PyRAF-based *lcogtsnpipe* pipeline (Valenti et al. 2016) built for LCO data, which has an interface to make PSF fitting and photometry extraction more effective. Since the field was not being observed by the SDSS, the B, V, g' , r' , and i' photometry was calibrated to the APASS catalog (Henden et al. 2009).

Liverpool Telescope

LT is a 2-meter fully robotic astronomical telescope owned and operated by the Astrophysics Research Institute of Liverpool John Moores University in north west England. Because of the ASAS-SN collaboration, ASASSN-14dc was followed by LT through July 2, 2014 to February 27, 2015 in u' , g' , r' , i' , and z' . The supernova is not visible in the images taken on September 11, 2015 (the flux at the location of the SN is around the same as the background, there is no stellar like PSF that can be pulled out), hence they are served as host-galaxy templates for the LT images. LT data come pre-reduced, including flat-field removal and bias subtraction etc. The image and median-combined templates were aligned with a star-

³<http://www.astro.washington.edu/users/becker/v2.0/hotpants.html>

matching algorithm. In the absence of enough point sources to tie the transformation, a transformation was performed just using the WCS information. Subtraction was also performed with HOTPANTS adapting the kernel parameters to reflect the seeing of the images. The photometry was extracted by a python routine I wrote based on PyRAF. For the same reason described in the previous section, all the photometry was calibrated to the APASS. However, APASS only provides magnitudes in B, V, g', r', and i'. For u' and z' band, color transformations based on Jordi et al. (2006) were used.

Swift UVOT

The *Swift* UVOT (Gehrels et al. 2004; Roming et al. 2005) observation was triggered immediately after the discovery for the purpose of catching a potentially associated Gamma-ray Burst (GRB). The follow up extended to August 10, 2014 in UVW1, UVM2, UVW2, U, B, and V. I obtained the UVOT galaxy template on August 4, 2016. The data reduction utilized the pipeline of the Swift Optical/Ultraviolet Supernova Archive (SOUSA; Brown et al. 2014). The reduction is based on that of Brown et al. (2009), including subtraction of the host galaxy count rates and uses the revised UV zeropoints and time-dependent sensitivity from Breeveld et al. (2011).

Milky Way extinction was based on the dust maps of Schlafly & Finkbeiner (2011) with $E(B-V) = 0.064$. I used the Cardelli et al. (1989) extinction law with $R_V = 3.1$ to correct all the photometry. I did not correct the host-galaxy extinction because no significant Na I D absorption can be seen in the spectrum. Thus, I assume that the host galaxy extinction is negligible

My photometric data from the LCO and the LT can be found in Table 3.1 and Table 3.2. The Swift data can be found on SOUSA. The data presented in the tables are not extinction corrected. Figure 3.2 shows the LT u'g'r'i'z' and LCO BVg'r'i' light curves for the first 250 days after the discovery combined with the Swift UV and UVOT UBV coverage for the first 50 days after the discovery.

Table 3.1: LT u'g'r'i'z' photometry of ASASSN-14dc

MJD^a	$Epoch^b(days)$	u'	g'	r'	i'	z'
56841.15	8.5	17.369 ± 0.049	16.442 ± 0.017	15.526 ± 0.009	15.756 ± 0.015	15.801 ± 0.023
56842.20	9.6	17.425 ± 0.045	16.458 ± 0.016	15.544 ± 0.009	15.765 ± 0.015	15.813 ± 0.023
56843.17	10.6	17.445 ± 0.053	16.464 ± 0.017	15.541 ± 0.009	15.763 ± 0.015	15.819 ± 0.024
56844.19	11.6	17.468 ± 0.045	16.471 ± 0.017	15.558 ± 0.009	15.771 ± 0.015	15.793 ± 0.023
56845.20	12.6	17.471 ± 0.045	16.489 ± 0.016	15.562 ± 0.009	15.789 ± 0.015	15.820 ± 0.023
56847.19	14.6	17.545 ± 0.046	16.506 ± 0.016	15.573 ± 0.009	15.787 ± 0.015	15.791 ± 0.023
56851.15	18.5	17.515 ± 0.050	16.549 ± 0.021	15.594 ± 0.011	...	15.816 ± 0.023
56854.13	21.5	17.648 ± 0.051	16.557 ± 0.018	15.607 ± 0.010	15.794 ± 0.016	15.782 ± 0.024
56857.13	24.5	17.619 ± 0.049	16.574 ± 0.017	15.601 ± 0.011	15.783 ± 0.015	15.789 ± 0.023
56860.16	27.5	17.624 ± 0.045	16.593 ± 0.017	15.629 ± 0.010	15.798 ± 0.015	15.795 ± 0.023
56863.10	30.5	17.734 ± 0.054	16.587 ± 0.017	15.641 ± 0.009	15.821 ± 0.015	15.778 ± 0.023
56866.09	33.5	17.599 ± 0.051	16.608 ± 0.017	15.656 ± 0.009	15.815 ± 0.015	15.788 ± 0.024
56869.08	36.5	17.730 ± 0.051	16.632 ± 0.017	15.673 ± 0.009	15.838 ± 0.015	15.782 ± 0.024
56873.07	40.5	17.836 ± 0.049	16.673 ± 0.017	15.728 ± 0.009	15.901 ± 0.015	15.818 ± 0.023
56876.11	43.5	17.830 ± 0.053	16.675 ± 0.019	15.741 ± 0.011	15.935 ± 0.016	15.858 ± 0.023
56879.05	46.4	17.860 ± 0.075	16.687 ± 0.020	15.746 ± 0.010	15.960 ± 0.017	15.853 ± 0.024
56883.07	50.5	17.886 ± 0.063	16.832 ± 0.019	15.835 ± 0.011	16.001 ± 0.018	15.891 ± 0.024
56886.03	53.4	15.854 ± 0.016
56889.19	56.6	18.062 ± 0.053	16.908 ± 0.018	15.902 ± 0.011	16.129 ± 0.017	16.106 ± 0.027
56892.08	59.5	18.291 ± 0.041	16.929 ± 0.017	15.965 ± 0.009	16.133 ± 0.016	15.966 ± 0.025
56895.13	62.5	18.129 ± 0.041	16.909 ± 0.017	15.996 ± 0.010	16.211 ± 0.016	16.027 ± 0.024
56899.02	66.4	18.320 ± 0.043	16.987 ± 0.020	16.043 ± 0.011	16.267 ± 0.018	16.065 ± 0.027
56901.99	69.4	18.246 ± 0.045	17.025 ± 0.018	16.084 ± 0.011	16.314 ± 0.016	16.107 ± 0.027
56905.09	72.5	18.442 ± 0.041	17.037 ± 0.018	16.134 ± 0.011	16.345 ± 0.017	16.149 ± 0.024
56907.97	75.4	18.313 ± 0.062	17.123 ± 0.029	16.116 ± 0.014	16.374 ± 0.018	16.054 ± 0.032
56914.09	81.5	18.428 ± 0.042	17.156 ± 0.024	16.212 ± 0.013	16.501 ± 0.022	16.231 ± 0.027
56917.04	84.4	18.479 ± 0.043	17.209 ± 0.018	16.268 ± 0.011	16.549 ± 0.016	16.315 ± 0.025
56922.98	90.4	18.623 ± 0.050	17.306 ± 0.019	16.349 ± 0.011	16.585 ± 0.018	16.227 ± 0.028
56930.03	97.4	18.772 ± 0.042	17.409 ± 0.019	16.464 ± 0.011	16.746 ± 0.016	16.417 ± 0.026
56932.95	100.3	18.778 ± 0.050	17.379 ± 0.023	16.460 ± 0.014	16.751 ± 0.019	16.523 ± 0.028
56936.08	103.5	18.720 ± 0.046	17.431 ± 0.021	16.544 ± 0.014	16.821 ± 0.019	16.503 ± 0.026
56942.01	109.4	18.841 ± 0.045	17.496 ± 0.022	16.589 ± 0.012	16.891 ± 0.017	16.546 ± 0.027
56946.94	114.3	19.101 ± 0.043	17.596 ± 0.018	16.678 ± 0.011	16.987 ± 0.018	16.620 ± 0.027
56953.01	120.4	...	17.708 ± 0.031	16.756 ± 0.030	17.069 ± 0.022	16.609 ± 0.041
56957.95	125.3	18.768 ± 0.104	17.623 ± 0.105	16.863 ± 0.083	17.076 ± 0.041	...
56965.03	132.4	...	17.822 ± 0.040	16.912 ± 0.018	17.290 ± 0.026	16.900 ± 0.029
56969.88	137.3	...	17.890 ± 0.042	16.945 ± 0.017	17.311 ± 0.023	16.871 ± 0.035
56974.84	142.2	...	17.970 ± 0.025	17.027 ± 0.014	17.404 ± 0.031	16.967 ± 0.039
56986.87	154.3	...	18.072 ± 0.023	17.119 ± 0.016	17.531 ± 0.021	17.130 ± 0.032
56992.93	160.3	...	18.119 ± 0.039	17.203 ± 0.024	17.439 ± 0.027	17.174 ± 0.034
56997.84	165.2	...	18.188 ± 0.046	17.259 ± 0.027	17.644 ± 0.030	17.205 ± 0.038
57003.89	171.3	...	18.242 ± 0.019	17.350 ± 0.014	17.736 ± 0.022	17.280 ± 0.032
57008.84	176.2	...	18.327 ± 0.021	17.436 ± 0.014	17.859 ± 0.025	17.363 ± 0.028
57009.85	177.2	...	18.338 ± 0.020	17.402 ± 0.014	17.801 ± 0.022	17.294 ± 0.028
57016.84	184.2	...	18.417 ± 0.019	17.525 ± 0.018	17.924 ± 0.023	17.436 ± 0.028
57025.95	193.3	...	18.482 ± 0.048	17.629 ± 0.031	18.129 ± 0.050	...
57036.90	204.3	...	18.692 ± 0.020	17.758 ± 0.013	18.152 ± 0.021	17.650 ± 0.030
57043.85	211.2	...	18.738 ± 0.019	17.835 ± 0.013	18.211 ± 0.021	...
57050.82	218.2	...	18.798 ± 0.038	17.898 ± 0.025	18.148 ± 0.028	17.708 ± 0.035
57057.84	225.2	...	18.909 ± 0.020	18.014 ± 0.015	18.283 ± 0.022	17.742 ± 0.032
57080.88	248.3	...	19.244 ± 0.059	18.120 ± 0.022	18.680 ± 0.038	18.143 ± 0.041

a: MJD=JD-2400000.5

b: Respect to the discovery date (MJD: 56832.61)

Table 3.2: LCO Bg'Vr'i' photometry of ASASSN-14dc

<i>MJD</i> ^a	<i>Epoch</i> ^b (<i>days</i>)	B	g'	V	r'	i'
56836.43	3.82	16.553 ± 0.026	16.359 ± 0.024	15.753 ± 0.022
56837.44	4.83	16.588 ± 0.026	16.412 ± 0.027	15.957 ± 0.041	15.525 ± 0.025	15.745 ± 0.019
56838.44	5.83	16.640 ± 0.034
56844.41	11.80	16.708 ± 0.026	...	16.117 ± 0.036
56862.18	29.57	16.956 ± 0.036
56876.81	44.20	16.976 ± 0.057	16.680 ± 0.026	...	15.726 ± 0.030	15.896 ± 0.023
56880.79	48.18	17.133 ± 0.079	16.715 ± 0.036	...	15.871 ± 0.038	16.005 ± 0.026
56888.79	56.18	17.094 ± 0.042	16.886 ± 0.027	...	15.845 ± 0.031	16.078 ± 0.029
56892.80	60.19	17.118 ± 0.029	16.943 ± 0.025	16.448 ± 0.041	15.905 ± 0.025	16.169 ± 0.017
56896.33	63.72	17.265 ± 0.028	16.957 ± 0.024	16.554 ± 0.033	16.080 ± 0.024	16.262 ± 0.017
56900.76	68.15	17.233 ± 0.027	16.913 ± 0.025	16.594 ± 0.042	...	16.332 ± 0.021
56905.02	72.41	17.332 ± 0.072	17.072 ± 0.039	16.527 ± 0.079	16.032 ± 0.037	16.336 ± 0.028
56909.05	76.44	17.626 ± 0.127	17.171 ± 0.040	...	16.138 ± 0.041	16.468 ± 0.027
56917.72	85.11	17.527 ± 0.045	17.207 ± 0.035	16.722 ± 0.069	16.109 ± 0.035	16.520 ± 0.030
56921.02	88.41	17.717 ± 0.052	17.358 ± 0.029	...	16.229 ± 0.038	16.686 ± 0.034
56927.67	95.06	17.537 ± 0.031	17.309 ± 0.030	16.863 ± 0.056	16.421 ± 0.029	16.714 ± 0.021
56932.60	99.99	17.831 ± 0.057	17.402 ± 0.030	...	16.429 ± 0.031	16.830 ± 0.031
56936.18	103.57	...	17.469 ± 0.025	17.119 ± 0.039	16.538 ± 0.040	16.919 ± 0.024
56943.94	111.33	...	17.508 ± 0.081	...	16.459 ± 0.066	16.918 ± 0.050
56947.91	115.30	18.171 ± 0.074	17.585 ± 0.038	...	16.562 ± 0.043	17.044 ± 0.047
56948.17	115.56	17.918 ± 0.040	17.607 ± 0.025	17.213 ± 0.045	16.680 ± 0.029	17.062 ± 0.022
56951.95	119.34	17.983 ± 0.062	17.696 ± 0.037	17.270 ± 0.085	16.700 ± 0.052	17.081 ± 0.062
56956.57	123.96	...	17.630 ± 0.036	...	16.559 ± 0.048	16.970 ± 0.051
56959.93	127.32	...	17.813 ± 0.035
56960.45	127.84	18.073 ± 0.028	17.718 ± 0.029	17.398 ± 0.037	16.778 ± 0.035	17.241 ± 0.026
56964.42	131.81	18.119 ± 0.144	17.904 ± 0.043	...	16.395 ± 0.169	17.354 ± 0.096
56971.55	138.94	18.218 ± 0.126	17.910 ± 0.056	...	16.735 ± 0.058	17.370 ± 0.055
56972.26	139.65	18.155 ± 0.036	17.894 ± 0.033	17.544 ± 0.049	16.844 ± 0.037	17.413 ± 0.031
56976.23	143.62	18.319 ± 0.039	18.023 ± 0.030	17.563 ± 0.057	16.917 ± 0.033	17.478 ± 0.043
56980.28	147.67	18.363 ± 0.042	17.923 ± 0.035	...	16.871 ± 0.034	17.488 ± 0.038
56985.37	152.76	18.585 ± 0.056	18.128 ± 0.033	...	17.105 ± 0.041	17.546 ± 0.052
56989.36	156.75	18.486 ± 0.036	18.136 ± 0.029	17.662 ± 0.058	17.109 ± 0.036	17.580 ± 0.031
56991.30	158.69	18.485 ± 0.048	18.066 ± 0.032	17.706 ± 0.045	17.141 ± 0.042	17.661 ± 0.032
56993.26	160.65	18.513 ± 0.048	18.156 ± 0.028	17.764 ± 0.051	17.138 ± 0.059	17.595 ± 0.049
57000.35	167.74	18.609 ± 0.080	18.132 ± 0.046	17.869 ± 0.059	17.549 ± 0.056	...
57003.32	170.71	18.531 ± 0.039	18.362 ± 0.041	17.964 ± 0.056	17.182 ± 0.047	17.854 ± 0.058
57007.32	174.71	18.590 ± 0.043	18.212 ± 0.043	...	17.448 ± 0.041	17.783 ± 0.033
57011.29	178.68	18.661 ± 0.043	18.414 ± 0.039	17.978 ± 0.055	17.248 ± 0.049	17.934 ± 0.042
57016.29	183.68	...	18.482 ± 0.081	...	17.515 ± 0.062	...
57018.20	185.59	18.747 ± 0.053	18.476 ± 0.043	18.040 ± 0.065	17.442 ± 0.056	18.056 ± 0.055
57038.22	205.61	19.087 ± 0.122	18.532 ± 0.051	...	17.522 ± 0.080	18.240 ± 0.070
57046.20	213.59	...	18.955 ± 0.105	...	17.789 ± 0.066	...
57050.12	217.51	19.039 ± 0.063	18.679 ± 0.045	18.347 ± 0.057	18.015 ± 0.049	...
57051.19	218.58	18.990 ± 0.044	18.720 ± 0.049	18.418 ± 0.068	17.825 ± 0.053	18.351 ± 0.083
57058.14	225.53	...	18.741 ± 0.126	...	17.909 ± 0.078	...
57072.15	239.54	...	18.929 ± 0.073	18.327 ± 0.074	18.006 ± 0.081	18.612 ± 0.080
57088.11	255.50	18.612 ± 0.106

a: MJD=JD-2400000.5

b: Respect to the discovery date (MJD: 56832.61)

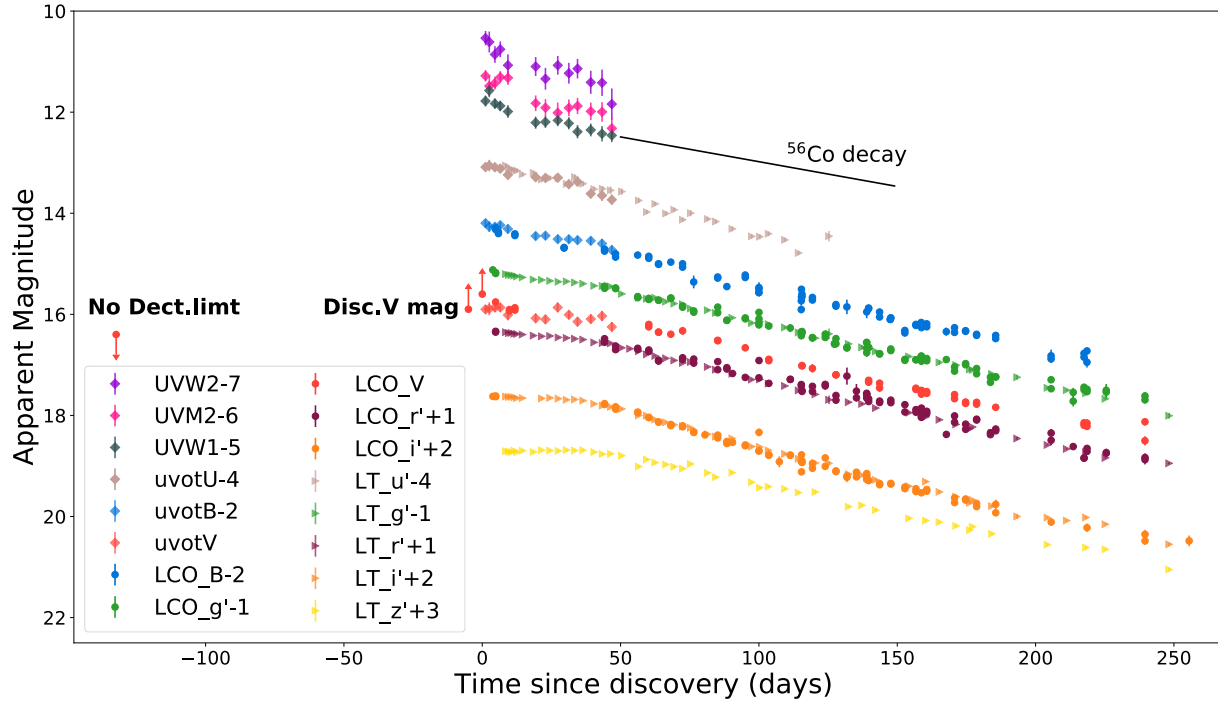


Figure 3.2: The multi-wavelength light curves of ASASSN-14dc. All the points are galactic extinction corrected. Photometry points from the *Swift* UVOT observation are in diamonds. LCO photometry points are in circles and the ones from LT are in triangles. The error bars are smaller than the symbols for most of the data. LCO BV are in the Vega system. LCO g'r'i' and LT u'g'r'i'z' are in the AB system. *Swift* points are in the UVOT system. Note that, UVOT U has been added an additional 1.02 mag to match the LT u' in AB system, which is the difference between the new AB and Vega zeropoints for UVOT (Breeveld et al. 2011). The discovery points in V and the no detection limits are shown as well. A decline rate of 0.98mag/100days (for light curve powered by radioactive decay) is plotted for comparison.

3.1.2 Optical Spectroscopy

All the spectra of ASASSN-14dc were extracted from the internal web interface *SNE x* ⁴ hosted by the LCO.

Most of the spectra were obtained from the FLOYDS robotic spectrographs on the LCOGT 2-meter telescopes at Haleakala Observatory, Hawaii. FLOYDS are a pair of nearly identical, low dispersion, robotic spectrographs deployed at the 2m Faulkes Telescopes, North and South (FTN and FTS). The instruments were designed with supernova classification and monitoring in mind, with a large wavelength coverage (~ 320 to 1000 nm) and a low resolution ($R \sim 300$ to 600 , depending on wavelength). FLOYDS spectra were reduced using the PyRAF- based *floydsspec*⁵ pipeline.

A Keck spectrum of ASASSN-14dc was obtained on 2014-11-20 UT at an airmass of 1.2 with the Low Resolution Imaging Spectrometer (LRIS; Oke et al. 1995). We used an exposure time of 600 seconds and the 1.0 arcsec slit rotated to the parallactic angle to minimize the effects of atmospheric dispersion (Filippenko 1982), in addition, LRIS has an atmospheric-dispersion corrector. In our LRIS configuration, coverage in the blue with the 600/4000 grism extends over the wavelength range 3200-5600 Å with a dispersion of 0.63 Å/pixel and a full-width at half-maximum intensity (FWHM) resolution of ~ 4 Å. We used the 5600 Å dichroic, and our coverage in the red with the 400/8500 grating extends over 5600-10200 Å with a dispersion of 1.16 Å/pixel and a resolution of FWHM ~ 7 Å. Spectra were reduced using the standard techniques optimized for Keck+LRIS by the CarPy package in PyRAF. The two-dimensional (2D) images were flat-fielded, corrected for distortion along the y (slit) axis, wavelength calibrated with comparison-lamp spectra, and cleaned of cosmic rays before extracting the 1D spectrum of the target. This spectrum was flux calibrated using a sensitivity function derived from a standard star observed the same night in the

⁴<http://supernova.exchange>

⁵<https://www.authorea.com/users/598/articles/6566>

same instrument configuration. The standard-star spectrum was also used to remove the telluric sky absorption features⁶.

I also obtained the spectra used to classify ASASSN-14dc with the 4.2-m William Herschel Telescope + ISIS double armed spectrograph 3 days after the discovery through Stephen Smartt from School of Maths and Physics at Queen’s University Belfast.

3.2 Analysis

3.2.1 Light Curves

The light curves decline since the discovery of the supernova in both UV and optical. This suggests that the ASASSN-14dc was discovered after the optical peak. However, some ‘plateau’ features seen in the i’ and z’ band that last from ~ 10 to 40 days since the discovery. The full optical light curves presented in Prieto et al. (2007) for SN 2005gj showed very similar behaviors in both i’ and z’ bands. The plateau in SN 2005gj lasted about 40 days as well and started ~ 40 days after explosion. A shorter plateau in g’ can be seen after the peak as well and it lasted about 20 days for the supernova. This similar short plateau in g’ can only be spotted for the first ~ 10 days of ASASSN-14dc. By this analogy, I can extrapolate the explosion date of ASASSN-14dc is about ~ 20 to 30 days before the discovery date of ASASSN-14dc and the g’ band peak took place about ~ 10 days prior to the discovery date. This has to be taken with caution. The secondary maximum present in the r’ and i’ light curves of SN 1991T and other SN Ia is completely absent in both ASASSN-14dc and SN2005gj but can be seen in both PTF11kx and SN2002ic.

By extrapolation, the supernova at peak is probably nearly as bright as the time it was discovered since it would just start to entering the short plateau in the g’ band. For a distance modulus of 36.35 mag, the absolute magnitude at the ‘peak’ in g would be ~ -20.23 and -21.00 in r’. By the empirical definition ($M_r < -21$) of the so called ‘Super-Luminous

⁶Keck spectra was reduced by Melissa L. Graham Department of Astronomy, University of Washington

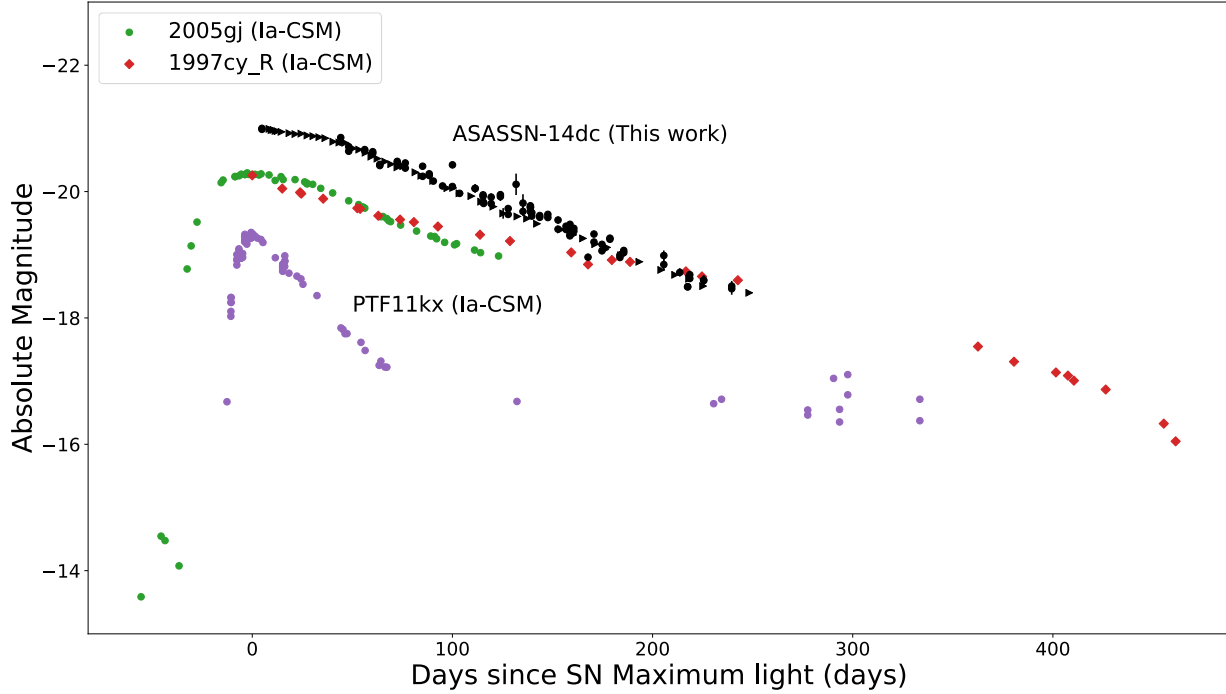


Figure 3.3: ASASSN-14dc light curve in r' compared to other SNe Ia-CSM. Typical SLSN is brighter than $M_r \sim -21$. ASASSN-14dc is right on the line, although this is an empirical definition. The date of the first photometric point of SN 1997cy was assigned as the date of its maximum brightness.

Supernova' (SLSN), ASASSN-14dc is one of them. In fact, it is among the brightest Ia-CSM candidates ever found. See the histogram in Silverman et al. (2013a) which shows the distribution of the peak brightness of Ia-CSM, IIc and SLSN etc in r' , and an updated version of the same plot can be found in Hosseinzadeh et al. (2017).

ASASSN-14dc has a constant decline rate of 0.015 ± 0.001 mag/day in u' . This is much slower when compared to the 0.027 ± 0.001 mag/day observed in SN 2005gj. But a slightly slower decline rate of 0.010 mag/day in B, V, g' , r' , and z' after 50 days can be seen in ASASSN-14dc. However, the decline rate of ASASSN-14dc in i' is as fast as 0.015 ± 0.001 mag/day after 50 days which is comparable to the decline rate of SN 2005gj in optical. Figure 3.3 and Figure 3.4 compares the ASASSN-14dc light curves with other Ia-CSM candidates and other types of SNe.

ASASSN-14dc is brighter than SN 2005gj at all times by ~ 0.2 - 0.6 mag depending on the filters and it is also brighter than SN 2002ic (Hamuy et al. 2003; Wood-Vasey et al. 2004),

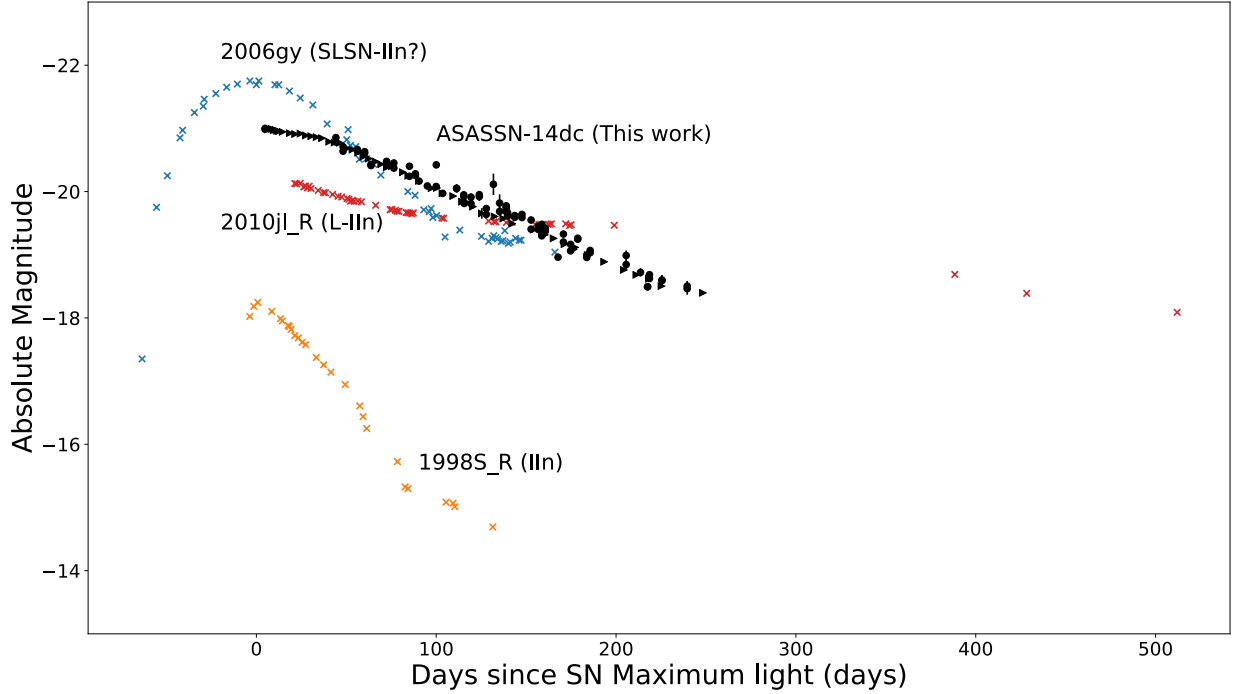


Figure 3.4: ASASSN-14dc light curve in r' compared to SNe II.

which is not shown in Figure 3.3. SN 2002ic is fainter than SN 2005gj as well. ASASSN-14dc is much brighter (~ 1.5 mag) than the PTF 11kx (Dilday et al. 2012). PTF 11kx has similar peak magnitude as the broad/bright SN1999aa/SN1991T and showed a similar decline rate as SN Ia in the first 100 days. However, its light curve reached a long lasting ‘plateau’ shape from ~ 150 days to 350 days (Silverman et al. 2013b) and it was 3 mag brighter than SNIa at similar times. The decline rate of ASASSN-14dc is very much like the decline rates observed in SN 2005gj and SN 2002ic. It is believed that the peak luminosity and decline rate difference between SN 2005 gj/SN 2002ic and PTF 11kx are due to the fact that the latter had weaker/late ejecta-CSM interaction. Simply from this perspective, ASASSN-14dc seems to have the strongest CSM interaction among them all. Also, this might explain the absence of the secondary peak in $i'z'$ in ASASSN-14dc and SN 2005gj but not in SN 2002ic and PTF 11kx, as relatively stronger ejecta-CSM interaction in ASASSN-14dc and SN 2005gj ‘dilute’ the underlying SN Ia feature. It is worth noting that, for PTF 11kx, the ejecta-CSM interaction persists even after 2 years (Silverman et al. 2013b) and 3.5 years

(Graham et al. 2017) after the SN explosion. This could explain the long lasting slow decline turn-on ~ 100 days post-explosion seen in the PTF 11kx light curve (see Figure 3.3). The explosion date of another Ia-CSM candidate, SN 1997cy (Germany et al. 2000) is highly uncertain. So in Figure 3.3, I assumed the first photometry point as the peak. The decline rate before ~ 50 days resembles ASASSN-14dc and SN 2005gj, however, it slowed down at later times. By the time of ~ 200 days, it had similar brightness in R as ASASSN-14dc while started ~ 0.5 mag fainter (it could be as bright as ASASSN-14dc at peak due to the unknown peak date). It might suggest that stronger CSM interaction turn on around 80 days due to a different CSM geometry or density or a combination of both. The light curve of ASASSN-14dc showed a similar behavior to SNe Ia-CSM and especially to SN 2005gj. It has a slow decline rate and it is highly possible that ejecta-CSM interaction is the additional energy source of the light curve. ASASSN-14dc is also brighter than most of the SNe Ia-CSM which suggests a even stronger ejecta-CSM interaction.

I also compare the ASASSN-14dc light curve with other Type II_n supernovae. SNe II_n are generally considered CSM interaction supernova with the ‘n’ indicating the narrow/intermediate width Hydrogen lines presented in the spectra. The light curves of Type II_n supernovae have huge diversity themselves. SN 2006gy is not only a SN II_n, but also the first SLSN to be discovered (e.g. Ofek et al. 2007, Smith et al. 2007). The peak brightness is about 1 mag brighter than ASASSN-14dc. However, huge dissimilarity can be seen as 2006gy fades rather quickly in the first 150 days despite an unusually slow rise time compared to ‘typical’ SN II_n. It is thought that SN 2006gy has a very compact and opaque CSM shell originating from a single eruption of ~ 20 solar masses of material from the progenitor around a decade prior the supernova explosion (Smith et al. 2010). This is unlikely to be the case for ASASSN-14dc as less mass is required for the observed luminosity and also the light curve stretches much longer which could imply a rather extended CSM distribution. SN 2010jl is also a SLSN II_n with a slower decline rate than ASASSN-14dc, and it remains fairly bright over the years after the explosion (Zhang et al. 2012). ASASSN-14dc faded below

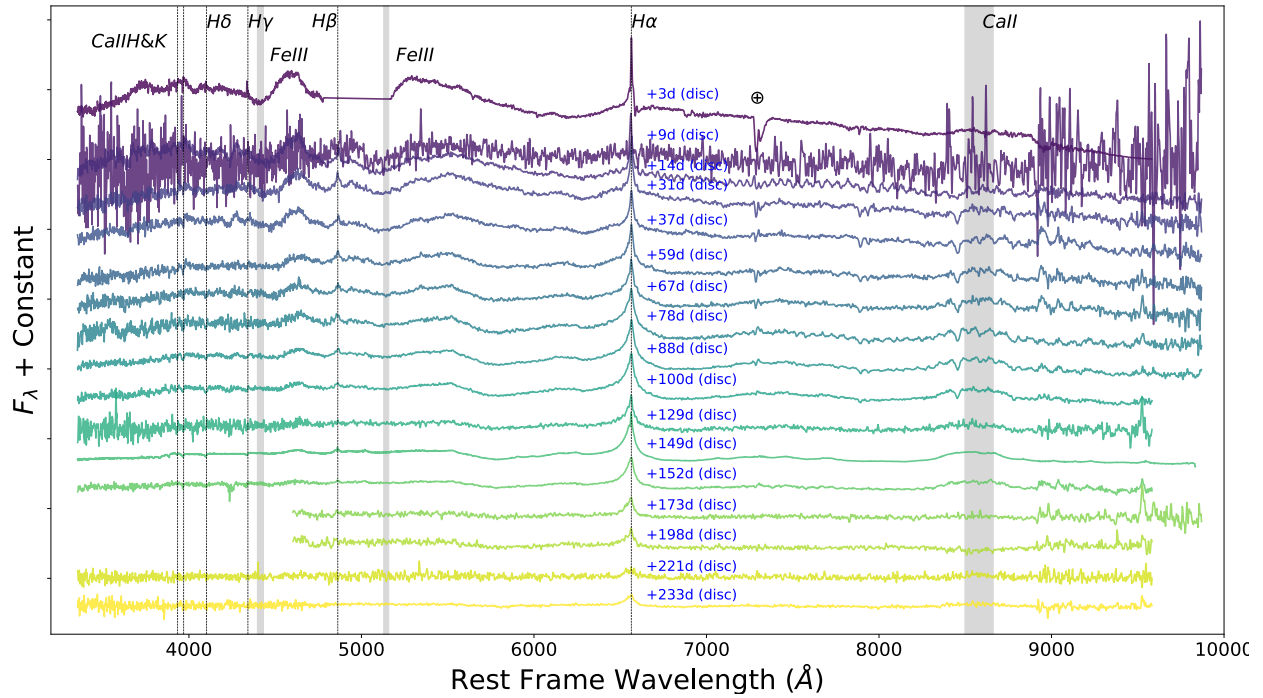


Figure 3.5: Spectral evolution of ASASSN-14dc. The phase of each spectrum is relative to discovery date of the supernova. The spectra are corrected for Galactic extinction and are shown in the rest frame of ASASSN-14dc. The \oplus symbol marks the positions of the strongest Telluric absorptions. A strong Telluric absorption around 6867\AA can be seen in the first spectrum as well. The first spectrum (3 days) is from the WHT+ISIS and the spectrum at epoch 149 days is from the Keck+LRIS. The rest are all from the LCO FLYODS.

SN 2010jl \sim 150 days while started to be \sim 0.8 mag brighter around the peak. An extended dense cocoon with mass of 10 solar mass or more in the CSM are suggested to be responsible for the observed light curve for SN 2010jl (Ofek et al. 2014). Linking to a young massive star cluster using *HST* direct imaging of the SN location post-explosion suggested a massive star ($> 30M_{\odot}$) as the progenitor for SN 2010jl (Fox et al. 2017). SN 1998S was not over luminous and the light curve declines sharply as the ejecta-CSM interaction only lasted for the first a couple of weeks. Also, spectropolarimetry has suggested that high asphericity was present which could imply a ring or disk-like CSM (Leonard et al. 2000). This is certainly not the case for ASASSN-14dc.

A slow light curve decline rate is a sign of ejecta-CSM interaction as an additional or dominant source of energy input for these interacting supernova. ASASSN-14dc is a super-luminous interacting supernova with its peak luminosity brighter than most of the SNe Ia-CSM and some luminous SN IIn. Its slow light curve decline rate suggests an ejecta-CSM interaction and this also can be confirmed spectroscopically which will be discussed in the next section.

3.2.2 Spectral Analysis

In Figure 3.5, I show the spectral evolution of ASASSN-14dc from soon after the discovery to \sim 230 days. Since there is no tight constraint for the explosion date, I am referring the phase with respect to the discovery date. The spectra are interaction dominated at the first epoch and was a little bluer than later epochs. All epochs can be characterized by multi-component H emission lines on top of a relatively flat continuum. Very broad Ca near-IR can be seen, and a blend of Fe lines has an appearance of a blue ‘pseudo-continuum’ below 5500Å (Silverman et al. 2013b, Silverman et al. 2013a, Inserra et al. 2016).

Using GELATO ⁷, ASASSN-14dc spectra are matched best with SN 2005gj at all epochs and can be matched with SN 1997cy, PTF 11kx at some epochs. Figure 3.6 shows the

⁷<https://gelato.tng.iac.es/>

spectral comparison with other SNe Ia-CSM at different epochs. The spectra of SN 2005gj and PTF 11kx were obtained through the Weizmann Interactive Supernova data REPOSITORY (Yaron & Gal-Yam 2012). I have performed the Galactic extinction and redshift correction accordingly. As already discussed in the light curve section, there is no tight constraint on the explosion date for ASASSN-14dc. Simply by light curve comparison, I extrapolate the explosion date ~ 30 days prior to the discovery. Indeed it happens that the spectrum at epoch 37 days can be matched best with SN 2005gj at 73.9 days since explosion. However, we should be cautious of treating this as the confirmation for my extrapolation of ASASSN-14dc's explosion date. The reason is that there is very limited line feature evolution from 3 days to 230 days in the ASASSN-14dc's spectra. The spectra are already interaction dominated at the discovery epoch and throughout the following 200 days. The spectra at 149 days can be matched best with PTF 11kx at 282 days (if using only PTF 11kx spectrum for the matches). As already discussed in the previous section, the light curve of PTF 11kx started to decline more slowly ~ 200 days after the peak along with the strengthening of the $H\alpha$ line and CSM interaction (Dilday et al. 2012; Silverman et al. 2013b; Graham et al. 2017). Stronger CSM interaction tends to veil the SNIa features more hence later epoch spectra of PTF 11kx can be matched best with ASASSN-14dc.

Noticeable evolution in the spectra is seen in the gradually decreasing Balmer lines and the emerging very broad Ca II NIR feature(8498Å , 8542Å , and 8662Å, then decreasing at later epochs. Also, the weakening of the red shoulder of the blue 'pseudo-continuum' can be seen. Other than these effects there are no significant changes in the spectra spanning ~ 250 days. He I 5876 and 7065 cannot be seen in the spectra of ASASSN-14dc. Oxygen lines, mainly [O I] 6300, 6364 and O I 7774, are claimed to be found in the Ia-CSM candidate SN 2012ca (Inserra et al., 2014) and they are blueshifted. The O I 7774 feature cannot be seen in ASASSN-14dc but the emission feature blue-ward of the trough of the very broad $H\alpha$ blue wing around 6240Å is rather clear through the ASASSN-14dc spectrum. However, Fox et al. (2015) found such blue-shifted lines are seen at the exact same velocity offset in different

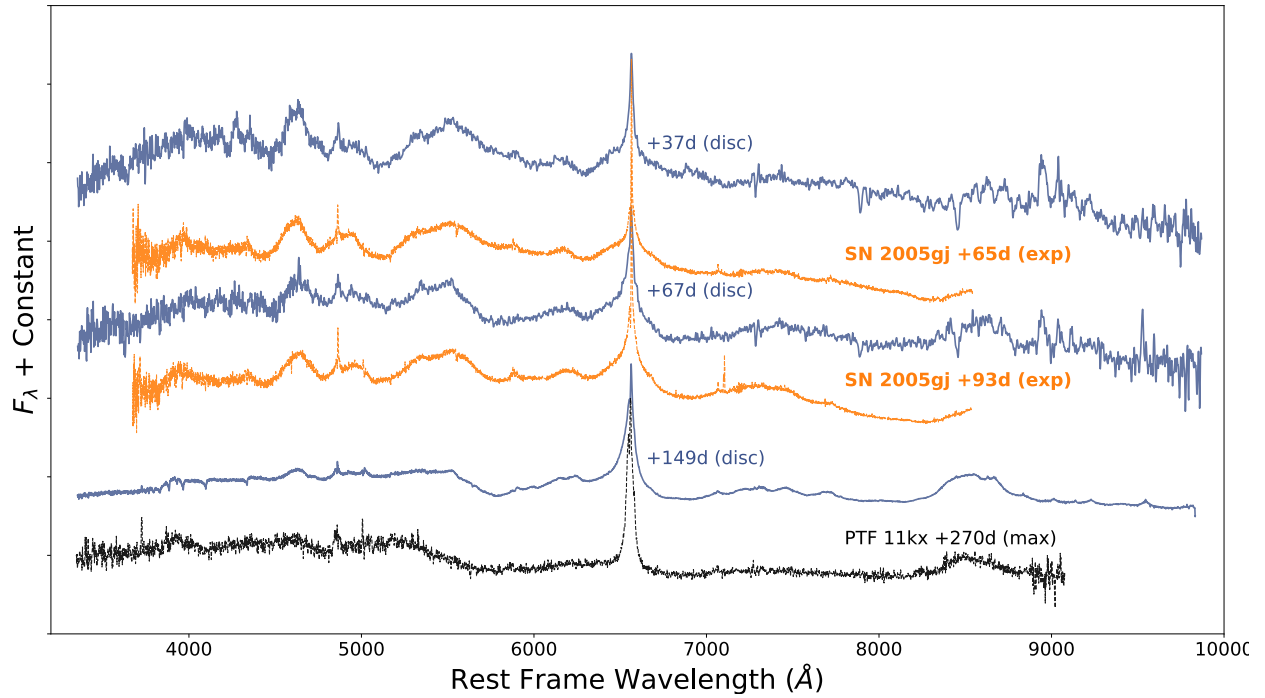


Figure 3.6: Comparison of spectra of ASASSN-14dc (blue) with other SNe Ia-CSM as SN 2005gj in orange and PTF 11kx in black. Spectra of SN 2005gj and PTF 11kx are scaled and shifted by an arbitrary constant for better comparison. All spectra are Galactic extinction and redshift corrected according to their own color index and redshift. Spectra of SN 2005gj are relative to its explosion date while the one from PTF 11kx is marked with respect to its peak date in the B band.

SNe like 2005ip, 2013dn, 2008J, 2009ip, and 1998S. This coincidence makes the explanation unlikely and they further suggested that [Fe II] 6248 might be responsible for this feature. A broad emission feature around 7400Å is visible in ASASSN-14dc from ~ 40 days to 150 days. As Silverman et al. (2013a) point out this might be due to a blend of [O II] 7319, 7330 and [Ca II] 7291, 7324. The absence or weakness of He and Oxygen distinguishes between SN Ia-CSM and SN IIn (Silverman et al. 2013a). ASASSN-14dc is consistent with other Ia-CSM supernovae in this respect.

In previous studies of SNe Ia-CSM (e.g. SN 2002ic: Hamuy et al. 2003; SN 2005gj: Aldering et al. 2006, Prieto et al. 2007), spectral decomposition revealed ‘diluted’ SN 1991T-like spectra plus a smoothly varying continuum, in which they tried to stress the idea of CSM interaction as an additional energy input. Aldering et al. (2006) pointed out that caution should be used when applying such a method and other people have already brought up this issue. Line profiles can change a lot (e.g. ‘muted’, inverted) when the line formation region has external illumination from CSM interaction (Branch et al. 2000; Chugai et al. 2004). Nevertheless, it is curious to see how the ASASSN-14dc spectra compare to SN 1991T. Figure 3.7 presents the decomposition result. I obtained the SN 1991T spectrum template from Nugent et al. (2002). After correcting the redshift and extinction for ASASSN-14dc, I decomposed the spectrum using a scaled SN 1991T spectrum, and a fourth order polynomial, which represents a smooth varying continuum from CSM interaction. The earliest WHT spectra can be best decomposed with the SN 1991T spectrum at 38 days after explosion which again agrees with my extrapolation of the explosion date of ASASSN-14dc. The latest SN 1991T template is at 93 days, hence I used it in the fit for the ASASSN-14dc spectrum at 67 days. Generally, most of the feature can be recovered except a deficit around 5900Å which might be due to forbidden Co line (Filippenko 1997) in SNIa. Also note that the broad feature around 6500Å in SN 1991T spectrum is not H α but a blend of [Fe II] and Co (Filippenko 1997) and this is probably the very broad feature (FWHM $\sim 10,000$ km/s) seen in the H α profiles. Hence, when calculating H α luminosity, equivalent width (EW)

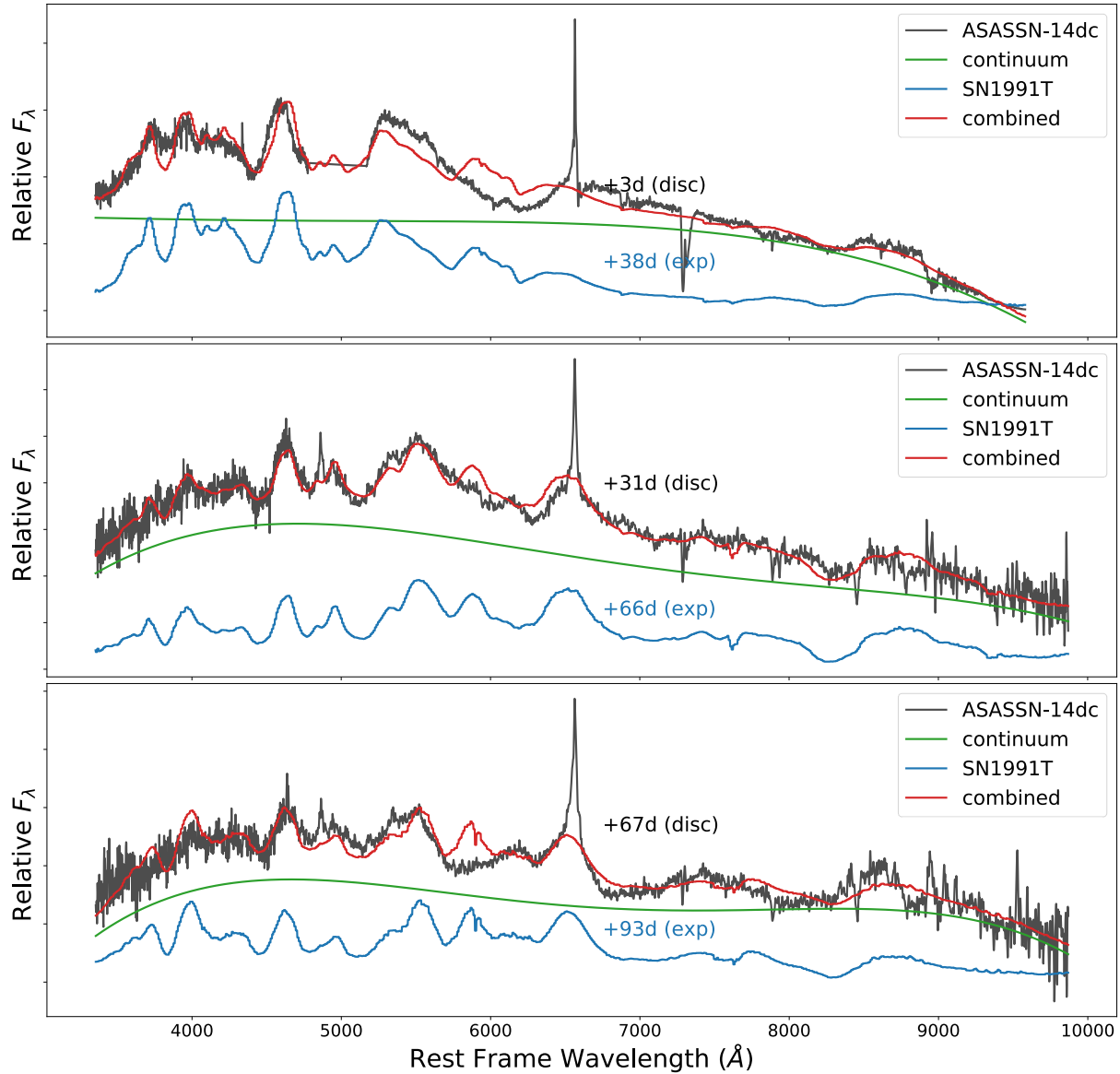


Figure 3.7: Spectral decomposition of ASASSN-14dc. I decompose the spectra into two components: (1) SN 1991T spectrum scaled by an arbitrary constant (blue line); (2) fourth order polynomial (green line). These two combined are in red. ASASSN-14dc spectra are in black and have been Galactic extinction and redshift corrected. Note that when emission features like the Balmer lines (e.g. at 6563 \AA , 4861 \AA) are added, you can have a full SN Ia-CSM. The purpose of this figure is to show that ASASSN-14dc spectrum can be interpreted as an underlying luminous SNIa (SN 1991T-like) being ‘diluted’ by ejecta-CSM interaction. This further supports that ASASSN-14dc is one of the SNe Ia-CSM and has a SNIa origin.

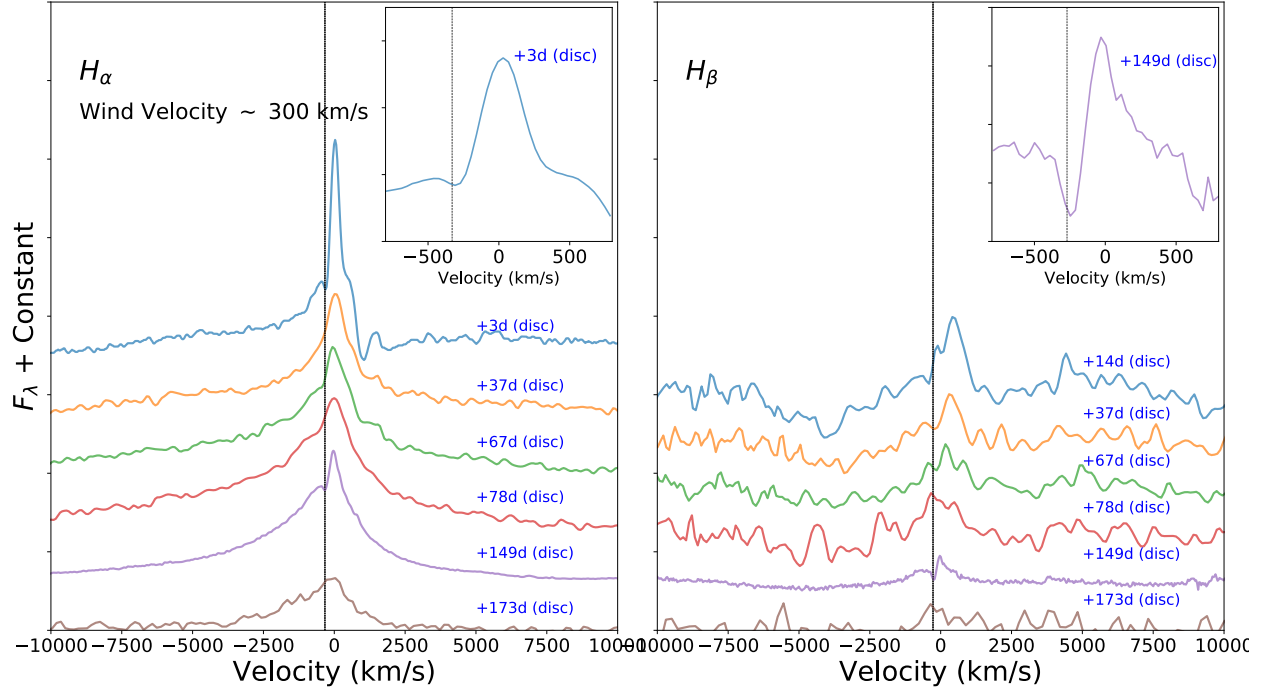


Figure 3.8: The evolution of $H\alpha$ and $H\beta$ lines. The P-Cygni profile can be seen in the day 3 and day 149 which have higher resolution. The wind velocity is ~ 300 km/s. $H\alpha$ can be characterized with an unresolved narrow and intermediate/broad width component. The narrow components have a typical FWHM of 200 to 400 km/s. The intermediate components have a typical FWHM of 2500 km/s, which is the sign of CSM interaction.

etc., such features should be excluded. Leloudas et al (2015) investigated how the flux ratio between the underlying SN and the continuum affected the spectroscopic classification of different types of interacting supernovae. I can easily calculate such ratios after this spectral decomposition. The ratio between the SN flux and continuum for ASASSN-14dc varies ~ 0.4 to 0.5 depends on epochs. This is within the range they found for SN Ia-CSM (0.17-0.69).

The $H\alpha$ line profile can be fitted best with a sum of two Gaussian components after excluding the underlying broad component. The motivation behind this is that a narrow component could represent recombination from photoionized un-shocked CSM while direct emission from the shock-heated CSM appears as the broad/intermediate width component. An even broader component could come from underlying broad SN iron lines. To exclude this very broader component, I used the SN 1991T template following the decomposition method

I just described. Since the SN 1991T template only lasts 94 days after its explosion, for later epochs, a third order polynomial was used to fit this broad component along with the two Gaussians for the rest of the profile. The narrow component has a FWHM of 200 to 400 km/s which is unresolved because of the low spectral resolution. The broad component has a FWHM of ~ 2500 km/s. There is little evolution in the FWHM of both components except that the broad component started with a smaller FWHM (~ 1500 km/s but increased to 2500 km/s ~ 30 days after discovery). $H\beta$ lines are generally unresolved through the spectra of ASASSN-14dc and contain significantly less flux when compared to the $H\alpha$ emission. It has a typical FWHM of several hundreds to 1000 km/s.

The luminosities of $H\alpha$ emission stayed pretty much the same in the first 150 days with $(2-3) \times 10^{41}$ erg s^{-1} then gradually decreased. This is higher than other SN-Ia CSM candidates which have $(1-9) \times 10^{40}$ erg s^{-1} (Silverman et al. 2013a). This is expected as ASASSN-14dc is among the brightest SNe Ia-CSM. The luminosity of $H\beta$ started around 5×10^{40} erg s^{-1} and decayed after the first epoch. The Balmer decrement (ratio between the $H\alpha$ flux and $H\beta$ flux) started around 2.5 and increased to ~ 14 in the first 150 days. Collisional excitation rather than recombination as the line formation cause has been suggested to explain this commonly observed feature among Ia-CSM supernovae (Aldering et al. 2006; Silverman et al. 2013a; Prieto et al. 2007). In this scenario, a large optical depth in $H\alpha$ can lead to a larger Balmer decrement (Drake & Ulrich 1980). This implies a high density and collisional excitation (Xu et al. 1992). Thus, one can picture that the SN ejecta ram into thin, dense Hydrogen-rich CSM and the Hydrogen may get collisional excited and cause the large Balmer decrement observed in the spectra of Ia-CSM.

The P-Cygni like profile can be best seen in two of the ASASSN-14dc spectrum with higher resolutions on day 3 and 149. The absorption-like minimum can be found around 300 km/s. This is the indication of un-shocked material moving outward, which is probably the material lost from the progenitor system. The velocity of this outflow is higher than the wind velocity found for other SNe Ia-CSM like PTF 11kx (65 km/s) (Dilday et al. 2012),

but comparable to SN 2005gj (Aldering et al. 2006; Prieto et al. 2007), SN1999E (Rigon et al. 2003) and SN 2012ca (Inserra et al. 2014) with ~ 200 km/s. SN 2005gj has been suggested to have a Luminous Blue Variable (LBV) as its Progenitor (Trundle et al. 2008), mainly based on the presence of a double P-Cygni profile in the $H\alpha$ line, a feature which is not present in ASASSN-14dc. The lack of strong He, O, Mg signatures also argues against the idea that ASASSN-14dc is core-collapse SN.

3.3 Discussion

I have presented the multi-wavelength photometry and spectroscopy of ASASSN-14dc obtained through the LCO and ASASSN supernova group during the first 250 days after discovery. Additional UV observations in the first 50 days were obtained with *SWIFT* UVOT. Despite the lack of spectra at maximum brightness and earlier, ASASSN-14dc shows lots of similarities with the Ia-CSM supernovae class, especially SN 2005gj, SN 2002ic, SN 1997cy, PTF 11kx, SN 2012ca etc.

SN Ia-CSM is interpreted as a SNIa embedded in a dense circumstellar material. The features of ASASSN-14dc and similarities with other SNe Ia-CSM can be summarized as follows:

(1) ASASSN-14dc has an absolute magnitude of ~ -21 magnitude in r' , which makes it among the brightest SNe Ia-CSM ever observed and also one of the super-luminous supernovae. The explosion date is not well constrained. However, from light curve and spectra comparison with other SNe Ia-CSM, I extrapolate the explosion date to be ~ 30 days before the discovery. The light curve decline rate is ~ 0.010 mag/day in B, V, g' , r' , and z' after 50 days since discovery which is similar to SN 2005gj. A higher decline rate can be seen in both u' and i' with ~ 0.015 mag/day. Its slow light curve decline rate and high luminosity suggest strong ejecta-CSM interaction which is consistent with other SNe Ia-CSM.

(2) The spectra of ASASSN-14dc can be matched best with SN 2005gj at all epochs and also other SNe Ia-CSM like SN 1997cy, PTF 11kx etc. at certain epochs. Just like

other SNe Ia-CSM, spectra of ASASSN-14dc can be characterized by ‘dilution’ of a SN 1991T (peculiar bright SNIa) spectrum with a smooth varying continuum. Blue ‘pseudo-continuum’ from blended iron-group element lines, strong broad Ca II near-IR triplet and strong multi-component $H\alpha$ emission lines can be seen in the spectrum. The lack of strong Helium and Oxygen signatures argue against ASASSN-14dc as a Type IIn supernova, which is also consistent with other SNe Ia-CSM. The ratio between the underlying SN Ia flux and the continuum is within the range found for many other SNe Ia-CSM.

(3) Broad (FWHM ~ 2500 km/s) $H\alpha$ emission lines are a sign of strong interaction between hydrogen-rich CSM and SN ejecta. Mostly unresolved narrow lines (FWHM ~ 200 - 400 km/s) indicate un-shocked CSM. The CSM wind velocity can be estimated from the P-Cygni profile detected in the two highest resolution spectra indicating a wind velocity ~ 300 km/s. This is the velocity of the material loss from the progenitor system.

(4) A large Balmer decrement (5~14) is seen throughout the ASASSN-14dc spectra. This is likely a consequence of collisional excitation as the main cause of hydrogen line formation when fast SN ejecta overtake slow moving dense thin CSM. All of these support the interpretation of the supernova ejecta interacting with dense circumstellar material.

It is clear that ASASSN-14dc is among the rare kind of SNe Ia-CSM and is ejecta-CSM interaction dominated. The lack of the secondary peak in the i' , z' light curves, slower decline rate compared to SN 2002ic and PTF 11kx, and higher luminosity than most of SNe Ia-CSM all point to stronger ejecta-CSM interaction in ASASSN-14dc.

3.3.1 Progenitor Models

If we accept that ASASSN-14dc and other SNe Ia-CSM have a SN Ia origin, what kind of SNe Ia progenitor system produced such events? This 1500 - 2500 km/s width component seen in the $H\alpha$ emission is very interesting. The velocity of the SN shock wave as it breaks out is on the order of 2×10^4 km/s. Our first spectrum which is 3 days after the discovery showed 1500 km/s component. In the following 150 days, the velocity of the component increased to

~ 2500 km/s and stayed pretty much constant for a long period of time. The velocity is still very small when compared to the SN velocity. Also, the fact that this intermediate width component increased the velocity a little bit contradicts the belief that SN shock velocity would gradually decrease as it moves outward. Hence this 1500 km/s ~ 2500 km/s width component cannot be due to the SN velocity but is rather due to interaction between the shock and CSM.

At least for ASASSN-14dc, we know that the interaction started 3 days after the discovery at least. If we assume that the explosion happened 30 days prior the discovery, using the SN shock velocity of 2×10^4 km/s, we have the inner radius of the CSM being $\sim 6 \times 10^{15}$ cm or smaller. We know the wind velocity of the CSM from the P-Cygni profile with a value ~ 300 km/s. This implies that the CSM was ejected by the progenitor system at least a decade before the supernova explosion. The number can serve as the upper limit for ASASSN-14dc as the ejecta-CSM interaction could happen even earlier. For SN 2005gj, Prieto et al. (2007) estimated that the ejecta-CSM interaction takes place only 3 days after the explosion. Then the delay time between the mass loss from the progenitor and the SN is even smaller. For PTF 11kx, the ejecta-CSM interaction started 59 days after the explosion but the CSM wind velocity is smaller ~ 100 km/s (Dilday et al. 2012). All of these cases show that the Hydrogen-rich circumstellar material was lost only in the past decades or so before the supernova explosion. Simply from this point of view the double-degenerate model for SN Ia with two CO white dwarfs spiraling-in through gravitational wave losses can be ruled out as it cannot account for the H and the time gap between the merger and progenitor mass loss is too long ($\sim 10^9$ yrs) compared to the calculation I just showed.

The estimated of CSM mass is somewhat uncertain depending on methods, assumptions on the CSM geometry (which is highly uncertain) etc., however, for many SNe Ia-CSM the required CSM seems to be in the order of one M_{\odot} (Silverman et al. 2013a; Dilday et al. 2012; Aldering et al. 2006; Silverman et al. 2013b; Graham et al. 2017, Hamuy et al. 2003; Inserra et al. 2016). The mass loss rate required for SNe Ia-CSM ranges from $(2-120) \times$

$10^{-4} M_{\odot} \text{ yr}^{-1}$ (Silverman et al. 2013a). Considering that ASASSN-14dc has an even higher luminosity, the CSM mass required should be within the same order or higher even.

I have constructed a bolometric light curve for ASASSN-14dc. I use a python-based supernova light curve model fitting tool *TigerFit*⁸, which is based on the work in Chatzopoulos, Wheeler & Vinko (2012). Assuming that the explosion date is 30 days prior to the discovery for ASASSN-14dc and choosing the CSM density profile of r^{-2} for a steady-state wind CSM and also a constant-density CSM shell, I fit the ASASSN-14dc bolometric light curve with the semi-analytical model in Chatzopoulos, Wheeler & Vinko (2012) for the case of ejecta colliding with an optically thick CSM. A better fit is achieved for the ejecta running into a constant-density CSM shell. The Nickel mass from the fit is $\sim 0.09 M_{\odot}$ and the ejecta mass $\sim 1.32 M_{\odot}$. This is acceptable if ASASSN-14dc has a SN Ia origin. The CSM mass and mass loss rate of the progenitor system from the fit is $\sim 1.34 M_{\odot}$ and $\sim 0.017 M_{\odot}/\text{yr}$, respectively. This is consistent with others' estimates (e.g. see Silverman et al. 2013a; In-serra et al., 2016). Note that, the fit has assumed spherical symmetry and this holds true for a lot of the estimates made by others.

So we need a mass loss rate $\sim 10^{-2} M_{\odot} \text{ yr}^{-1}$ or higher from the progenitor system with $\sim 1 M_{\odot}$ material lost from the progenitor system only decades before the supernova explosion. Also, the material would be traveling in a velocity of several hundreds km/s.

There is this SN 1.5 (Iben & Renzini 1983) model, in which the thermonuclear explosion is caused by the Chandrasekhar-mass Carbon-Oxygen core of a single massive AGB star. This naturally explain the H-rich CSM and is favored by Hamuy et al. (2003) and Chugai et al. (2004) for SN 2002ic and acknowledged in Prieto et al. (2007). The model is not favored for PTF 11kx as there is a 59 day delay between the ejecta-CSM interaction and the supernova explosion (Dilday et al. 2012). However, for ASASSN-14dc, I only have spectra 3 days after the discovery, so I cannot judge this model based on this point. Chugai et al. (2004) raised the question that for a AGB star to form a Chandrasekhar-mass Carbon-Oxygen core,

⁸<https://github.com/manolis07gr/TigerFit>

the radiatively driven winds from the AGB have to be weak enough. This implies a very low-metallicity environment and has been suggested by Zijlstra (2004). Chugai et al. (2004) further made an interesting point that if all SNe Ia-CSM are from this SN 1.5 model which might only work in low-metallicity host galaxies, more SNe Ia-CSM should be seen when we can reach $z \sim 2-3$ or higher. There is little we know about the host galaxy of ASASSN-14dc. This remains a future work. However, to account for the CSM mass ($\sim 1M_{\odot}$) required for SNe Ia-CSM, a complete loss of the envelope via some ‘super-wind’ before the mass of the core reaches to the Chandrasekhar mass is necessary and this is not understood well. Moreover, there is no information regard to the ejected material velocity.

It seems that the single-degenerate model for SN Ia might provide an answer for us. However, can any of the classic SD model work? Dilday et al. (2012) has proposed that a recurrent-nova progenitor system should account for the slow 100 km/s mass outflow and multiple shells of CSM they found for PTF 11kx. They however estimated that the CSM mass is $\sim 5.36 M_{\odot}$ times a covering factor K in the case that CSM is not distributed spherically symmetrically or is clumpy. But still, this is too high for recurrent-nova system with mass loss rate of $\sim 10^{-7}M_{\odot}/\text{yr}$ (Patat, et al. 2011). A later reanalysis by Graham et al. (2017) estimate the total CSM mass for PTF 11kx is $0.06 M_{\odot}$. But this is still much higher than the $2 \times 10^{-6} M_{\odot}$ Moore & Bildsten et al (2012) produced from a model in which recurrent-nova eruptions periodically eject material and sweep up Red Giant wind.

Han & Podsiadlowski (2006) showed that with a relatively massive ($\sim 3 M_{\odot}$) donor star (main-sequence or slightly evolved), the system will experience a delayed dynamical instability which causes a large mass loss rate ($10^{-4} M_{\odot}/\text{yr}$) in the last few 10^4 years before the SN explosion in order to explain the large amount of CSM observed in SNe Ia-CSM. They treat this as part of the ‘super-soft model’. However, there is no information about the velocity of material being ejected and the authors were not sure what would really happen at the last stage of the mass transfer.

So we know of no SD model that can expel $\sim 1M_{\odot}$ material at ~ 100 km/s only decades

before the supernova explosion. However, Soker et al., (2013) lay out a possible solution. A merger happens between a white dwarf and the still hot, degenerate core of an Asymptotic Giant Branch star at the termination of the common envelope (CE) phase and this is labeled as the ‘core-degenerate’ (CD) model. To be specific, Soker et al., (2013a) lists the evolutionary route for this to happen. A total mass of the WD and the degenerate core being super-Chandrasekhar and even large than 2 solar mass is required. The ratio between the envelope and the WD should be larger than 3 (Soker 2013b). To avoid the delay between the termination of the CE phase and the supernova explosion, the degenerate core of the AGB star should be less dense than the WD so that the core would accrete onto the WD to have a prompt merger. And neither the mass of the WD nor the degenerate core should exceed $1.1 M_{\odot}$, so that the production of ONe WD is avoided (Kashi & Soker 2011). They show that this is a version of the ‘core-degenerate’ (CD) model. So from this model, CSM originated from the complete common envelope ejection with a speed of several hundreds km/s. It can produce the ~ 1 solar mass of CSM required for SNe Ia-CSM and since this merger happens right-after or shortly after the common envelope ejection, in particular, the small time gap between the ejecta-CSM interaction observed in PTF 11kx can be accounted for. So it looks like this would be the most-likely progenitor system for ASASSN-14dc and possibly for other SNe Ia-CSM as well.

3.4 Summary

I have presented the large photometric and spectroscopic follow-up for ASASSN-14dc and showed that it resembles a luminous Type Ia supernova exploding inside of a solar mass dense hydrogen-rich CSM traveling at 300 km/s and extending out to 10^{16} cm. Ejecta-CSM interaction likely powers its slowly declining light curve and super-luminous nature. ASASSN-14dc joins SN 2005gj, PTF 11kx etc. as one of the very rare kind Ia-CSM event. The critical issue for these objects is the nature of their progenitor system.

The merger between a CO white dwarf and another CO white dwarf (DD model) as the

SNIa progenitor system cannot explain the presence of hydrogen-rich CSM surrounding the supernova. This immediately points to the SD model. However, it not possible for any kind of companion star in the SD model to eject $1M_{\odot}$ hydrogen-rich material at several hundreds km/s all within the last decades before the supernova explosion, as I showed for ASASSN-14dc and other SNe Ia-CSM. So both classic SD and DD models fail to produce objects like these.

Fortunately, a version of the ‘core-degenerate’ model (merger of a WD and the still hot degenerate core of a AGB star) fills all the requirements. A solar mass of CSM originates from the ejection of the common envelope with the prompt violent merger following right after the CE ejection to create the thermonuclear runaway supernova explosion. So for ASASSN-14dc and other SNe Ia-CSM, the ‘core-degenerate’ model seems to be the only suitable model to explain all the observed features. So for SNe Ia-CSM, a rare kind of SNe only comprising 0.1-1% of all SNIa might have companion of a still hot degenerate CO core of a AGB star.

4. Ex-companion of a Core-Collapse Supernova’s Progenitor?

4.1 Is Muzzio 10 the Ex-companion Star of the PSR B1509-58’s Progenitor?

SNR G320.4-01.2 (MSH 15-52, RCW 89) is a SNR in the constellation Circinus with a radius of 17', and a distance of 3.8-6.6 kpc by HI absorption (Caswell et al. 1975; Kerr et al. 1986). Gaensler et al. (1999) further argued that the whole x-ray and radio region of SNR G320.4-01.2 is a single SNR with distance of 5.2 ± 1.4 kpc.

At the center of the SNR is one of the youngest, most energetic pulsars, PSR B1509-58 (PSR J1513-5908, 2E 1509.9-5856). The pulse period is 150 ms, while the spin-down age (nearly $P/2\dot{P}$) is 1700 years, the spin-down luminosity is 1.8×10^{37} erg/s and the inferred dipole surface magnetic field is 1.5×10^{13} G (Kaspi et al. 1994; Livingstone et al. 2005). This fast pulsar is visible brightly in the X-ray and radio. The pulsar has not been seen in the optical, with a $V=22.4$ foreground star on top of the pulsar position, although a ‘polarization excess’ inside the PSF of the foreground star suggests that the pulsar is there with $R=25.7$ mag (Wagner & Seifert 2000). PSR B1509-58 itself is too weak to show H I absorption, hence no distance can be inferred from it. However, dispersion measurements using five other nearby (within 20 degrees radius) pulsars yields a distance range of 4.2-8.4 kpc. An $H\alpha$ emission nebula RCW 89 sits in the SNR region as well. It coincides with the brightest radio portion of SNR G320.4-01.2 and one of the two x-ray nebulae in the SNR region. A bridge of non-thermal emission was found to be connecting what appears to be the pulsar jet and the thermal emission of RCW 89 (Tamura et al. 1996). The energy content from X-ray spectral analysis is consistent with the scenario that the nebula is powered by the pulsar jet. Using Chandra, Yatsu et al. (2005) examined temperatures and ionization parameters of bright emitting knots in RCW 89 aligned in a ‘horseshoe’ shape and found that they increase and decrease respectively in the clockwise direction. This suggests a picture of

energy transfer via pulsar jet precession. More importantly, they confirmed that energy from the pulsar rotation loss is sufficient to heat the nebula with a heating timescale of 1400 yr, which is consistent with pulsar’s spin-down age of 1700 yr. These results provide evidence that PSR B1509-58 is interacting with the SNR, hence they should be at the same distance. The expansion age of the X-ray filaments is ~ 1800 yr, which further confirms that RCW 89 is the SN ejecta of the progenitor of PSR B1509-58 (Yatsu et al. 2006).

Just 18.1” north of the pulsar (see Figure 4.1), there is a massive O4.5III(fp) star called ‘Muzzio 10’. This is a bright hot star at $V=11.63$ ($B-V=0.58$), and has been detected previously in *Chandra* ACIS-I images. We have taken a good-quality high-resolution spectrum ($R=28,000$, $S/N=50$, $4500-9000\text{\AA}$) with the help of Frederick Walter on the CTIO 1.5m telescope, where the velocities of sodium D absorption are the same as for the HI absorption of the SNR, yielding a distance between 3.8-6.6 kpc. I also found that the rotational velocity of Muzzio 10 is high at ~ 400 km/s from my spectrum. This puts the FWHM of any line from the star to about 12\AA including critical lines from europium and samarium, which must have small equivalent widths. This means rotational broadening would basically kill the idea of looking for r-processed elements on such star. This star is a likely member of the Cir OB1 association, with a distance of ~ 4.6 kpc (Lortet et al. 1987). The UCAC4 combined catalog has a measured proper motion (μ) of 5.9 ± 3.1 mas/year with the star coming from the northeast. At a distance of 4.5 kpc, the transverse velocity is 130 km/s. This means that Muzzio 10 is a runaway star, and one of the fastest ones.

Various groups have recognized the possibility of a connection between Muzzio 10 and the pulsar, always just briefly stated, but no one has published any tests or predictions (e.g. Arendt 1991; Gaensler et al. 1999; Koo et al. 2011). The probability is low for finding a fast runaway O star within 18.1” of a young pulsar in the middle of a SNR, unless they are causally connected. The obvious idea is that a SN blast around 1700 years ago created the RCW 89 expanding shell, the resultant neutron star is zipping away and now seen as PSR B1509-58, while the companion of the exploding star became unbound and flew away from

the explosion site at its prior orbital speed and is now seen as Muzzio 10.

Just $\sim 12''$ to the northeast of Muzzio 10 (and $\sim 27''$ north of the pulsar), there is a unique mid-infrared source (IRAS 15099-5856) that is extended (Koo et al. 2011). This IRAS source is consistent with models of thermal emission from dust and shows prominent crystalline silicate emission that can be seen in the spectrum. The heating mechanism was initially suspected to be the synchrotron radiation of the pulsar wind nebula. However, the required optical luminosity of the pulsar to achieve the IR luminosity measured for the infrared source cannot be met (Koo et al. 2011). A collisionally heated dust model was also proposed for explaining the thermal IR radiation, although the drawback of this model is that there is no direct evidence of thermal X-ray emission (Arendt 1991). The origin of the crystalline silicates is suggested to be from the mass outflow from the progenitor of the supernova remnant. This means that the IR cloud was there even before the supernova event. The link between Muzzio 10 and the progenitor of the SNR was established as such an IR cloud could survive the supernova blast wave if it is in a close binary system. Thus the IR emission could be a result of the heating from hot Muzzio 10 (Koo et al. 2011). It also happens that the relatively poor UCAC4 proper motion places Muzzio 10 just close to the position of the peak of the infrared source for a time 1700 years ago. This further strengthens the idea of the likely association between the pulsar and Muzzio 10. Another obvious idea would be that this cloud was made from low-velocity or fallback material from the original SN, with both the pulsar and the ex-companion star flying out of the cloud and leaving it behind. With the hope of finding r-processed elements in the atmosphere of Muzzio 10 gone due to the high rotational velocity, the IR cloud could well be a perfect place for looking for r-processed elements as it has low or zero rotation and should be contaminated by the supernova event.

The case for Muzzio 10 being a long-sought ex-companion of a CCSN is good. *The most likely way to get proof is to measure accurate proper motions for the pulsar and Muzzio 10 and show them to be consistent with the same location around 1700 years ago.* Only with such

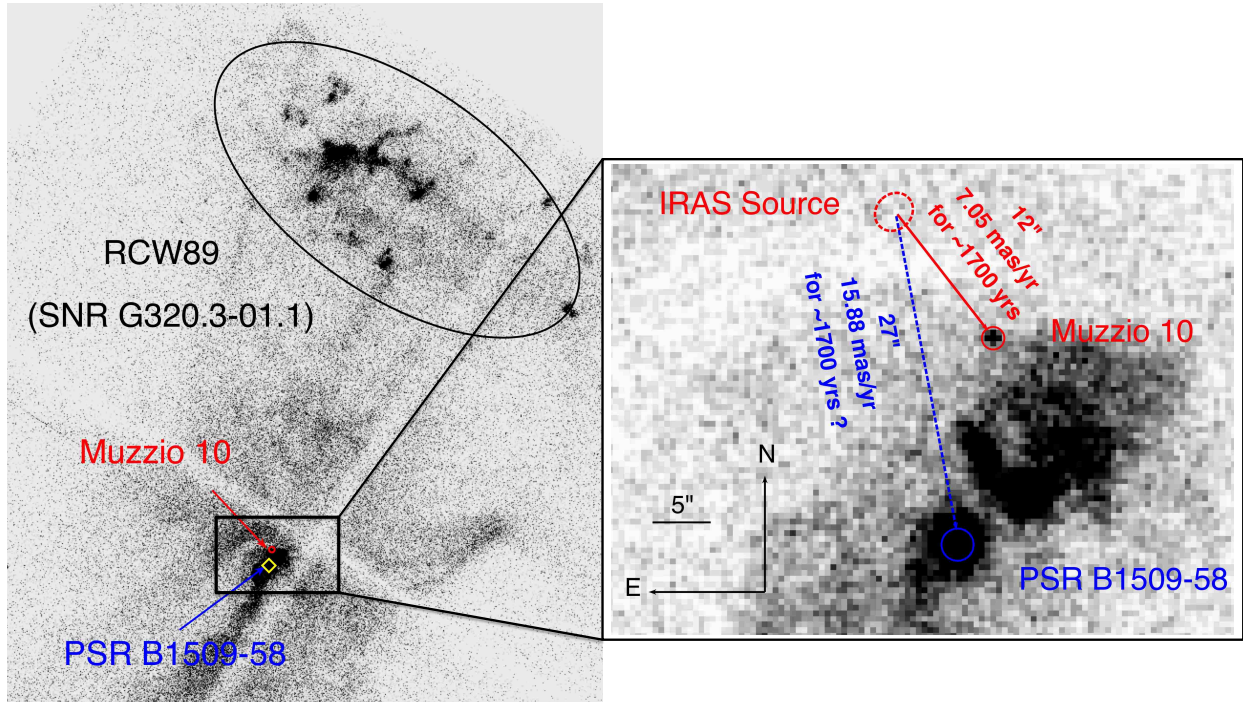


Figure 4.1: This shows about half of the *Chandra* ACIS-I image of the field of the pulsar in the year 2005 with 45.5 ksec of exposure. To the north of both Muzzio 10 and the pulsar is the shell of the supernova remnant as indicated in the black ellipse. The blow-up box on the right shows the relative relations of the pulsar, Muzzio 10, and the IRAS source. So here we have a massive O star within 18.1'' of a pulsar in the center of the SNR. Interstellar absorption proves that both RCW 89 and Muzzio 10 are at similar distances from Earth. Muzzio 10 has a poorly-known proper motion from UCAC4 that points to it being coincident with the IRAS source at a time ~ 2000 years ago (if the SN event happened ~ 2000 yrs ago, Muzzio 10 would need a proper motion of ~ 7 mas/yr to travel to the current location as shown in the figure), and so the peak of the infrared dust cloud might be the site of the SN explosion. The proper motion of Muzzio 10 gives a transverse velocity of 130 km/s, which is to say that it is one of the faster runaway stars, just as expected for an ex-companion star of a SN explosion. *If* the proper motions of the pulsar and Muzzio 10, extrapolated back 1700 years, place them both at a coincident position (likely near the IRAS source), then I have proof that Muzzio 10 is the ex-companion of a CCSN.

a proof can Muzzio 10 or the infrared source be used for the several astrophysics questions.

Here I will present my result from measuring the proper motion of Muzzio 10 using the Fine Guidance Sensor (FGS) on the *HST* with a one-year baseline and proper motion of PSR B1509-58 using the *Chandra* images with a 16-year baseline.

4.2 Observations and Data Analysis

4.2.1 *HST* Observations and Data Reduction

Muzzio 10 has a relatively poor proper motion from the UCAC4 catalog, $\mu=5.9\pm 3.1$ mas/year, with a $\sim 50\%$ uncertainty. I know of no archival plates or old positions that can improve this measure, or that can serve as useful first epoch images. The UCAC4 proper motion could loosely suggest the likely connection of Muzzio 10 coming from the unique IRAS infrared cloud. However, the UCAC4 is based on Tycho-2 and has some offsets with respect to the *International Celestial Reference System* (ICRS). Hence, it is not accurate enough for the purpose I am doing here. The FGS on *HST* can measure the proper motion with enough accuracy to get an arc-second position for the time 1700 years ago.

The observations were carried out under my *HST* GO proposal (14365 Cycle 23). The first epoch FGS observations were taken on 1 January 2016, with the second epoch being taken on 1 January 2017. The exactly one-year separation was intended to remove the effect of parallax (it is very small, 0.2 mas for a distance of 4.5 kpc). Selected stars in the Muzzio 10 and PSR B1509-58 field were sequentially observed in POSITION mode by FGS1r, a two-axis interferometer, in position (POS) ‘fringe-tracking’ mode with the F583W filter. Each visit had 28 exposures of 9 stars ($V < \sim 14.5$ mag). Several stars were observed multiple times so that the telescope drift, which is astrometrically significant, can be modeled and eliminated during the data reductions. Each visit was set to a specific orient angle to cover my target and reference stars. Each visit took up one whole orbit. The FGS instrument is described in Nelan (2007). Benedict et al. (2007) describes the reduction and calibration of

the data.

I received the pre-reduced (photometric, time dependent optical field angle distortion(OFAD), differential velocity aberration, and drift corrected) data directly from *HST* which provide the x, y coordinates and error bars of the each star for each visit and their position angles. This is the starting point of the analysis.

4.2.2 *Chandra* Observations and Data Reduction

PSR B1509-58 has its old radio position given with a 1.0" error radius. The best constraint is $\mu < 52$ mas/year in the north/south direction and there has been no improvement in recent years (Gaensler & Kaspi 2015, private communication). In the X-rays, no significant proper motion was detected with *Chandra* images with just a 5-year baseline (2000 to 2005). The pulsar has not been seen in optical light, and *HST* has never looked at the field. With these limits, 1700 years ago, the pulsar could have been anywhere within 1.5 arc-minutes of the center of the SNR, and this is useless to demonstrate a positional coincidence with Muzzio 10.

Fortunately, *Chandra* already has a number of Advanced CCD Imaging Spectrometer (ACIS)-I images from 2000 and 2005, and these can serve as the first epoch images. So the only way to get the proper motion of the pulsar will be taking a new set of ACIS-I images now so that I can have a 16-year baseline to measure the pulsar's proper motion. My *Chandra* proposal (GO 17500589 Cycle 17) requested 20k seconds of exposure time just like the observation made in 2000. All the other parameters are set to be identical to the previous observations, except the roll angle of the field of view (FOV). But the rotation of the field will be taken care of in the astrometry solution. In all of the images, the pulsar has been placed at or very close to the aim point to ensure the later best positional determination for the pulsar. Table 4.1 listed all the available data and the observation information from *Chandra*, including the one from my own proposal.

I retrieved event files from the *Chandra* X-Ray Center Data Archive. I followed the

Table 4.1: All the available *Chandra* ACIS-I images

Date	MJD	Obs.ID	Instrument	Exposure Time
2000 Aug. 14	51770.56	754	ACIS-I	19.03 ks
2005 Oct. 18	53661.01	6117	ACIS-I	45.5 ks
2017 Feb. 14	57786.97	18023	ACIS-I	18.3 ks

‘ACIS Data Preparation Analysis Guide’ to reprocess all the data to ensure that the latest calibration updates are applied to all the datasets. The new Level=2 Event File will be my starting point. Chandra Interactive Analysis of Observation software (CIAO version 4.9) were used for my analysis. I generated images of the field by selecting photons in the 0.3~10 keV energy range with no binning applied.

Source detection was done using the WAVDETECT package, utilizing Mexican-Hat wavelets with scales ranging from 1 to 16 pixels, spaced by a factor of 2. The default detection threshold of 10^{-6} was selected to avoid missing faint sources. A larger threshold than the inverse of the total pixels in the image could lead to the detection of strong background fluctuations as sources. However, for the absolute astrometry as I am trying to do here, I will have to cross match all the sources detected by the program with an external catalog to find out their photometric information and proper motions. Thus, mistreating background fluctuations does not matter in this case as they would not be matched with any stellar objects and they would not be used in my analysis. However, objects with low counts could be easily missed if the threshold was set too high.

There are 88, 166 and 74 sources being extracted from the 2000, 2005 and 2017 images, respectively. To do astrometry, I have to figure out how many sources are common in multiple epochs. I used the 2000 image as the reference frame and the rest will be compared to it. Adopting a maximum source separation of 2 arc-seconds, I found 32 coincidences in the 2000 and the 2005 images. The rest are either background fluctuations or knots in the supernova shell which could come and go. However, there are only 9 common sources can be matched for the 2000 and the 2017 pair. The 2000 image has an exposure time of 19 ks which is similar to my latest 2017 image with 18.3 ks of exposure. I have checked the locations of

the sources that can be seen in the 2000 image but not the 2017 images, indeed, the count rates are indistinguishable from the surrounding background. For the same sources that can be seen in both epochs, the ones in the 2017 image have an up to a factor of 2 fewer count rates for faint and off-axis sources. The brightest object, the pulsar, has a similar count rate in both images. I think this is mostly caused by the known instrumental degradation in the past nearly two decades.

4.3 Astrometry

4.3.1 Astrometric Model

Both the *HST* and the *Chandra* roll with the observations, so the position (X, Y) of the target and reference stars change with each observation set. An overlapping plate model has been utilized through my astrometry analysis. The plate model would provide scale, rotation, and offset to the later epochs for them to match the reference frame. In my case, the first FGS observation and the *Chandra* observation made in 2000 were used as the reference frame, respectively.

To perform absolute astrometry, one would need absolute proper motions of the reference stars from catalogs. Thus the astrometric model should also account for the time-dependent movements of each star, for example, the absolute parallax and the absolute proper motion. For FGS, I should also correct for instrumentally caused lateral position shifts depending on the stars' B-V color. Since I observed all the targets in one filter, there is no need to correct for the cross-filter term.

$$\epsilon = A \times (X - mx \times dt) + B \times (Y - mx \times dt) + C \quad (4.3.1)$$

$$\eta = D \times (X - my \times dt) + E \times (Y - my \times dt) + F \quad (4.3.2)$$

Where:

$$mx = -pm_{RA} \times \cos(\theta) + pm_{Dec} \times \sin(\theta) \quad (4.3.3)$$

$$my = pm_{RA} \times \sin(\theta) + pm_{Dec} \times \cos(\theta) \quad (4.3.4)$$

For Chandra, X and Y are the measured coordinates in pixels of the ACIS-I images. ϵ and η will be the measured coordinates of the reference frame, the 2000 image. mx and my are the proper motions of each star in each frame's local coordinate system, which is converted from the absolute proper motions (pm_{RA} and pm_{Dec}) extracted from the new UCAC5 catalog (Zacharias et al. 2017). θ is the angle between the local y axis and the North direction. Also, the pixel scale (0.492 arc-second/pixel) of the ACIS-I chips was used to convert the proper motion to the unit of pixel/yr. dt is the epoch difference from the reference frame. Parameters A through F control scale, rotation, and offsets.

For FGS, the coordinates (X , Y) are measured in the unit of arc-seconds. A lateral color correction (the instrumentally caused lateral position shift) has to be applied.

$$X = X' + lcx \times (B - V) \quad (4.3.5)$$

$$Y = Y' + lcy \times (B - V) \quad (4.3.6)$$

In this case, X' and Y' are the measured coordinates from the FGS in the unit of arc-seconds. lcx (-0.00109455) and lcy (-0.00109455) are the lateral color corrections¹, and $B-V$ is the $B-V$ color of each star. I extracted the $B-V$ color for all the targets in the FGS from the AAVSO Photometric All-Sky Survey (APASS). FGS observations provided the roll angle for each observation so that θ can be figured out. The same plate model described above were used for the FGS astrometry analysis with the first epoch observation (the 2016 one) set to be the reference frame.

¹private communication with Barbara McArthur

Table 4.2: Reference stars used for the FGS astrometry solution

Name	RA(J2000)	DEC(J2000)	B	V	B-V	$\sigma_{(B-V)}$	PM_{RA} (mas/yr)	PM_{Dec} (mas/yr)	$\sigma_{PM_{RA}}^2$	$\sigma_{PM_{Dec}}^2$
TYC 8706-841-1	228.378	-59.146	11.838	10.621	1.217	0.05	-15.1	-11	1	1
2MASS 15141685-5907185	228.570	-59.121	13.632	12.931	0.701	0.04	-2.2	-2.7	1	1
TYC 8706-178-1	228.312	-59.145	11.681	11.235	0.446	0.05	-2.8	-3.9	1	0.81
2MASS 15142375-5906280	228.599	-59.108	14.605	13.592	1.013	0.04	-39.1	-32.2	1.21	1.21
2MASS 15133147-5906560	228.381	-59.116	13.962	13.275	0.687	0.05	-3.6	-1	1	1
2MASS 15144285-5904252	228.678	-59.074	12.975	12.514	0.461	0.04	-1.6	-1	1	1
TYC 8706-582-1	228.528	-59.114	12.203	11.606	0.597	0.04	-1.7	-2.2	1	1
2MASS 15141317-5905357	228.554	-59.093	14.510	13.542	0.968	0.05	-4.4	0.5	1.21	1.21
2MASS 15131421-5909540	228.309	-59.165	16.272	14.396	1.876	0.06	-6.3	-6.1	1.44	1.44

4.3.2 The Proper Motion of Muzzio 10 from *HST* FGS Data

Figure 4.2 shows the FOV of the FGS 1r with Muzzio 10 sitting in the center of the field and surrounded by 9 reference stars. Table 4.2 listed their magnitudes, colors from APASS and proper motions from UCAC5.

Occasionally, bad measurements of the positions or stars in an unknown binary system or wrongly measured proper motion of the reference stars could bias the plate solution. To check for this, I applied a leave-one-out technique to see whether there is any big χ^2 drop when a star’s data are excluded during the fitting. The process was done using only the reference stars. Each time, one of the reference stars is excluded and a minimized total sum of χ^2 is computed from fitting the plate model. It turns out that when one of the reference stars, 2MASS 15144285-5904252 (number 9 in Figure 4.2), is excluded, the total sum of χ^2 dropped a lot compared to the others (from ~ 50 to 25). It could mean that the proper motion is wrong by a lot, or the positions from the FGS are bad since this star sits close to the edge of the FOV, or the star could be in an un-recognized binary system. Thus, in the following analysis, this star was left out.

To get the proper motion of Muzzio 10 and the associated error bar, I took a bootstrapping approach. In this approach, an initial minimization of the plate model (described in the previous section) including Muzzio 10 and all the reference stars except 2MASS 15144285-5904252 has been done. The fitted plate model parameters and the proper motion of Muzzio 10 have been reapplied to the plate model to calculate the residuals between the modeled

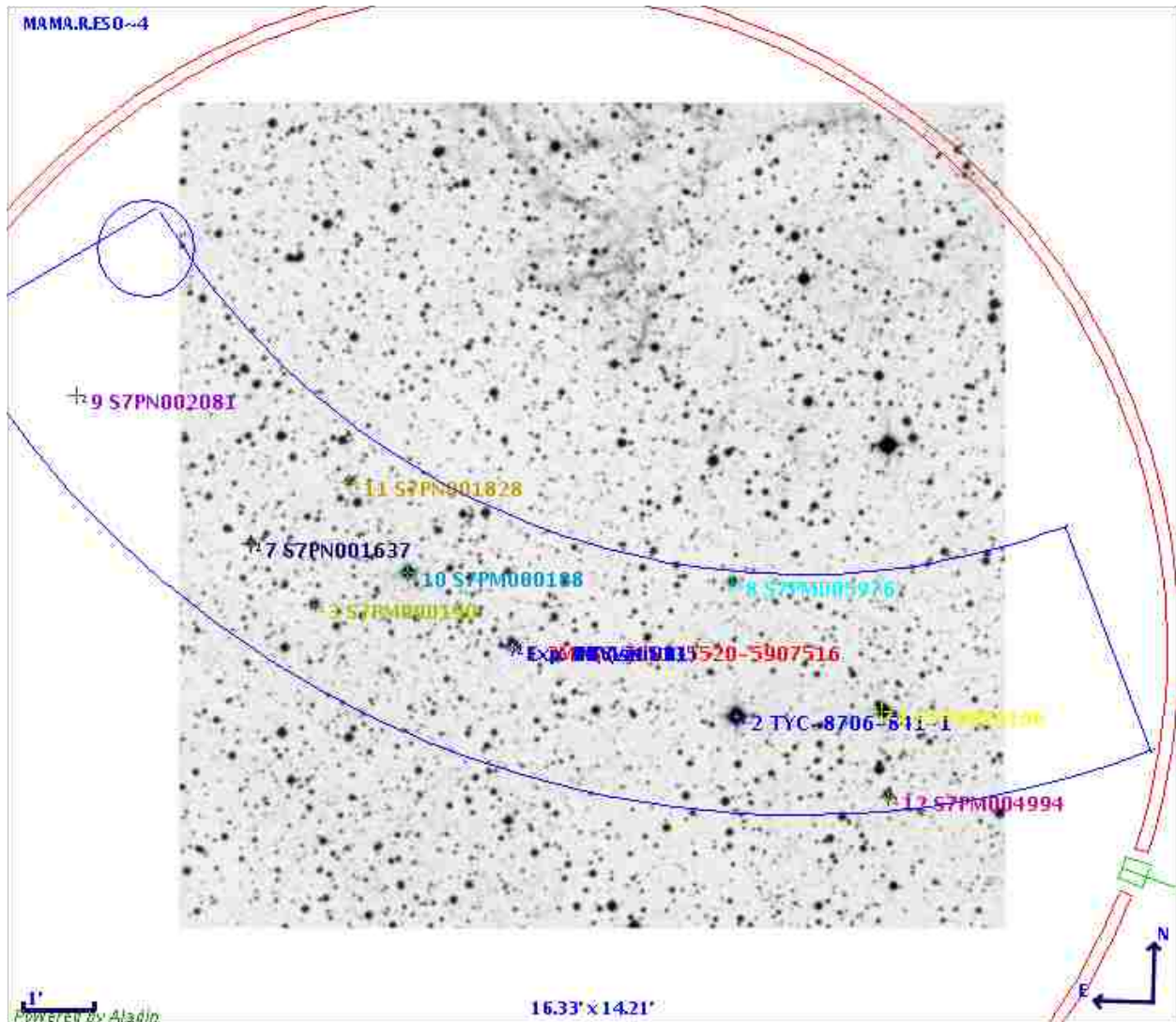


Figure 4.2: The ‘pickle’-like shape is the FOV of the FGS 1r with Muzzio 10 sitting in the center of the field (the one with an overlapped blue and orange label) and is surrounded by 9 reference stars. The image is overlaid with the Digitized Sky Survey image. All the reference stars have previously measured proper motions from the UCAC5 catalog. They are evenly distributed around Muzzio 10 to avoid a direction biased plate model constraint. Star 9 will be excluded during the astrometry analysis.

coordinates and the reference frame coordinates. I used a bootstrap method to generate N new residual samples for both X and Y directions. These new samples of bootstrapped residuals were added back to the modeled coordinates and let us call them bootstrapped coordinates. For N of 2000, I can have 2000 sets of new bootstrapped coordinates. Along with the second epoch coordinates, I ran the same minimization repeatedly for 2000 times. In Figure 4.3, I plot the distribution of the proper motion I got for Muzzio 10 from the 2000 bootstrap samples. A 1-D Gaussian distribution has been fitted to them and I am quoting the fitted centers of the distributions as my result along with the $1-\sigma$ error bar derived from it.

The proper motion of Muzzio 10 is $-3.84 \pm 0.76 * \cos(Dec)$ mas/yr in the Right Ascension (R.A.) and -2.21 ± 0.87 mas/yr in the Declination (Dec.). The size of the $1-\sigma$ error bar is comparable to what can be expected from FGS observation. Muzzio 10 has a total projected proper motion of 4.43 mas/yr coming from the northeast with an angle of 240.8 degree from north.

The newly released UCAC5 catalog happens to have the new proper motion measured for Muzzio 10 as well. UCAC5, unlike the previous release, e.g. UCAC4, is based on the new Tycho-*Gaia* astrometric solution (TGAS) and it does not suffer the large offset discovered in UCAC4. The proper motion of Muzzio 10 from UCAC5 is $-3.8 \pm 1 * \cos(Dec)$ mas/yr in the R.A. and -2.2 ± 1 mas/yr in the Dec. Note that, during my plate model fitting routine, there is no prior for Muzzio 10, only the proper motion of the reference stars are fed into the plate model. Muzzio 10's proper motion is fitted simultaneously along with the plate parameters. Thus, the UCAC5 result confirms my FGS measurement, although with a slightly worse accuracy.

4.3.3 The Proper Motion of PSR B1509-58 from *Chandra* ACIS-I Data

For the 32 coincidences in the 2000 and the 2005 images not including the pulsar, I found 15 of them have entries in the Two Micron All-Sky Survey (2MASS) catalog. The rest could

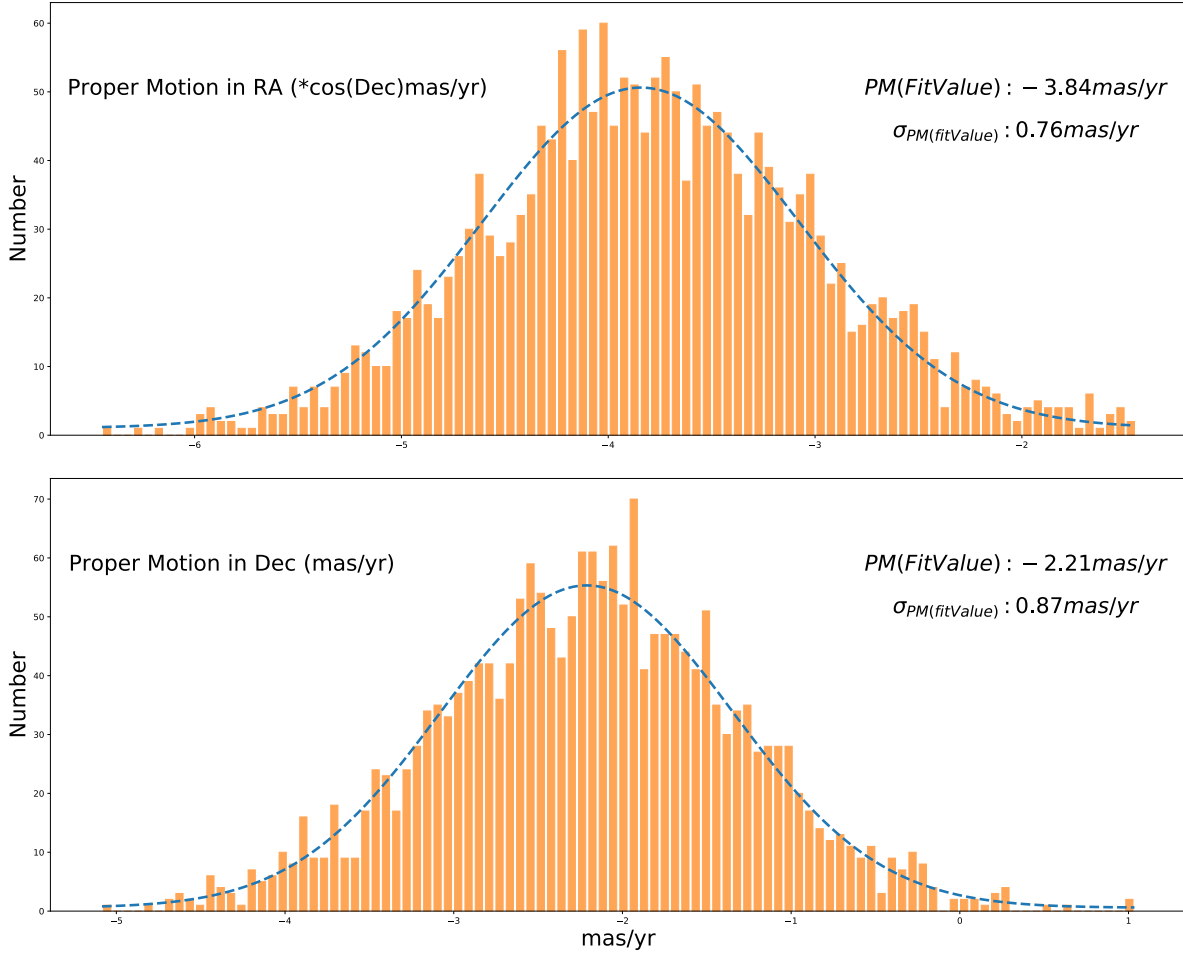


Figure 4.3: The distribution of the proper motion of Muzzio 10 in both R.A. and Dec. from 2000 bootstrap samples. A 1-D Gaussian has been fitted to the distribution. I adopt the fitted centers of the distributions as the proper motions along with the 1- σ error bars. The 1- σ error bars are comparable to what can be expected from FGS measurement.

either be knots in the supernova remnant or background fluctuation misidentified as a point source. Only 8 of the 15 sources that have a 2MASS ID and proper motion measured from UCAC5. So I have 8 reference stars to help to solve the plate model and the pulsar’s proper motion for the 2000 and 2005 epochs.

Unfortunately, for the 9 common sources (including the pulsar) found in the 2000 and the 2017 epochs, there are merely 2 sources that have proper motions from the UCAC5. 5 of them are actually knots in the SNR shell in the northern region (as recognized by being larger than point sources within the region with nebulosity). The plate model parameters A, B, D, E actually have a degeneracy among them. They can all be expressed in a function of a scale factor and a rotation angle. Along with the offsets C and F, I need at least four reference stars to even constrain the plate model. The trouble of not being able to find more reference stars has already been discussed in the data reduction section. I saw no other ways to improve on this issue. Hence, I decided to use what I got. An obvious try would be using the 5 knots in the supernova remnant. I constructed a simple expansion model in which I compute the angular distance between each knot and the pulsar and their positional angle, assuming all the knots were traveling at the same speed, hence a factor $1/T$ is needed to compute the proper motion of each knot in which T represents the ‘expansion age’ of the SNR shell in some level. I did not use any specific number for T, and it is fitted simultaneously along with the plate parameters and the pulsar’s proper motion. Also, a 10% $1-\sigma$ error has been assigned to the knot’s proper motion. This is probably the best I can do. 5 knots plus the two sources with UCAC5 entries were used to solving the plate model and the pulsar’s proper motion for the 2000 and 2017 epochs pair.

Table 4.3 listed all the reference sources that are used to constrain the plate models for *Chandra* observation. Figure 4.4 compares the common sources detected for different epochs.

Following the similar leave-one-out test, I found no significant χ^2 drop. The same plate model and bootstrap routine for the reference vs the 2005 epoch and the reference versus the 2017 epoch were used. However, I could not constrain the plate model well in either

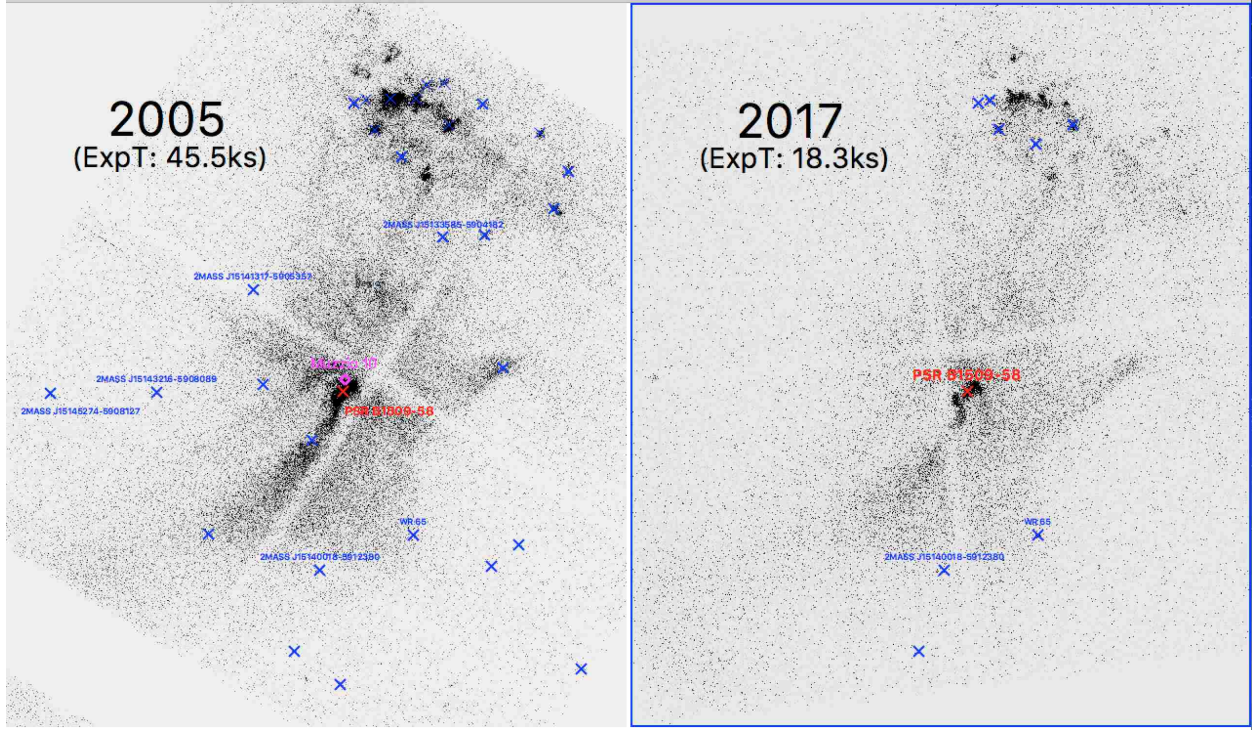


Figure 4.4: Left: The common sources found in both the 2005 and 2000 images marked with the ‘X’. All the sources have been cross-matched with the 2MASS and the UCAC5 catalog. Only 8 sources have proper motions from the UCAC5 excluding the pulsar. They are all marked with their 2MASS ID or name. Right: The same as the left. However, only 9 common sources can be matched between the 2000 and the 2017 image. Only two of them have UCAC 5 proper motion. See the text for detail.

Table 4.3: Reference stars used for the *Chandra* astrometry solution

Name	RA(J2000)	DEC(J2000)	PM_{RA} (mas/yr)	$\sigma_{PM_{RA}}^2$ (mas/yr)	PM_{Dec}	$\sigma_{PM_{Dec}}^2$
WR65	228.4237542	-59.19581716	-4.2	1	-3.6	1
Muzzio10	228.4802546	-59.13105315	-3.84	0.76	-2.21	0.87
2MASS 15140018-5912380	228.5002691	-59.21056329	-4.3	1	-2.3	1
2MASS 15143216-5908089	228.6334649	-59.13615902	5.3	4.3	4.6	4.3
2MASS 15133585-5904182	228.3999498	-59.07156297	-9.3	11.8	1.7	11
2MASS 15141317-5905357	228.5544324	-59.09341532	-4.4	1.1	0.5	1.1
2MASS 15145274-5908127	228.7196672	-59.13661602	-6.7	3.9	-0.9	4
2MASS 15151922-5910125	228.8287708	-59.1705189	-10.2	6.8	19.8	4.4

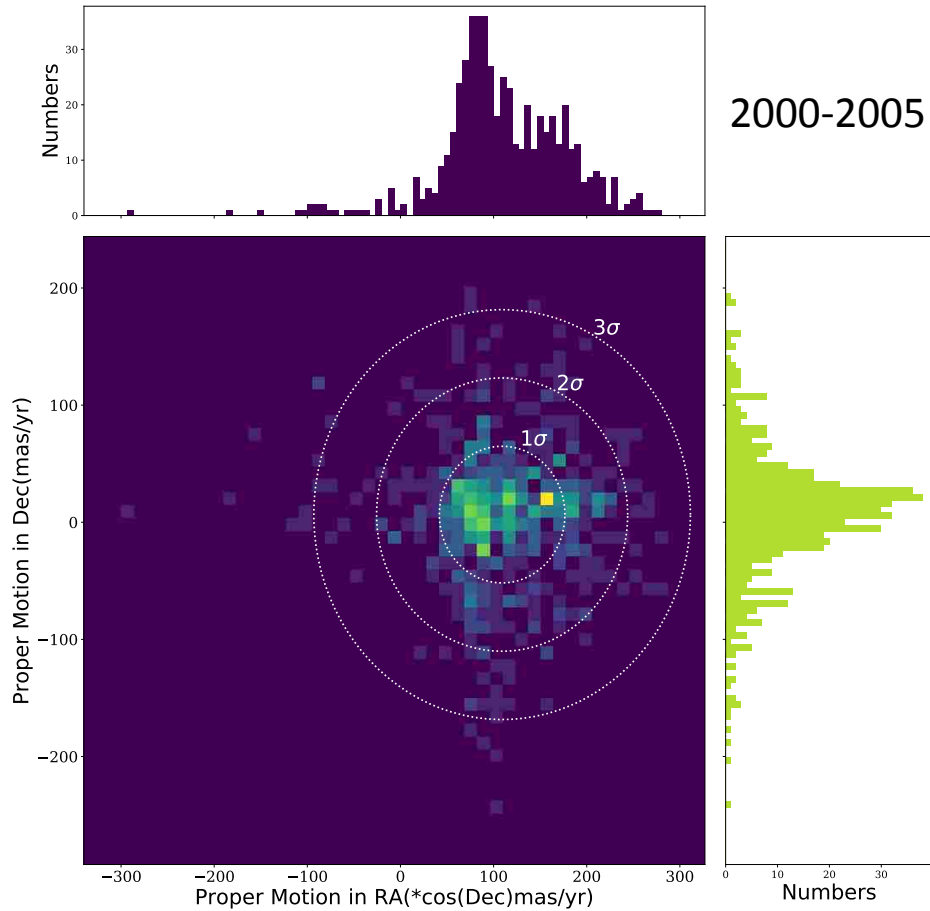


Figure 4.5: The distribution of the pulsar proper motion derived from the plate model and using the bootstrap method using the 2005 and 2000 epochs. The 1σ error on the pulsar proper motion is ~ 50 mas/yr. This kills the hope of pointing out the place where the pulsar could come from. Hence, I cannot make the claim that Muzzio 10 and the pulsar came from the same location. See the text for detail.

pair. Figure 4.5 and Figure 4.6 show the distribution of the pulsar's proper motions from the bootstrap methods along with the error circles. The $1\text{-}\sigma$ error radius is as high as approximately 50 mas/yr in both cases. This means I have nothing useful to constrain the pulsar proper motion. Remember, the distance between the pulsar and the peak of the IR source is about 27 arc-seconds. If I extrapolate the pulsar's location 1700 years ago, the $1\text{-}\sigma$ error radius of the position would be as large as 1.4 arc-minutes. This is useless to determine whether Muzzio 10 and the pulsar would intercept back 1700 years ago.

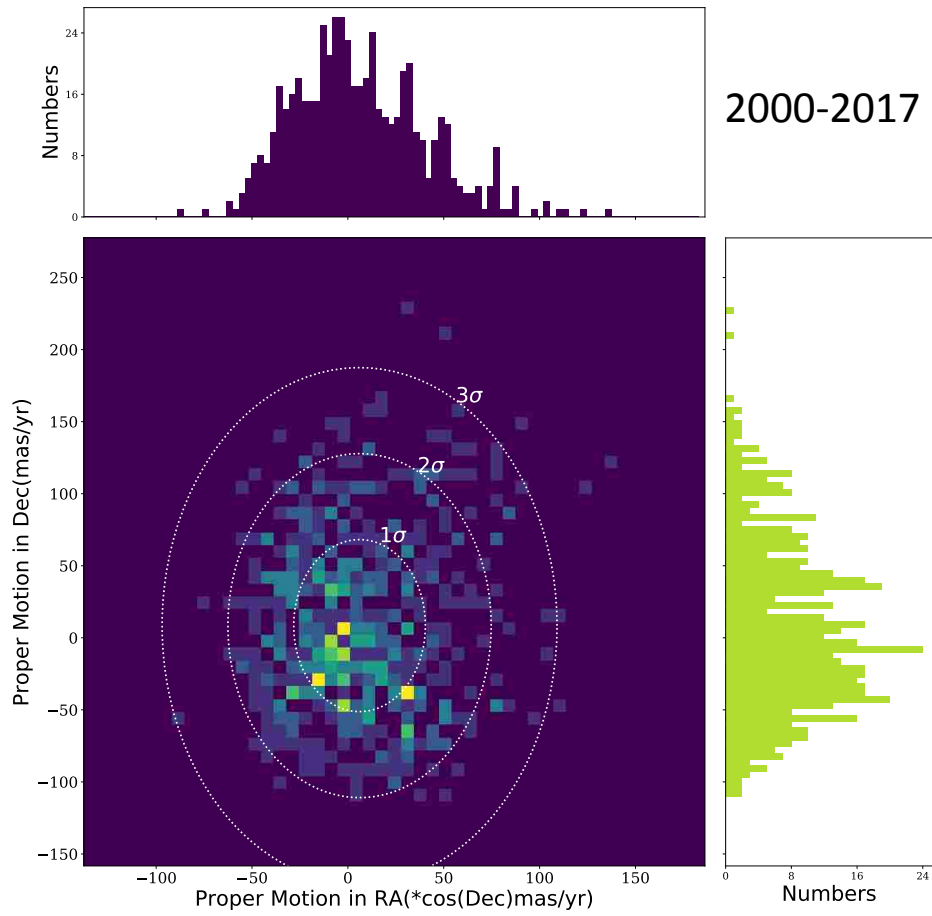


Figure 4.6: The same as the Figure 4.5, but from the 2017-2000 epoch pair. The 1σ error on the pulsar proper motion is ~ 50 mas/yr as well.

4.4 Conclusion and Discussion

I measure the proper motion of Muzzio 10 with the FGS on *HST* to better than one mas/yr accuracy. Muzzio 10 has a proper motion of $-3.84 \pm 0.76 * \cos(Dec)$ mas/yr in Right Ascension and -2.21 ± 0.87 mas/yr in Declination. For a distance of 4.6 kpc, Muzzio 10 would have a transverse velocity of ~ 94.6 km/s. Muzzio 10 remains a runaway star. If I adopt an age of 1700 years, the location of Muzzio 10 1700 years ago would be the first solid circle in Figure 4.7. However, the ‘expansion age’ I got from my fit to the expanding X-ray filaments is around 2900 years. With this age, the peak of the IR source would sit about $2\text{-}\sigma$ away from the position of Muzzio 10 about 2900 years ago. Then I can still casually connect the IR source and Muzzio 10. Unfortunately, I could not provide a tight constraint on the pulsar’s proper motion. The $1\text{-}\sigma$ error radius of the pulsar position 1700 years ago is as large as 1.4 arc-minutes, compared to the distance between the IR source and the pulsar is about 27 arc-seconds.

I think the problem is two fold, firstly, the poor position determination of the reference stars and secondly the lack of reference stars in my latest (2017) *Chandra* image. Two factors can affect the uncertainty of the sources’ positions: the source signal-to-noise ratio and the separation between the source and the on-chip aimpoint as the point-spread function (PSF) degradation is a function of the off-axis angle. Larger off-axis angle would have worse PSF, hence, larger positional error. My primary target, the bright pulsar is located at or close to the aimpoint in all three epochs and its positions can be determined with $1\ \sigma$ error of ~ 0.03 pixels (~ 0.015 arc-seconds) per coordinate in both the 2000 and the 2017 epochs. A slightly better $1\ \sigma$ error of ~ 0.02 pixels per coordinate can be achieved in the 2005 image, which has a longer exposure time (45.5 ks). With the pixel scale of the ACIS-I chips 0.492 arc-second/pixel, this means I can measure the pulsar’s position to an accuracy of 10-15 mas. However, the position of a typical faint source located several arc-minutes off-axis can have an average of order 0.5 pixels (~ 0.25 arc-seconds) per coordinate. For 2000 and 2017 images with less exposure time, the positional error for faint, large off-axis angle sources can be a

factor of 2 more larger when compared to the 2005 epoch. Astrometry depends largely on how accurately you can determine the references' positions as they are the key to constrain the plate model.

The 2005 and 2000 images have 'adequate' reference stars, but the $1\text{-}\sigma$ error of the pulsar proper motion is still very large. I expected the pulsar to have a proper motion ~ 15 mas/yr. For a baseline of 5 years, the pulsar would have traveled ~ 75 mas in total. However, the residual between the modeled coordinates and the reference are \sim several hundred milli-arcseconds in both directions. So the fact that I do not have accurate reference star positions resulted in the poor constraint on the plate model and the offset I want to measure is too small compared to the residuals.

The major problem with the 2000 and 2017 pair is probably due to the lack of enough reference stars. What if I had the 2017 image with a 45.5 ks exposure time just as the 2005 images instead of the 18.3 ks I got? This means that I can have enough reference stars and long enough baseline to have the pulsar moved a comparable angular distance to the average residual. I simply copied the data from the 2005 image and retained the coordinates of all the reference star but add a small perturbation to them according to their error bars. So that I am creating a simulated second epoch data with the same amount of reference stars as the 2005 image. I make the proper motion of these reference star to be zero but kept their error bar on the proper motion. Still using a 16 years baseline, I re-run the routine using the 2005 image as the reference image and the simulated data as the second epoch. This would be a test to see what if I have enough reference stars and what kind of error bar I can get for the proper motion. The result is that I can get an error bar of 5 mas/yr in both directions. Now this would be acceptable and adequate to make a claim of pulsar's position ~ 2000 years ago. It seems like that if I asked for a 45ks image, I might be able to get the answer. However, the produced proper motion is about 5 mas/yr away from zero which a value of zero in both directions should be expected from this simulated data. I am still thinking about the reason behind it and maybe the method is underestimating the error.

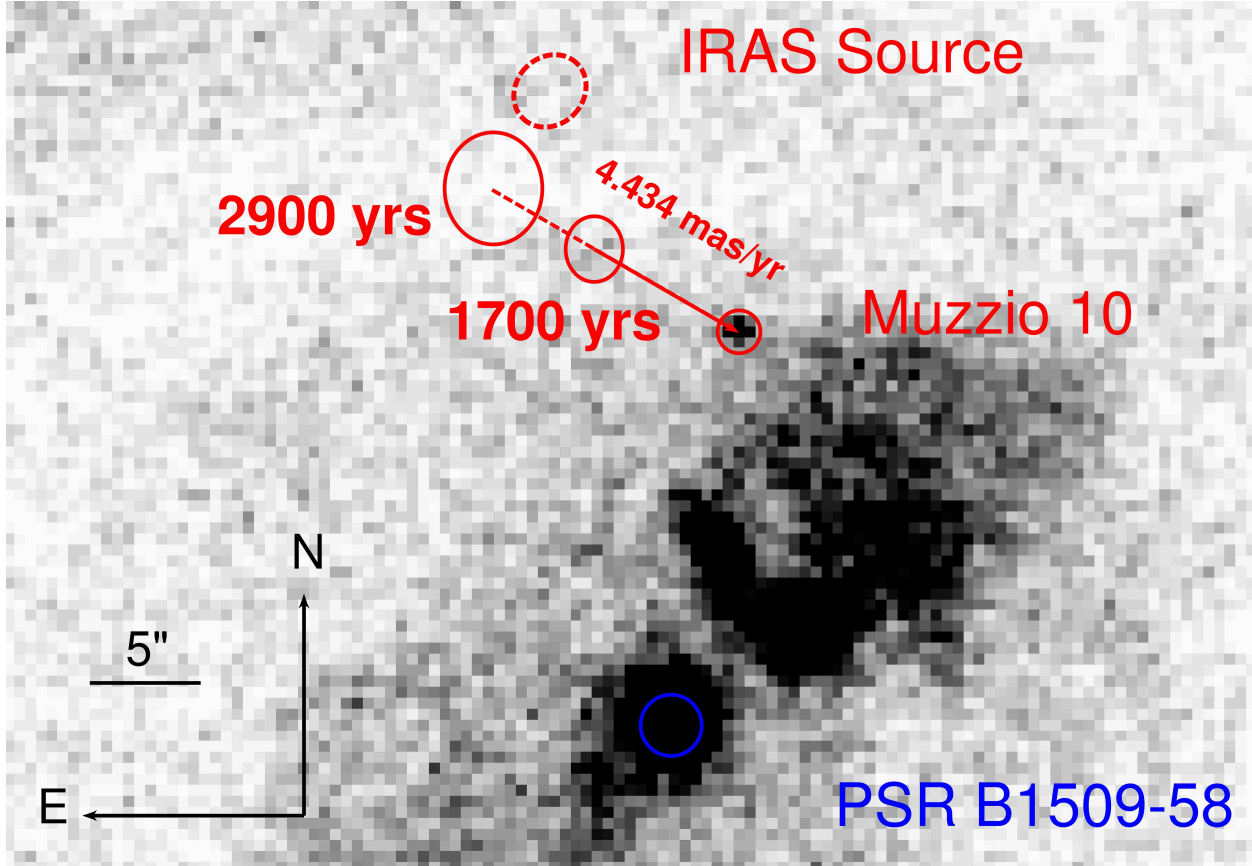


Figure 4.7: The proper motion of Muzzio 10 can be measured to a sub-milli-arcsecond level. It has a proper motion of $-3.84 \pm 0.76 * \cos(Dec)$ mas/yr in the R.A and -2.21 ± 0.87 mas/yr in the Dec. The transverse velocity of Muzzio 10 is ~ 94.6 km/s for a distance of 4.5 kpc. The two red solid circles indicate the $1-\sigma$ positional error region of Muzzio 10 if traced back to certain years ago. Unfortunately, I cannot make similar prediction for the pulsar, thus I can not claim Muzzio 10 is the ex-companion of the progenitor of PSR B1509-58. See the text for detail.

Next step, I will create a simulated data with known proper motion for the pulsar instead of using zero and see whether I can recover it with a reasonable error bar.

Muzzio 10 has a fast rotational velocity (~ 400 km/s). The similar case VFTS102 discovered in Dufton et al. (2011) is suggested to be spun-up due to the binary nature. Muzzio 10 is also a runaway star. The chance of having a massive, fast-rotating runaway O-star randomly next to a young pulsar is very low. Although I was not be able to constrain the proper motion of the pulsar tightly and make a decisive conclusion about the implied connection, the case should be looked into again with, for example, *Chandra* data with longer

baseline and longer exposure time might be able to perform the astrometry with required accuracy for this task. Also, I could try to apply for HST to try to get the optical counterpart of the pulsar and if I can find it, I could come back re-image the field five years later to do the astrometry.

5. Discussion and Conclusions

The goal of my thesis project was trying to investigate the progenitor systems of thermonuclear supernovae and core-collapse supernovae through the eyes of their ex-companions or SNe themselves. I have approached the problems from multiple angles.

To explore the progenitor system of thermonuclear supernovae (Type Ia supernovae), I first investigated the famous Tycho supernova remnant. Since 2004, Tycho star G has been considered as the most popular ex-companion candidate for the progenitor of Tycho's SN. If star G is the ex-companion, then a single-degenerate model would be required and the nature of the ex-companion star (a G type subgiant) would strongly point to a recurrent-nova progenitor (like U Sco). The companion star would survive the supernova explosion and then be found inside of the supernova remnant. While, if a SNIa explosions are produced by the double-degenerate channel, in which two carbon-oxygen white dwarfs with total mass higher than the Chandrasekhar mass would merge and have a thermonuclear runaway explosion, there would be no companion star left inside the supernova remnant as the two white dwarfs were destroyed during the supernova explosion. This is the reason behind the whole Tycho star G question, because it can distinguish between SD and DD models of SN Ia. However, people have overlooked one critical question of what is the position in the sky of the original supernova explosion. The original paper (Ruiz-Lapuente et al. 2004) that claimed star G as the ex-companion star was based on a search region centered on the geometric center of the supernova remnant. The position of the geometric center is not what is relevant for knowing the explosion position of the supernova, because there will inevitably be some offset between the two positions. To see this, we can imagine an idealized case where the SNR is expanding into the ISM with a density gradient, so that one side is running into a higher gas/dust density than the other side. The expansion towards the high density side will be slowed, while the expansion away from it will be relatively fast. The SNR shape as seen from the side will have its geometric center at the point halfway from the slow edge and its fast edge. In this case, the geometric center will be offset significantly from the explosion center

in the direction away from the dense side. So only looking for an ex-companion around the geometric center is not quite right in most cases. This is true for Tycho's SNR as it is out of round and has different densities around the rim of the remnant (Williams et al. 2013). This is the indication that Tycho's SN swept up different amount of material in different directions. This further strengthens the idea that we should look for the ex-companion star around the explosion site not at the geometric center of the remnant. I applied a one-dimensional expansion model for 19 positions around the edge of the remnant, where the swept-up material has measured densities, and I determined the center of expansion with a chi-square fit to the 19 measured radii and velocities. I found that the explosion site is far away from the geometric center and mostly outside the region previously searched for ex-companion stars. Most importantly, star G is too far away from the explosion site and is rejected to 8.2σ confidence level. Similarly, another ex-companion candidate star B is rejected at the 5.1σ level, and star E is rejected at the 4.1σ level. Hence, Tycho star G, B, E are unlikely to be the ex-companion star of the progenitor of Tycho's SN. So I have rejected Tycho star G as the ex-companion star, and this had previously been a strong argument for the SD scenario (Xue & Schaefer 2015).

Another approach I took to probe the progenitor system of SN Ia is through a rare kind of supernova, SN Ia-CSM. They were originally classified as type IIn supernovae but later studies showed them have a SNIa origin. Several candidates (SN 1997cy: Germany et al. 2000; SN 2002ic: Hamuy et al. 2003; SN 2005gj: Aldering et al. 2006, Prieto et al. 2007) were discovered. They resemble each other and their spectrum showed strong narrow and intermediate components in the Hydrogen lines which is a sign of strong H-rich circumstellar material (CSM) interaction. However, the pre-peak spectra were not dominated by CSM interaction, instead it resembled the peculiar bright/broad Type Ia supernova like SN 1991T and SN 1999aa. Although a core-collapse origin has been suggested by some people (Benetti et al. 2006; Trundle et al. 2008), the discovery of PTF 11kx confirmed that the central explosion is a SNIa event. About a dozen these kind of objects were found in the last two

decades, although most of them were classified as SN IIn initially (Silverman et al. 2013a). The sample gathered in Silverman et al. (2013a) is largely selected based on the similarity in the spectral features. SNe Ia-CSM often have slow-declining light curves, peaking at absolute magnitudes brighter than about -19 mag. Their spectra can be interpreted as strong multi-component Hydrogen lines (the cause of all the SN IIn classifications initially) superimposed on CSM interaction ‘diluted’ Type Ia spectra. I have gathered photometric and spectroscopic data for ASASSN-14dc, a supernova discovered by the All-Sky Automated Survey for SuperNovae (ASAS-SN). It showed close similarity with those SN Ia-CSM, but it is the brightest SNe Ia-CSM ever found and its peak luminosity is in the super-luminous supernova regime. I presented the multi-band follow up and spectroscopic observation for this supernova and claimed that it is one of the SNe Ia-CSM despite the lack of pre-peak spectrum. I have showed that the CSM must be lost from the progenitor only decades prior to the supernova explosion with a typical Hydrogen-rich CSM mass for SNe Ia-CSM of order one solar mass. This challenges the traditional views of SNIa formation. The large amount of H and the fact that they are lost from the progenitor system not too long ago before the SN strongly argue against the classical double-degenerate model. This is equally challenging for single-degenerate model. Typical single-degenerate systems with a non-degenerate companion (e.g., red-giant, main sequence star) can not achieve the high mass loss rate required for SNe Ia-CSM. Typical mass loss rates of recurrent-nova systems and symbiotic systems are $\sim 10^{-7} M_{\odot}/\text{yr}$ (Patat et al. 2011). Even from a model Moore & Bildsten et al (2012) produced, in which recurrent-nova eruptions periodically eject material and sweep up Red Giant wind can only produce $2 \times 10^{-6} M_{\odot}$ in the CSM. So the single-degenerate model does not work either. A possible solution would be the so called ‘core-degenerate’ (CD) model (Soker et al., 2013, Soker et al., 2014). In this model, the merger happens between a white dwarf and the still hot, degenerate core of an Asymptotic Giant Branch star at the termination of the common envelope phase. Specifically, the core would accrete onto the cool WD to avoid the delay between the SN explosion and CE ejection. The

one solar mass or more of Hydrogen-rich CSM required by SNe Ia-CSN would originate from the complete common envelope ejection followed by the prompt merger. It is consistent with my finding that CSM should be ejected not long before the supernova explosion. It seems like the CD model is the only suitable model for ASASSN-14dc and its SNe Ia-CSN follows as neither the DD nor SD model works. More interesting questions would be, what fraction of Type Ia events can be produced by this method? Especially, can CD model produce normal SN Ia if the delay between the common envelope ejection and SN explosion is long enough to let the CSM travel far from the system?

The ex-companion star of a core-collapse supernova's progenitor is also very interesting, as such a star could provide clues to many astrophysical topics. For example, what would a massive star look like after being 'baked' by a really close core-collapse supernova explosion? Does a core-collapse SN in a binary system produce a run-away star? Is the asymmetric explosion of core-collapse SNe the cause of high velocity stars? The most exciting possibility would be looking for r-processed elements in the atmosphere of a surviving companion star after being 'baked' in a core-collapse supernova. I was lucky to find such a candidate and was able to successfully proposed to *HST* and *Chandra* to conduct my research. The candidate Muzzio 10 is a O-type star and it is also a run-away star. It sits ~ 18 arc-second to the north of PSR B1509-58 in SNR G320.4-01.2 with comparable distance. This makes it a very appealing ex-companion candidate of the progenitor of the pulsar. I proposed to *HST* to use FGS to measure the proper motion of Muzzio 10 and *Chandra* to measure the proper motion of the pulsar just to see whether they came from the same place ~ 2000 years ago. Using FGS on *HST*, I was able to measure the proper motion of Muzzio 10 accurately and it is coming from the direction I expected. Unfortunately, I was not able to constrain the proper motion of the pulsar to any useful accuracy. The main reason could be the instrumental degradation causing the significant less detections of my reference stars which are crucial to perform precise astrometry. I plan to apply for more time through *Chandra* to re-do the task or apply to *HST* to look for the pulsar's optical counterpart and measure the proper motion

of the pulsar through this way. The chance of casually having a massive run-away star close to a young pulsar is very low. I still think that they are connected.

Supernovae are extremely interesting objects and there are still plenty of questions need to be explored and solved. I plan to investigate them further if possible.

Besides the main work of my dissertation, I have worked on a project that is photometric calibration related and the result is useful for calibration programs in e.g. supernova cosmology. The study is on the variability of DA white dwarfs and I performed the study using data from the *Kepler* and K2 mission. The details of the work can be found in Appendix B.

Bibliography

- [1] Alard, C. 2000, AASupp, 144, 363
- [2] Aldering, G., Antilogus, P., Bailey, S., et al. 2006, ApJ 650, 510
- [3] Aniano, G., Draine, B. T., Calzetti, D., et al. 2012, ApJ, 756, 138
- [4] Arendt, R. G. 1991, AJ, 101, 2160
- [5] Arnould, M., Goriely S., & Takahashi K., 2007, Physics Reports, 450, 97
- [6] Baade, W. 1945, ApJ, 102, 309
- [7] Badenes, C., Borkowski, K. J., Hughes, J. P., et al. 2006, ApJ, 645, 1373
- [8] Bedin, L. P., Ruiz-Lapuente, P., Gonzalez H, J. I., et al. 2014, MNRAS, 439, 354
- [9] Benedict, G. F., McArthur, B. E., Feast, M. W., et al. 2007, AJ, 133, 1810
- [10] Blaauw, A. 1961, Bulletin of the Astronomical Institutes of the Netherlands, 15, 265
- [11] Blondin, S. & Tonry, J. L. 2007, ApJ, 666, 1024
- [12] Boubert, D., Fraser, M., Evans, N.W., et al. 2017, arXiv:1704.05900
- [13] Branch, D., Jeffery, D. J., Blaylock, M., & Hatano, K. 2000, PASP, 112, 217
- [14] Breeveld, A. A., Landsman, W., Holland, S. T., et al. 2011, Gamma Ray Bursts 2010. AIP Conference Proceedings, 1358, 373
- [15] Brown, P. J., Breeveld, A. A., Holland, S., Kuin, P., & Pritchard, T. 2014, Astrophysics and Space Science, 354, 89
- [16] Brown, P. J., Holland, S. T., Immler, S., et al. 2009, AJ, 137, 4517
- [17] Brown, T. M., Baliber, N., Bianco, F. B., et al. 2013, PASP, 125, 1031
- [18] Burbidge E. M., Burbidge G. R., Fowler W. A., Hoyle F., 1957, Reviews of Modern Physics, 29, 547
- [19] Carlton, A.K., Borkowski, K. J., Reynolds, S. P., et al. 2011, ApJLett, 737, L22
- [20] Cassam-Chena, G., Hughes, J. P., Ballet, J., & Decourchelle, A. 2007, ApJ, 665, 315
- [21] Caswell J. L., Murray J. D., Roger R. S., Cole D. J., Cooke D. J., 1975, A&A, 45, 239
- [22] Chatzopoulos E., Wheeler J. C., Vinko J., 2012, ApJ, 746, 121
- [23] Chen, T.-W., Jerkstrand, A., Smartt, S. J., et al. 2014, The Astronomer's Telegram, 6284

- [24] Chiotellis, A., Kosenko, D., Schure, K. M., Vink, J., & Kaastra, J. S. 2013, MNRAS, 435, 1659
- [25] Chugai, N. N., Chevalier, R. A., & Lundqvist, P. 2004, MNRAS, 355, 627
- [26] Claeys, J. S. W., de Mink, S. E., Pols, O. R., Eldridge, J. J., Baes, M. 2011, A&A, 528, A131
- [27] Dalcanton, J. J., Williams, B. F., Lang, D., et al. 2012, ApJSupp, 200, 18
- [28] Decourchelle, A., Sauvageot, J. L., Audard, M., et al. 2001, A&A, 365, L218
- [29] Dessart, L., Hillier, D. J., Li, C., Woosley, S. 2012, MNRAS, 424, 2139
- [30] Dilday, B., Howell, D. A., Cenko, S. B., et al. 2012, Science, 337, 942
- [31] Dinell, B., Neuhuser, R., Yerli, S. K., et al. 2015, MNRAS, 448, 3196
- [32] Drake, S. A., & Ulrich, R. K. 1980, BAAS, 12, 798
- [33] Duin, R. M. & Strom, R. G. 1975, A&A, 39, 33
- [34] Dwarkadas, V. V., & Chevalier, R. A. 1998, ApJ, 497, 807
- [35] Edwards, Z. I., Pagnotta A., & Schaefer B. E. 2012, ApJL, 747, 19
- [36] Filippenko, A. V. 1982, PASP, 94, 715
- [37] Filippenko, A. V. 1997. Annu. Rev. Astron. Astrophys. 35, 309
- [38] Folatelli, G., Bersten, M. C., Benvenuto, O. G., et al. 2014, ApJ, 793, L22
- [39] Fox, O. D., Silverman, J. M., Filippenko, A. V., et al., 2015, MNRAS, 447, 772
- [40] Fox, O. D., Van Dyk, S. D., Dwek, E., et al. 2017, ApJ, 836, 2
- [41] Freiburghaus, C., Rosswog, S., & Thielemann, F. K., 1999, ApJL, 525, L121
- [42] Gaensler, B.M., Brazier, K.T.S., Manchester, R.N., Johnston, S., & Green, A.J., 1999, MNRAS, 305, 724
- [43] Gehrels, N., Chincarini, G., Giommi, P., et al. 2004, ApJ, 611, 1005
- [44] Germany, L. M., Reiss, D. J., Sadler, E. M., et al. 2000, ApJ, 533, 320
- [45] Ghavamian, P., Raymond, J. C., Hartigan, P., & Blair, W. P. 2000, ApJ, 535, 266
- [46] Gonzalez Hernandez, J. I., Ruiz-Lapuente, P., Tabernero, H. M., et al. 2012, Nature, 489, 533
- [47] Gonzalez Hernandez, J. I., Ruiz-Lapuente, P., Filippenko, A. V., et al. 2009, ApJ, 691, 1
- [48] Graham, M. L., Harris, C.E., Fox O. D. et al. 2017, arXiv:1706.02266

- [49] Hamuy, M., Phillips, M. M., Suntzeff, N. B., et al. 2003, *Nature*, 424, 651
- [50] Han, Z. & Podsiadlowski, P. 2006, *MNRAS*, 368, 1095
- [51] Harutyunyan, A. H., Pfahler, P., Pastorello, A., et al. 2008, *A&A*, 488, 383
- [52] Hayato, A., Yamaguchi, H., Tamagawa, T., et al. 2010, *ApJ*, 725, 894
- [53] Henbest, S. N. *MNRAS*, 1980, 190, 833
- [54] Henden, A. A., Welch, D. L., Terrell, D., Levine, S. E. 2009, *The AAVSO Photometric All-Sky Survey*, AAS 214, 0702.
- [55] Holoiien, T. W.-S., Stanek, K. Z., Shappee, B. J. et al. 2014, *The Astronomer's Telegram*, 6267
- [56] Hosseinzadeh, G., Arcavi, I., Valenti, S., et al. 2017, *ApJ*, 836, 2
- [57] Hoogerwerf, R., de Bruijne, J. H. J., & de Zeeuw, P. T. 2000, *ApJL*, 544, L133
- [58] Hughes, J. P. 2000, *ApJL*, 545, L53
- [59] Iben, I. Jr., A. Renzini, 1983, *ARA&A*, 21, 271
- [60] Iben, I. Jr. & Tutukov, A. V. 1984, *ApJS*, 54, 335
- [61] Iben, I. Jr. & Tutukov, A. V. 1985, *ApJS*, 58, 661
- [62] Ihara, Y., Ozaki, J., Doi, M., et al. 2007, *PASJ*, 59, 811
- [63] Inserra, C., Smartt, S. J., Scalzo, R., et al. 2014, *MNRAS*, 437, L51
- [64] Inserra, C., Fraser M., Smartt, S. J., et al. 2016, *MNRAS* 459, 2721
- [65] Jennings, Z. G., Williams, B. F., Murphy, J. W., et al. 2012, *ApJ*, 761, 26
- [66] Jennings, Z. G., Williams, B. F., Murphy, J. W., et al. 2014, *ApJ*, 795, 170
- [67] Jordi, K., Grebel, E. K., Ammon, K., 2006, *A&A*, 460, 339
- [68] Kaplan, D. L., Chatterjee, S., Gaensler, B.M., & Anderson, J. 2008, *ApJ*, 677, 1201
- [69] Kashi A., Soker N., 2011, *MNRAS*, 417, 1466
- [70] Kaspi, V., Manchester, R., Siegman, B., Johnston, S., & Lyne, A. 1994, *ApJL*, 422, L83
- [71] Katsuda, S., Petre, R., Hughes, J. P., et al. 2010, *ApJ*, 709, 1387
- [72] Kerr F. J., Lynden-Bell D., 1986, *MNRAS*, 221, 1023
- [73] Kerzendorf, W. E., Childress, M., Scharwachter, J., Do, T., & Schmidt, B. P. 2014, *ApJ*, 782, 27

- [74] Kerzendorf, W. E., Schmidt, B. P., Laird, J. B., Podsiadlowski, P., & Bessell, M. S. 2012, *ApJ*, 759, 7
- [75] Kerzendorf, W. E., Yong, D., Schmidt, B. P., et al. 2013, *ApJ*, 774, 99
- [76] Kerzendorf, W. E., Schmidt, B. P., Asplund, M., et al. 2009, *ApJ*, 701, 1665
- [77] Kochanek, C. 2009, *ApJ*, 707, 1578
- [78] Koo, B.-C., McKee, C. F., Suh, K.-W., et al. 2011, *ApJ*, 732, 6
- [79] Korobkin, O., Rosswog, S., Arcones, A. et al., 2012, *MNRAS*, 426, 1940
- [80] Krause, O., Tanaka, M., Usuda, T., et al. 2008, *Nature*, 456, 617
- [81] Lee, J.-J., Koo, B.-C., & Tatematsu, K. 2004, *ApJL*, 605, L113
- [82] Leonard, D.C, Filippenko, A.V., Barth, A.J., & Matheson, T. 2000, *ApJ*, 536, 239
- [83] Liu, Z. W., Pakmor, R., Ropke, F. K., et al. 2013, *A&A*, 554, 109
- [84] Livingstone, M. A., Kaspi, V. M., Gavriil, F. P., & Manchester, R. N. 2005, *ApJ*, 619, 1046
- [85] Livio, M., & Riess, A. G., 2003, *ApJ*, 594, 2
- [86] Lortet, M. C., Georgelin, Y.P., & Georgelin, Y. M. 1987, *A&A*, 180, 65
- [87] Marietta, E., Burrows, A., & Fryxell, B. 2000, *ApJS*, 128, 615.
- [88] Maund, J. R. & Smartt, S. J. 2009, *Science*, 324, 486
- [89] Meyer, B. S., Mathews, G. J., Howard, W. M. et al., 1992, *ApJ*, 399, 656
- [90] Moore, K., & Bildsten, L. 2012, *ApJ*, 761, 182
- [91] Nelan, E. P. 2007, *Fine Guidance Sensor instrument Handbook* (16th ed.; Baltimore, MD: STScI)
- [92] Nugent, P., Kim, A. G., & Perlmutter, S. 2002, *PASP*, 114, 803
- [93] Ochner, P., Benetti, S., Cappellaro, E. et al. 2014, *The Astronomer's Telegram*, 6660
- [94] Ofek, E. O., Cameron, P. B., Kasliwal, M. M., et al. 2007, *ApJL*, 659, 13
- [95] Ofek, E. O., Zoglauer, A., Boggs, S. E. et al. 2014, *ApJ*, 781, 42
- [96] Oke, J. B.; Cohen, J. G.; Carr, M. et al. 1995, *PASP*, 107, 375
- [97] Pagnotta, A. & Schaefer, B. E. 2015, *ApJ*, 799, 101
- [98] Pagnotta, A., Walker, E. S., & Schaefer, B. E. 2014, *ApJ*, 788, 173

- [99] Pan, K.-C., Ricker, P. M., & Taam, R. E. 2012, *ApJ*, 750, 151
- [100] Patat, F., Chugai, N. N., Podsiadlowski, Ph. et al. 2011, *A&A* 530, A63
- [101] Perlmutter, S., Aldering, G., Goldhaber, G., et al. 1999, *ApJ*, 517, 565
- [102] Prieto, J. L., Garnavich, P. M., Phillips, M. M. et al. 2007, arXiv:0706.4088
- [103] Qian, Y.-Z. 2012, *AIP Conf. Proc.*, 1484, 201
- [104] Qian, Y.-Z., Vogel, P., & Wasserburg, G. J., 1998, *ApJ*, 506, 868
- [105] Rest, A., Welch, D. L., Suntzeff, N. B., et al. 2008, *ApJ*, 681, 81
- [106] Reynoso, E. M. & Goss, W. M., 1999, *AJ*, 118, 926
- [107] Reynoso, E. M., Moffett, D. A., Goss, W. M., et al. 1997, *ApJ*, 491, 816
- [108] Riess, A., Filippenko, A. V., Challis, P., et al. 1998, *AJ*, 116, 1009
- [109] Ripley, J. L., Metzger, B. D., Arcones, A. et al., 2014, *MNRAS*, 438, 3243
- [110] Roming, P. W. A., Kennedy, T. E., Mason, K. O., et al. 2005, *Space Science Reviews*, 120, 95
- [111] Ruiz-Lapuente P. 1997, *Science*, 276, 1813
- [112] Ruiz-Lapuente P. 2014, *New Astronomy Reviews*, 62, 15
- [113] Ruiz-Lapuente, P., Comeron, F., Mendez, J., et al. 2004, *Nature*, 431, 1069 (RL04)
- [114] Schaefer, B. E. & Pagnotta, A. 2012, *Nature*, 481, 164
- [115] Schlafly, E. F., & Finkbeiner, D. P. 2011, *ApJ*, 737, 103
- [116] Schmidt, B. P., Kerzendorf, W. E., Frebel, A., et al. 2007, in *Accretion and Explosion: the Astrophysics of Degenerate Stars*
- [117] Silverman, J. M., Nugent, P. E., Gal-Yam, A. et al. 2013a. *ApJS*, 207, 3
- [118] Silverman, J. M., Nugent, P. E., Gal-Yam, A. et al. 2013b, *ApJ*, 772, 125
- [119] Smith, N., Chornock, R., Silverman, J. M., 2010, *ApJ*, 709, 856
- [120] Smith, N., Li, W., Foley, R. J., et al. 2007, *ApJ*, 666, 1116
- [121] Soker, N., Kashi, A.; Garca-Berro, E et al., 2013a, *MNRAS*, 431, 1541
- [122] Soker, N., 2013b, *New Astron.*, 18, 18
- [123] Soker, N., Garca-Berro, E., & Althaus, L. G., et al., 2014, *MNRAS*, 437, L66
- [124] Tan, S. M. & Gull, S. F. 1985, *MNRAS*, 216, 949

- [125] Tamura, K., Kawai, N., Yoshida, A., & Brinkmann, W. 1996, PASJ, 48, L33
- [126] Tetzlaff, N., Dincl, B., Neuhuser, R., & Kovtyukh, V. V. 2014, MNRAS, 438, 3587
- [127] Thompson, T. A., Burrows, A., & Meyer, B. S., 2001, ApJ, 562, 887
- [128] Trundle C., Kotak R., Vink J. S., Meikle W. P. S., 2008, A&A, 483, L47
- [129] Turatto, M., Suzuki, T., Mazzali, P. A., et al. 2000, ApJL, 534, 57
- [130] Valenti, S., Howell, D. A., Stritzinger, M. D., et al. 2016, MNRAS, 459, 3939
- [131] Vink J., Yamazaki, R., Helder, E. A., & Schure, K. M. 2010, ApJ, 722, 1727
- [132] Wagner, S. J., & Seifert, W. 2000, Pulsar Astronomy 2000 and Beyond, Proceedings of the 177th Colloquium of the IAU held in Bonn, Germany, 30 August - 3 September 1999, ed. M. Kramer, N. Wex, & N. Wielebinski, ASP Conf. Ser., 202, 315
- [133] Wanajo S., 2013, ApJL, 770, L22
- [134] Warren, D. C. & Blondin, J. M. 2013, MNRAS, 429, 3099
- [135] Warren, J. S., Hughes, J. P., Badenes, C., et al. 2005, ApJ, 634, 376
- [136] Webbink, R. F. 1984, ApJ, 277, 355
- [137] Whelan, J. & Iben, I. Jr. 1973, ApJ, 186, 1007
- [138] Williams, B. J., Borkowski, K. J., Ghavamian, P., et al. 2013, ApJ, 770, 129
- [139] Williams, B. J., Borkowski, K. J., Reynolds, S. P., et al. 2011, ApJ, 729, 65.
- [140] Wongwathanarat, A., Janka, H.-Th., & Müller, E 2013, A&A 552, A126
- [141] Wood-Vasey, W. M., Wang, L., & Aldering, G. 2004, ApJ, 616, 339
- [142] Woosley, S. E., Wilson, J. R., Mathews, G. J. et al., 1994, ApJ, 433, 229
- [143] Xu, Y., McCray, R., Oliva, E., & Randich, S. 1992, ApJ, 38
- [144] Xue, Z. & Schaefer, B. E. 2015, ApJ, 809, 183
- [145] Yaron, O., Y & Gal-Yam, A. 2012, PASP, 124, 668
- [146] Yatsu, Y., Kawai, N., Kataoka, J., Kotani, T., Tamura, K., & Brinkmann, W. 2005, ApJ, 631, 312
- [147] Yatsu, Y., Kawai, N., Kataoka, J., Tamura, K., & Brinkmann, W. 2006, in Proc. The X-ray Universe 2005, ed. A. Wilson (Noordwijk: ESA Publications Division), 379
- [148] Yoon, S.-C., Cantiello, M. 2010, ApJL, 717, L62
- [149] Zacharias, N., Finch, C., & Frouard, J. 2017, AJ, 153, 166

- [150] Zhang, T., Wang, X., Wu, C., et al. 2012, *AJ*, 144,131
- [151] Zijlstra, A. A. 2004, *MNRAS*, 348, L23
- [152] Zinnecker, H., & Yorke, H. W. 2007, *ARA&A*, 45, 481

APPENDIX A. Permission to Reproduce Copyrighted Material

AMERICAN ASTRONOMICAL SOCIETY

This agreement must be signed and returned to the editorial office before the American Astronomical Society (AAS) can publish your paper. In the event the article is not judged acceptable for publication in the journal you will be notified in writing and the copyright and all rights conferred by this agreement shall revert to you.

PUBLICATION AND TRANSFER OF COPYRIGHT AGREEMENT Manuscript number: ApJ98062R1

Article title: 'Star G' in Tycho's Supernova Remnant Is Far From The Site Of The Supernova Explosion And Is Not An Ex-companion Star Of The Progenitor

Names of authors: Zhichao Xue Bradley Schaefer

Author Rights: AAS grants to the author(s) (or their below-named employers, in the case of works made for hire) the following rights. All copies of the Article made under any of these rights shall include notice of the AAS copyright.

- (1) All proprietary and statutory rights other than copyright, such as patent rights.
- (2) The right after publication by the AAS to grant or refuse permission to third parties to republish all or part of the Article or a translation thereof. In the case of whole articles only, third parties must first obtain permission from the AAS before any right of further publication is granted. The AAS may choose to publish an abstract or portions of the Article before the AAS publishes it in a journal.
- (3) The right to use all or part of the Article in future works and derivative works of their own of any type, and to make copies of all or part of the Article for the authors' use for educational or research purposes.
- (4) In the case of a work made for hire, the right of the employer to make copies of the Article for the employer's internal use, but not for resale.

Copyright Assignment: Copyright in the Article is hereby transferred to the AAS for the full term of copyright throughout the world, effective as of date of acceptance of the Article for publication in a journal of the AAS. The copyright consists of all rights protected by copyright laws of the United States and of all foreign countries, in all languages and forms of communication, and includes all material to be published as part of the Article in any format or medium. The AAS shall have the right to register copyright to the Article in its name as claimant, whether separately or as part of the journal issue or other medium in which the Article is included.

Authorized signature _____

Date _____

Certification of Government Employment: An article prepared by a government officer or employee as part of his or her official duties may not be eligible for copyright, if the authors are all employed by one of the governments of Australia, Canada, New Zealand, the UK, or the US. If *all* the authors of the article are such government employees, one of the authors should sign here. If *any* of the authors is *not* such a government employee, do not sign in this box.

Author signature _____

Date _____

After signing the form, please scan and upload via the peer review system at <http://apj.msubmit.net> or fax to 905-538-7173.

APPENDIX B. Testing DA White Dwarf Variability using the *Kepler* and K2 mission

B.1 Introduction

Supernova cosmology is a vast and important enterprise, with extensive upcoming ground-based (e.g. Dark Energy Survey) and space-based photometry of supernova light curves, so as to provide the primary measure of Dark Energy. The effort of using Type Ia Supernovae as ‘standard candles’ has discovered the acceleration of the Universe (Perlmutter et al. 1999; Riess et al. 1998). As we are seeking more precise measurement of Dark Energy, the dominant source of error is now the photometric uncertainty in calibrating the supernova light curves (Stubbs & Brown 2015). Work has been done using local Standards (Landolt 1983; Landolt 1992) to calibrate SNe light curves, while to advance, better calibrations are needed. The goal is to get calibrations better than 1%, and hopefully much better than 1%, as such is needed to measure the Dark Energy parameters (Stubbs & Brown 2015).

When we talk about flux calibration, it means figuring out a way to use some known constant photon spectral flux standard to calibrate the instrument via the means of comparing between measured instrumental magnitude differences from different passbands and the actual photon flux ratio at the top of the atmosphere. This makes DA white dwarfs (DA WDs), which are WDs with pure-hydrogen atmospheres, the perfect choice. Isolated DA white dwarfs possess several properties that make them ideal calibration standards (Holberg 1982; Holberg et al. 1991). First, DA WDs not in close binaries, nor near the ZZ Ceti instability strip should be extremely photometrically stable. Since DA WDs have fully radiative, pure-hydrogen photospheres, their opacity can be calculated to a high precision, and it has been shown repeatedly that calculated model atmospheres covering wide ranges of temperature and surface gravity can represent continuum flux distributions and line profiles of these stars accurately. Thus only an effective temperature and a surface gravity would be adequate for modeling the atmosphere of these stars. A detailed spectroscopic analysis of

the Balmer line profiles would determine these two parameters to a considerable precision without any kind of photometry. With these type of stars' energy distributions exhibiting strong wavelength dependencies due to the covering of a wide range of effective temperature (T_{eff}) and surface gravity ($\log g$), synthetic photometry for stars with different energy distributions and broad ranges of colors become possible (Holberg et al. 2006).

A variety of situations could make DA WDs fail as standard stars. DA WD models from different groups reportedly produce discrepancies at 1% level (Bohlin et al. 2014). Those discrepancies are often seen in the width of hydrogen lines and general shape of the continuum spectra. However, high-resolution observations of those lines should be able to guide the tuning of model parameters and, eventually, address the issue.

For future large sky surveys, like LSST, a single one-second exposure of most known DA WDs would be saturated and become completely useless as local calibration standards. Faint DA WDs should be pursued in such a program.

Empirically, we can work out a set of transformation equations (including zero points and color terms etc.) for a desired passband using local field standards, in this case, DA WDs. Thus, temporal variability in DA WDs should be the primary concern. For example, BD+17° 4708, one of the 3 HST fundamental flux standards, exhibits 4% change in apparent magnitude over a six-year interval (Bohlin & Landolt 2015). Other possibilities include an unresolved low-mass companion star induced relativistic beaming, reflection/re-radiation/ and transiting effects, combinations between WD rotation and magnetic spots or spots from accreting interstellar-medium (e.g. Maoz et al. 2015, Østensen et al. 2011), and pulsations of various types (including the WD being in the ZZ Ceti instability strip (e.g. Winget et al. 1982)). For these cases, some fraction of the WDs will have the effects prominent enough to be recognized, in which case the star would not be used as a standard star. Nevertheless, in many cases, the situation will be completely unrecognizable, which could be horrific as is the case of BD+17° 4708. The question at hand is the frequency of unrecognized situations wherein the DA WD suffers substantial variability.

Supernova cosmology now needs $<1\%$ photometry (as the limiting factor in measuring Dark Energy), and this requires standard stars that are truly constant to roughly the 0.1% level. DA WDs are being touted as the answer, with large programs now underway to calibrate them. But no one has asked the question as to whether they are really stable to the 0.001 mag level. Ground-based telescope often can not achieve this level of photometric accuracy, while space telescopes like the *Hubble Space Telescope* (HST) do not have the cadence to test for variability on most time scales. However, there is one spacecraft (*Kepler*) that can provide a unique opportunity with unprecedented photometric accuracy and continuous observation.

The *Kepler* spacecraft was launched in March 2009 with a goal of detecting Earth size planets within the habitable zone of Sun-like stars through the transit method. The spacecraft has a 0.95-meter aperture telescope with a CCD array consisting of 21 modules on the focal plane. It utilizes no filter but the whole system has an equivalent bandpass of 4300 - 9000Å. The measure of source intensity as observed through this bandpass is called the Kepler magnitude (Kp). *Kepler* has performed observations covering a field of view of 116 square degrees on the Cygnus-Lyra region for more than four years with unprecedented photometric accuracy (tens of parts per million for bright targets) and non-stop. Nearly 5000 exoplanet candidates have been discovered and it has also revolutionized other fields of astronomy like eclipsing binary characterization, asteroseismology, and stellar variability studies etc.

Unfortunately, in May 2013, the spacecraft had its second reaction wheel failure, which resulted in the loss of fine pointing accuracy required for high precision photometry. To extend the mission as far as it can, several solutions were applied. By aligning the spacecraft along the ecliptic, pointing drift can be corrected by solar pressure on the spacecraft and periodic thruster firing. This extended mission has been called K2. Unlike the *Kepler* mission, K2 runs a series of sequential observing ‘Campaigns’ of fields distributed around the ecliptic plane. Each campaign has a shorter duration approximately 80 days than a ‘quarter’ in the *Kepler* mission (Howell et al. 2014).

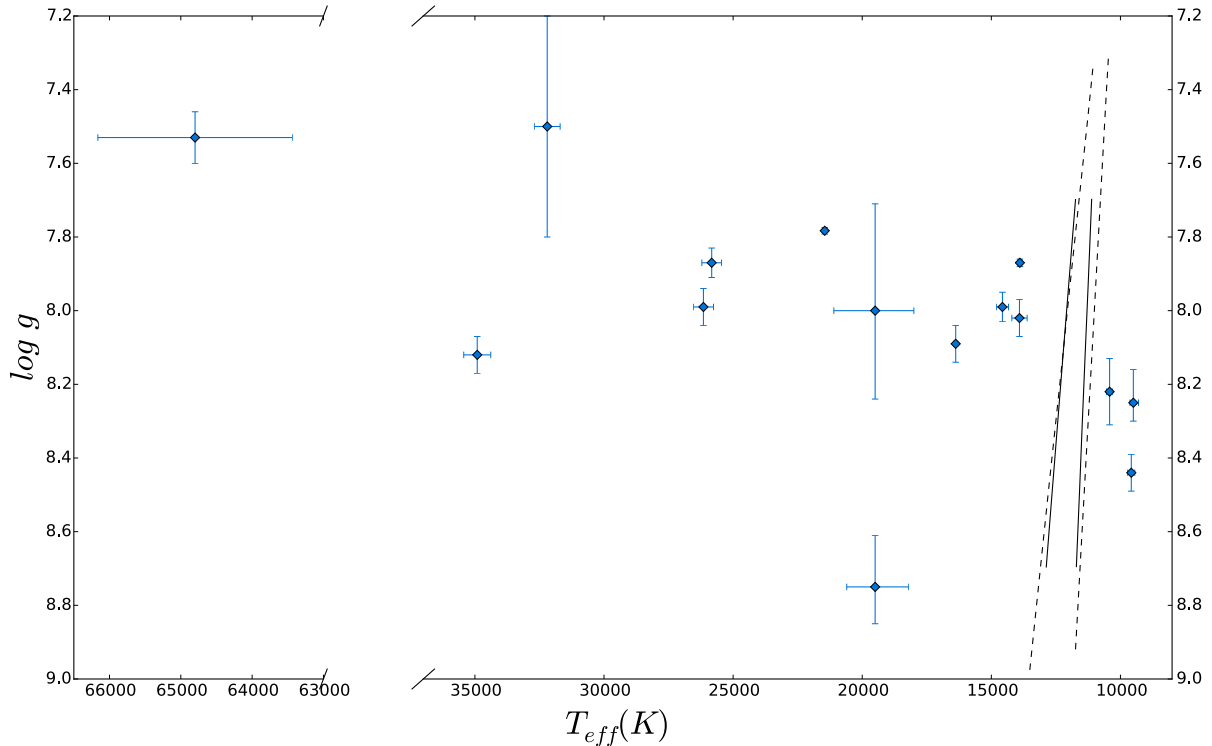


Figure B.1: Positions of the 15 DA WDs that are selected based on the criteria described in Section B.2.1 in the T_{eff} - $\log g$ space along with the empirical (dashed line) and the theoretical (solid line) instability strip from Gianninas et al. (2005) and Fontaine et al. (2003). None of the 15 DA WDs fall in the instability strip.

In this work, I will select out DA WDs that were observed by both the *Kepler* and K2 mission based on several criteria. I will present my measurements for the variability in DA WDs from their light curves for different time scales ranging from several hours to several days. Period searching would also be performed for all the WDs. I will test whether DA WDs can be stable enough (better than 0.1%) to push better calibration for supernova cosmology programs and calculate the fraction of WDs that are too variable to be calibration standards.

B.2 Target Selection and Data Reduction

B.2.1 Target Selection

There are many DA WDs in the *Kepler* and K2 fields. Our group here at LSU made several proposals to the K2 mission (GO6063, 5003, 4003), so I can draw my sample from them. I later expanded the search for any available DA WDs from the *Kepler* mission and K2 Campaign 0 to 6. However, not all of them are suitable for this test. I have selected targets based on the following criteria:

- Each must be a spectroscopically confirmed DA WD, as only WDs with a pure hydrogen atmosphere are the best candidates for better calibrations and to test their variability is the main purpose of this work.
- Each must be apparently a single star. Effects from known companions (another WD, planets, accretion from the companion, etc.) in the same system usually can be easily spotted through different light curve modulations, which will forfeit the purpose of my test. All of my targets have been checked against public available databases like *Simbad* and the literature to exclude known photometric and spectroscopic binaries.
- Crowding can also introduce unwanted and perhaps variable flux for the objects I am testing. Depending on different situations, contamination from one or more nearby objects can induce variability not originating from the target or decrease the measured target intrinsic variability. Especially in the K2 mission, telescope pointing drift has been a dominant systematic error in the photometric points. A close by object moving in-and-out of the photometry aperture (due to very small drifts in the telescope pointing) can cause pseudo-variability, even though both stars are constant in nature. Also, a much brighter nearby object can dominate the collected flux and decrease the variability calculated for the target. For all of my targets, I have firstly checked Digitized Sky Survey (DSS) to very deep limit to make sure there are no close objects. Then, I checked target pixel files with the photometric aperture that were used to create the

light curve products and made sure there is no crowding or contamination. Only with this, can I be sure that I am measuring the fluxes only from my targets.

- Cool DA WDs sometimes can fall into the ZZ Ceti instability strip, which has a temperature range from 10800K to 12300K (Bergeron et al. 2004; Mukadam et al. 2004). DA WDs in this narrow region in the T_{eff} - $\log g$ plane are considered to be pulsating DA WD or DAV. They exhibit stellar pulsation-driven by the partial ionization of atmospheric hydrogen to the order from several percents to tens of percent. Recently, several studies using *Kepler* and K2 data have discovered new outburst-like phenomenon (up to $\approx 15\%$, lasting a fraction of day, and recurring irregularly on timescales of days) beside normal pulsation modes in at least six known DAV WDs (e.g. Bell et al. 2015, Hermes et al. 2015, Bell et al. 2016). Using DAVs in any calibration program will certainly introduce systematic uncertainties either from their pulsation modes or this newly discovered outburst phenomenon. Fortunately, both theoretical (Fontaine et al. 2003) and empirical bounds (Gianninas et al. 2005) have been set for this kind of object in the T_{eff} - $\log g$ parameter space. Previous modeling and spectral fitting have determined the effective temperature and surface gravity for my targets. These properties are used to exclude DA WDs that fall into the instability strip. Figure B.1 shows both the theoretical and empirical instability strip in T_{eff} - $\log g$ space and all the targets that are used in this work.
- The *Kepler* mission can achieve photometric precision better than ~ 100 ppm (i.e., 0.01% accuracy) for targets that are brighter than Kp=16. The limiting factor for observations of faint sources is believed to be caused by source confusion. The K2 mission has slightly degraded photometric precision, although I will be still looking at ~ 200 ppm for targets at Kp=16¹. As I intend to examine the DA WD variability down to the 0.1% level, I should really look at WDs no fainter than 16th Kepler magnitude.

¹<https://keplerscience.arc.nasa.gov/the-kepler-space-telescope.html>

Table B.1: Parameters of the 15 DA WDs

KIC	NAME	Campaign	$Kepmag$	$T_{eff}(K)$	$\log g$	Type	Reference
212687157	BD-07 3632	6	12.422	14570^{+235}_{-235}	$7.99^{+0.04}_{-0.04}$	DA	1
202059074	LAWD 21	0	13.400	26150^{+391}_{-391}	$7.99^{+0.05}_{-0.05}$	DA	1
211821115	GALEX J081237.8+173701	5	13.491	16380^{+80}_{-80}	$8.09^{+0.05}_{-0.05}$	DA	2
201907706	PG 1141+078	1	14.418	64800^{+1363}_{-1363}	$7.53^{+0.07}_{-0.07}$	DA	1
212148813	PG 0839+232	5	14.550	25830^{+382}_{-382}	$7.87^{+0.04}_{-0.04}$	DA	1
201286675	GD 135	1	14.585	13895^{+77}_{-77}	$7.87^{+0.01}_{-0.01}$	DA	3
212657308	PG 1350-090	6	14.616	9580^{+136}_{-136}	$8.44^{+0.05}_{-0.05}$	DA	1
201880326	PG 1129+072	1	15.033	13910^{+296}_{-296}	$8.02^{+0.05}_{-0.05}$	DA	1
203705962	LP 861-31	2	15.141	10420^{+120}_{-120}	$8.22^{+0.05}_{-0.09}$	DA	4
210991241	HS 0331+2240	4	15.391	21452^{+54}_{-54}	$7.783^{+0.009}_{-0.009}$	DA	5
8682822	2MASS J19172058+4452397	Cygnus Q8	15.814	19500^{+1300}_{-100}	$8.75^{+0.14}_{-0.1}$	DA	6
4829241	LAMOST J191927.67+395839.30	Cygnus Q8	15.825	19500^{+1500}_{-1600}	$8^{+0.29}_{-0.24}$	DA	6
4242459	EGGR 580	Cygnus Q8	15.868	9500^{+200}_{-130}	$8.25^{+0.09}_{-0.05}$	DA	6
11822535	RE J1943+500	Cygnus Q9	14.817	34910^{+523}_{-523}	$8.12^{+0.05}_{-0.05}$	DA	1
11514682	2MASS J19411253+4925073	Cygnus Q9	15.692	32200^{+500}_{-500}	$7.5^{+0.3}_{-0.3}$	DA	7

Reference: (1): Gianninas et al. 2011; (2): Limoges et al. 2013; (3): Koester et al. 2001; (4): Kawka & Vennes 2006 (5): Koester et al. 1997; (6): Doyle et al. 2016; (7): Østensen et al. 2011

Based on the criteria described above, I selected out 15 DA WDs that are spectroscopically confirmed DA WDs, not in the instability strip, photometrically and spectroscopically not in a binary or multiple system, with no crowding or contamination, and brighter than $Kp=16$. There are 5 of them in the *Kepler* field and the other 10 are in the K2 Campaign 0-6. Table B.1 listed the properties of these 15 DA WDs.

B.2.2 *Kepler* and K2 Photometry Data Reduction

The *Kepler* spacecraft has two modes of observation, long cadence (LC; 30-minute exposures) and short cadence (SC; 1-minute exposures). In this work, I only used the long cadence light curve for testing DA WDs variability. For the *Kepler* mission, there are also two kinds of photometric products, Pre-search Data Conditioning Simple Aperture Photometry (PDCSAP) and Simple Aperture Photometry (SAP). The SAP light curve is just a time series of fluxes summed within an optimal aperture.

PDCSAP light curves are SAP light curves corrected for systematic artifacts. This is achieved by subtracting a set of ‘Cotrending Basis Vectors’ (CBVs) out of the SAP light curves, which are created quarterly from carefully selected quiet targets on each detector channel to characterize systematic artifacts (e.g. Smith et al. 2012; Stumpe et al. 2012,

2014; Van Cleve et al. 2015). The same technique was implemented for the K2 mission as well. A total number of 16 CBV would be generated for each quarter. However, with a closer look at CBVs, one would spot many variations on all ranges of time scales and amplitudes within the CBVs themselves. This means intrinsic stellar variabilities in light curves could be contaminated by those CBVs if they are co-trended that way. It would be fine for the purpose of exoplanet searches but it would sabotage a study like what I am doing. Also, as I am trying to put limits on the WD variability on a long range of time scales, it would be hard to track down how the PDC pipeline altered the light curves. Thus, in my analysis, I used the unaltered SAP product to put limits on the WD variability.

The K2 mission also brought up a new significant systematic error in stars' light curves. Stellar centroids on the CCD chips would drift across pixels due to the satellite's pointing drift plus the thrust firing every 6 hours to correct the spacecraft pointing. This creates a 'saw-tooth' feature in the light curves from the K2 mission. Plenty of efforts have been made to correct the position-dependent systematic errors, which showed significant improvement in reducing the 'saw-tooth' features while preserving intrinsic stellar variabilities. For example, **K2SFF** (Vanderburg & Johnson 2014) and **K2VARCAT** (Armstrong et al., 2015) de-trend light curves by de-correlating the photometry with the stellar centroid motion across pixels. Recently, a newly published de-trending pipelines **EVEREST** (Luger et al. 2016) utilizing Pixel Level Decorrelation (Deming et al. 2015, PLD) is believed to produce some better results when compared to other de-trending methods. I started my analysis for targets in the K2 campaigns using the **K2VARCAT** de-trended light curves. So this was kept consistent through my analysis from campaign 1 to 6. Only when light curves from the **K2VARCAT** still clearly show the 'saw-tooth' feature, do I turn to the products from the **EVEREST**. All Kepler data are archived and publicly available from the Mikulski Archive for Space Telescopes (MAST).

Even with these de-trending methods, light curves from the K2 mission still showed some prominent long-term trends during the ~ 80 day data acquisition period with all different

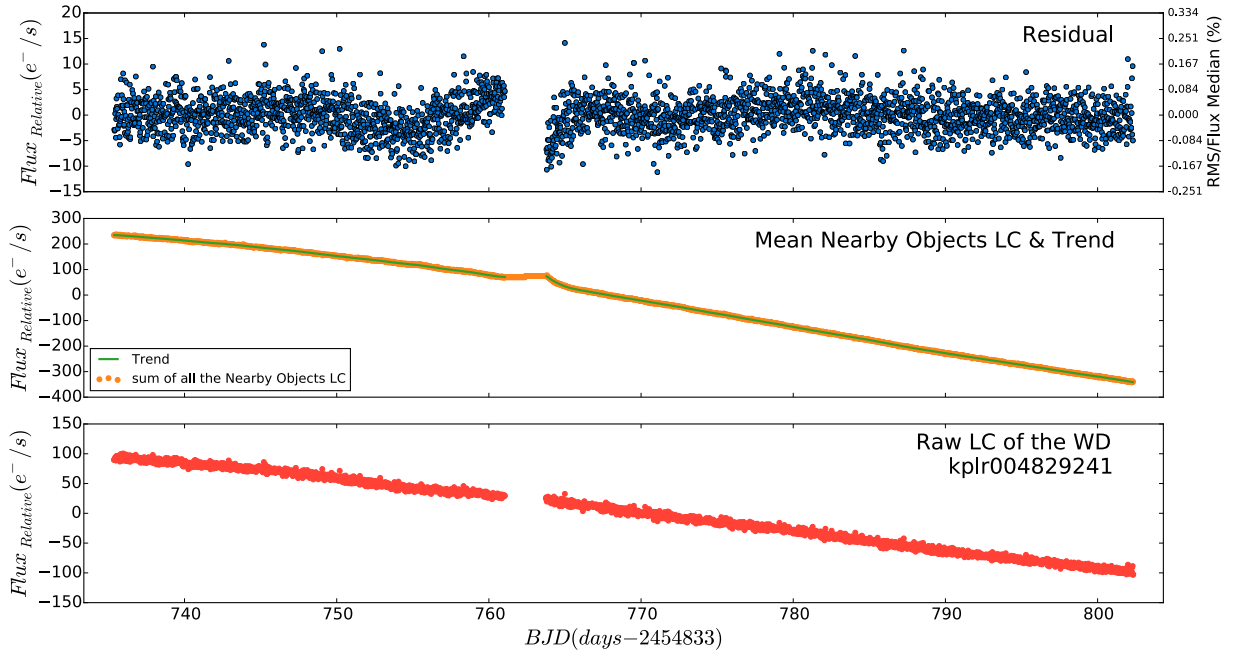


Figure B.2: Example of the light curve of KIC 4829241, a DA WD in the *Kepler* field with $K_p = 15.825$. *Kepler* light curves are using the Barycentric Julian Date (BJD), which is the Julian Date (JD) corrected for differences in the Earth’s position with respect to the barycentre of the Solar System. The bottom panel shows the raw light curve straight from the SAP. This flux has been subtracted by the median flux of this WD to show the relative variability more clearly. A long term trend can be clearly seen. The middle panel shows the averaged light curves (median subtracted) of nearby objects (see Section B.2.2 for detail). A similar trend can be spotted as in the WD’s light curve and nearby objects’ light curve. The green curve is the trend created by applying a Savitzky-Golay filter with a large window size (larger than the longest time scale I would test, which is 3 days). This trend would be the one used to de-trend this long-term variation. See Section B.2.2 for detail. The top panel shows the de-trended light curve of KIC 4829241. This method can flatten the light curve, in other words, correct the long term systematic variation partially. There are still some residual trends can be seen on either side of the gap in the top panel, with these being not intrinsic to the target DA WD. Then the light curve in the top panel would be used to test variability on a variety of timescales. For example, the 6-hour variability for KIC 4829241 is 0.050%. This would be an excellent local standard for SN cosmology if they want the calibration error to be better than 1%.

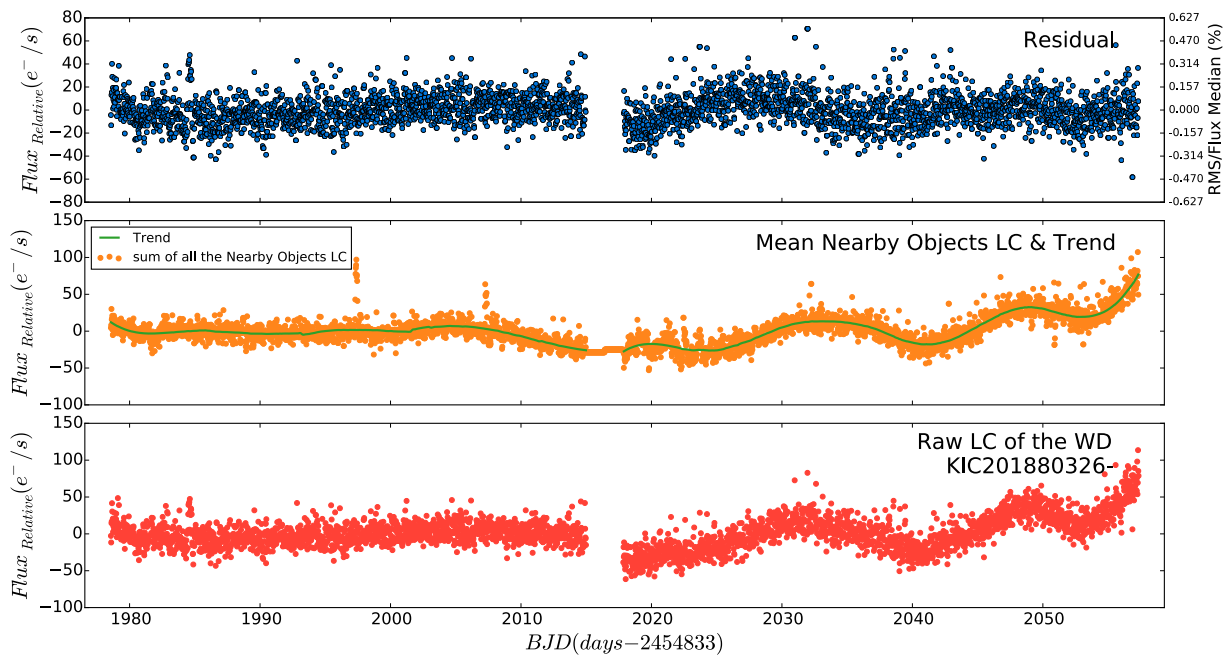


Figure B.3: As in Figure B.2, KIC 201880326 is a DA WD in K2 Campaign 1 with $K_p = 15.033$. The bottom panel shows the raw light curve straight from **K2VARCAT** with median flux of the WD being subtracted. The 6 hour variability for ktwo201907706 is 0.086%. Again, the flattened light curve (top panel) shows systematic trends that are either intrinsic or instrumental. For my purpose, even with these uncorrected trends, I can still put an upper limit on the variability of this WD.

kinds of shapes, see the bottom panel of Figure B.2 & B.3. Very likely, most of them are due to the systematic artifacts due to thermal environment change in the CCD over the time or telescope focus change which in turn affects the stellar PSF on the images. SAP light curves have similar long-term trends as well, see Figure B.2 & B.3. This is bad for my analysis as well, as I would want to put limits on the variability on the scale of several days. Simply taking peak-to-peak amplitudes would be unreasonable and useless, even with data binning.

Thus, I have tried to develop a way to de-trend the long-term trend in both the *Kepler* and K2 light curves. By examining nearby objects around my targets (generally within a 5 arcmin radius), I spot similar trends in those objects' light curves as the one in the WDs. This is suggesting that my targets were experiencing similar systematic changes along with nearby others. This immediately inspired me to develop the idea of using nearby stars light curves to de-trend my targets. I first locate non-extended sources within ~ 5 arcmin radius around each WD in my sample. Selecting out obviously variable targets (sinusoidal, eclipsing etc.), I then average their fluxes and create an averaged light curve of nearby objects. Applying a Savitzky-Golay high-pass filter (Savitzky & Golay 1964) for this light curve with a window size larger than any time scale I will test for variation and be left with a simple smooth trend curve for the local field. This prevents any variations on the time scale below the window size from the nearby objects being injected into my target light curves. Using this equation $Residual = Flux_{raw} - (C[0]*Trend + C[1])$, $Flux_{raw}$ is the flux of WDs with position-dependent artifacts being corrected by **K2VARCAT** or SAP, $Trend$ is the one just created from nearby objects and it is normalized. $C[0], C[1]$ are some constants, a least square fit would try to minimize the Residual. The median flux of the WD before this de-trending can be added on this residual to recreate the WD light curve. My method for correcting for the long-term trend is effectively differential photometry using nearby field stars for comparison. With this, I can test the WD variability on several different time scale.

Table B.2: Summary of Result

KIC	Campaign	Kepler Mag.	Median Flux (e^-/s)	$\frac{\text{RollingRMS}}{\text{MedianFlux}}$ (3hour ^a)	$\frac{\text{RollingRMS}}{\text{MedianFlux}}$ (6hour ^a)	$\frac{\text{RollingRMS}}{\text{MedianFlux}}$ (1day ^a)	$\frac{\text{RollingRMS}}{\text{MedianFlux}}$ (3days ^a)	$\frac{\text{PeaktoPeak}}{\text{MedianFlux}}$ (3days ^b)	Pipeline
212687157	6	12.422	150300	0.020%	0.028%	0.037%	0.041%	<0.34%	K2VARCAT
202059074	0	13.4	50084	0.047%	0.056%	0.064%	0.072%	<0.09%	K2VARCAT
211821115	5	13.491	49364	0.032%	0.040%	0.059%	0.074%	<0.64%	K2VARCAT
212657308	6	14.616	20330	0.048%	0.053%	0.059%	0.062%	<0.30%	K2VARCAT
201907706	1	14.418	20030	0.070%	0.075%	0.084%	0.085%	<0.32%	K2VARCAT
201286675	1	14.585	18885	0.063%	0.068%	0.075%	0.081%	<1.22%	K2VARCAT
212148813	5	14.55	18116	0.068%	0.073%	0.080%	0.083%	<0.47%	K2VARCAT
201880326	1	15.033	12753	0.080%	0.086%	0.093%	0.097%	<0.17%	K2VARCAT
11822535	Cygnus Q9	14.817	11601	0.032%	0.034%	0.036%	0.037%	<0.24%	SAP
203705962	2	15.141	11417	0.056%	0.058%	0.063%	0.069%	<0.97%	EVEREST
210991241	4	15.391	9865	0.059%	0.062%	0.066%	0.070%	<0.56%	EVEREST
4829241	Cygnus Q8	15.825	5985	0.048%	0.050%	0.052%	0.053%	<0.08%	SAP
8682822	Cygnus Q8	15.814	5309	0.055%	0.057%	0.060%	0.061%	<0.57%	SAP
11514682	Cygnus Q9	15.692	5093	0.058%	0.061%	0.063%	0.065%	<0.29%	SAP
4242459	Cygnus Q8	15.868	4557	0.062%	0.065%	0.067%	0.069%	<0.47%	SAP

a: The window size for computing the rolling RMS

b: Peak to peak amplitudes were calculated using binned light curves with a 3-day window

B.3 Discussion and Summary

B.3.1 Analysis and Result

Instead of calculating the Root Mean Square (RMS) for the whole light curves which would be dominated by the uncorrected long-term systematic artifacts, I computed rolling RMS for a variety of timescales. I mainly test the WD variability in 3-hour, 6-hour, 1-day and 3-day time windows. That is, for example, a 6-hour RMS is calculated via taking the RMS within a rolling window of 12 contiguous long-cadence data, and taking the median of the RMS as the result for this time-scale. Table B.2 summarized the results, in which I quoted the value of RMS over the median flux of the WD in percentage. I closely checked all the light curves I used for the testing, some of them still showed uncorrected features due to the spacecraft drifting. For cases with extremely poor quality, I redo the analysis with the products from **EVEREST**. No doubt, those uncorrected features would bring up the RMS values. Thus, the values quoted in Table B.2 should be considered as upper limits.

I am also interested in the peak-to-peak amplitudes for these WDs over the selected quarter (for targets in the *Kepler* mission) or campaign (for K2 targets). The example of BD+17 4708 showed that WD can vary on a long time scale. Although I have attempted to

correct the long term systematics in the *Kepler* and K2 data using the method described in Section B.2.2, it does not work 100% of the time. Again, this made me realize that I could only put limits on this test. Directly taking a peak-to-peak amplitude would be unreasonable as the maxima or the minimum point can be affected by noise. Instead, I applied a 3-day binning to all the light curves and take the peak-to-peak amplitudes as an upper-limit, see Table B.2. Thus my peak-to-peak amplitudes represent an upper-limit on the variability on time scales of 3 to 80 days.

Maoz et al. (2015) reported periods found for several DA WDs in the *Kepler* mission. There are some overlaps between their and my samples. So for all the 15 DA WDs in this work, I performed a Fourier Transform on all of them. For KIC 8682822, both this work and Doyle et al. (2016) did not recover the reported 4.7246 days period reported in Maoz et al. (2015). It might be possible that Maoz et al. (2015) used the PDCSAP data which are light curves de-trended by CBVs while I am using SAP data that are not de-trended using CBVs. This was the concern that CBVs might induces additional variabilities in the first place. I did not recover the 9.8934 days period found for KIC 11514682 by Maoz et al. (2015). For the rest of the sample in this section, I did not found any significant period for any of them.

As summarized in column 5 to 8 in Table B.2 , all these 15 DA WDs, which are spectroscopically confirmed DA WDs, not in the instability strip, have no known companions and if brighter than $K_p=16$ can vary as little as 0.02% (RMS over median flux) and not exceed 0.1% over the time scale of 3-hour, 6-hour, 1-day and 3-day. Considering these values are limits essentially, I am safe to conclude that DA WDs can truly be stable to the 0.1% level or better. There is no reason to assume WDs that are fainter than the $K_p=16$ could not be stable to the 0.1% level. The cutoff was mainly set due to the spacecraft photometric precision concern. Thus, DA WDs can be used as photometric standards and any calibration needs can be achieved to the 1% level or better.

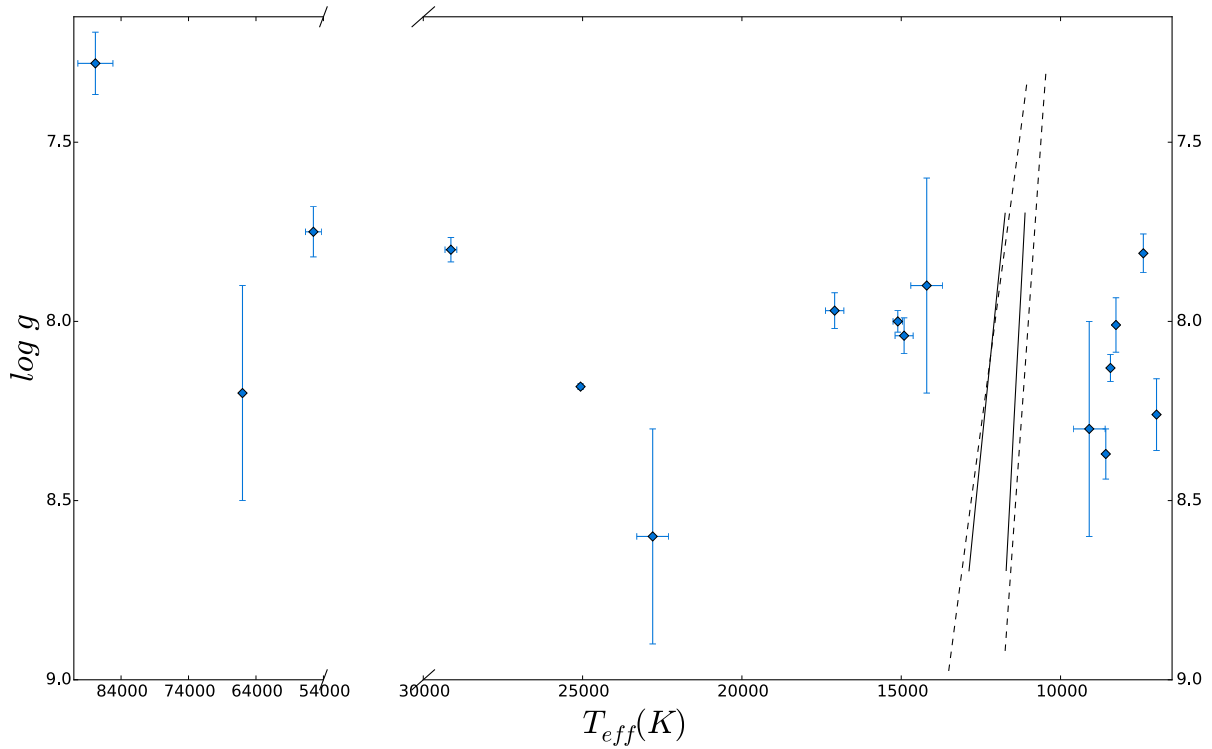


Figure B.4: Positions of the 16 DA WDs in the extended sample described in Section B.3.2 in the T_{eff} - $\log g$ space along with the empirical (dashed line) and the theoretical (solid line) instability strip from Gianninas et al. (2005) and Fontaine et al. (2003). None of the 16 DA WDs fall in the instability strip.

Table B.3: Parameters of the DA WDs in the extended sample

KIC	NAME	Campaign	$Ke p_{mag}$	$T_{eff}(K)$	$\log g$	Type	Reference
11337598	KIC 11337598	Cygnus Q3	16.105	22800^{+500}_{-500}	$8.6^{+0.3}_{-0.3}$	DA	1
212749589	PG 1314-067	6	16.18	17090^{+289}_{-289}	$7.97^{+0.05}_{-0.05}$	DA	2
10198116	KIC 10198116	Cygnus Q4	16.412	14200^{+500}_{-500}	$7.9^{+0.3}_{-0.3}$	DA	1
206197016	PB 7199	3	16.537	87805^{+2600}_{-2600}	$7.28^{+0.087}_{-0.087}$	DA	3
211923589	HS 0852+1916	5	16.542	14910^{+284}_{-284}	$8.04^{+0.05}_{-0.05}$	DA	2
5769827	KIC 5769827	Cygnus Q6	16.619	66000^{+200}_{-200}	$8.2^{+0.3}_{-0.3}$	DA	1
212173448	PG 0836+237	5	16.726	55490^{+1177}_{-1177}	$7.75^{+0.07}_{-0.07}$	DA	2
11604781	KIC 11604781	Cygnus Q10	16.739	9100^{+500}_{-500}	$8.3^{+0.3}_{-0.3}$	DA	1
202059078	2MASS J06443019+2731115	0	17	6988^{+40}_{-40}	$8.26^{+0.1}_{-0.1}$	DA	3
201854020	SDSS J112731.55+062305.1	1	17.082	8434^{+24}_{-24}	$8.13^{+0.038}_{-0.038}$	DA	3
201870446	SDSS J113109.06+064306.0	1	17.253	7402^{+30}_{-30}	$7.81^{+0.054}_{-0.054}$	DA	3
201260717	SDSS J112318.74-030248.8	1	17.3	15108^{+149}_{-149}	$8^{+0.03}_{-0.03}$	DA	3
201597644	SDSS J111509.50+020029.0	1	17.419	29133^{+185}_{-185}	$7.8^{+0.034}_{-0.034}$	DA	3
201433590	SDSS J113738.37-002721.7	1	17.909	8580^{+50}_{-50}	$8.37^{+0.07}_{-0.07}$	DA	4
201438515	SDSS J113725.16-002259.0	1	17.981	8261^{+46}_{-46}	$8.01^{+0.076}_{-0.076}$	DA	3
210403895	HS 0345+1324	4	18.056	25064^{+67}_{-67}	$8.182^{+0.008}_{-0.008}$	DA	5

Reference: (1): Østensen et al. 2011; (2): Gianninas et al. 2011; (3): Kleinman et al. 2013; (4): Tremblay et al. 2011; (5): Koester et al. 2009

Table B.4: Statistical Results of the 16 WDs in the extended sample

KIC	Campaign	Kepler Mag.	Median Flux (e^-/s)	$\frac{RollingRMS}{MedianFlux}$ (3hour ^a)	$\frac{RollingRMS}{MedianFlux}$ (6hour ^a)	$\frac{RollingRMS}{MedianFlux}$ (1day ^a)	$\frac{RollingRMS}{MedianFlux}$ (3days ^a)	$\frac{PeaktoPeak}{MedianFlux}$ (3days ^b)	Period [days]	Pipeline
11337598	Cygnus Q3	16.105	2522	0.11%	0.11%	0.12%	0.12%	<0.06% ^d	0.09	SAP
212749589	6	16.18	3997	0.2%	0.22%	0.25%	0.25%	<0.97%	None	K2VARCAT
210403895	4	16.2 ^c	3888	0.15%	0.17%	0.18%	0.2%	<0.43%	None	K2VARCAT
10198116	Cygnus Q4	16.412	2204	0.07%	0.08%	0.08%	0.08%	<0.39%	None	SAP
206197016	3	16.537	2966	0.81%	1.43%	2.64%	2.7%	<6.88% ^d	0.83	K2VARCAT
211923589	5	16.542	3326	0.2%	0.21%	0.23%	0.24%	<0.77%	None	K2VARCAT
5769827	Cygnus Q6	16.619	2676	0.12%	0.13%	0.14%	0.14%	<1.49%	None	SAP
212173448	5	16.726	2071	0.34%	0.36%	0.38%	0.4%	<1.17%	None	K2VARCAT
11604781	Cygnus Q10	16.739	2271	0.12%	0.12%	0.14%	0.18%	<0.35% ^d	4.87	SAP
202059078	0	17	2154	0.47%	0.54%	0.61%	0.64%	<1.92%	None	K2VARCAT
201854020	1	17.082	1976	0.35%	0.39%	0.44%	0.46%	<0.93%	None	K2VARCAT
201870446	1	17.253	1722	0.37%	0.39%	0.43%	0.44%	<0.72%	None	K2VARCAT
201260717	1	17.3	1380	0.58%	0.62%	0.66%	0.69%	<1.69%	None	K2VARCAT
201597644	1	17.419	1307	0.46%	0.49%	0.52%	0.53%	<0.82%	None	K2VARCAT
201433590	1	17.909	944	0.65%	0.69%	0.73%	0.74%	<1.38%	None	K2VARCAT
201438515	1	17.981	913	0.72%	0.78%	0.84%	0.88%	<1.78%	None	K2VARCAT

a: The window size for computing the rolling RMS

b: Peak to peak amplitudes were calculated using binned light curves with a 3-day window

c: It had a Kep. Mag. of 18.056. I adjusted it to ~ 16.2 based on the optical magnitudes from *SIMBAD* and the calculated median flux

d: The peak to peak amplitudes for WDs with periods were computed using smoothed folded light curves based on the periods reported in the table

B.3.2 Extended Sample of Faint DA WDs

My initial sample can answer the question of whether DA WDs are stable at the 0.1% level. However, a bigger question at hand would be for randomly selected DA WDs, what is the chance that it is varying more than 1% and hence will fail as a photometric standard. I extend my sample by including WDs fainter than Kp=16 while still being constrained by the other criteria listed in Section B.2.1. The photometric precision for targets fainter than Kp=16 (in both *Kepler* and K2) will be significantly poorer than those brighter than 16. According to Figure 6 in Armstrong et al., (2015), the photometric precision for K2 targets with Kp=18 could be ~ 1000 ppm or worse. In practice, I found that it can be two times worse (e.g. the photometric precision for targets with Kep. Mag.18 can be as low as ~ 2000 ppm) in late K2 campaigns and also according to the comparison between the **K2VARCAT** and the **EVEREST** made in Luger et al. (2016).

To make my statistics useful, I made a cut-off by 18th Kepler Magnitude for my extended sample. From both the *Kepler* and K2 data, I found another 16 DA WDs brighter than

Kp=18. Table B.3 listed their campaign numbers and parameters. Again, I tested them against both the theoretical and empirical instability strip. None of them falls into the instability strip, see Figure B.4. I performed similar analysis for these additional 16 WDs, the results are summarized in Table B.4 . Due to the drastic drop in the photometric precision for faint targets, the values reported in Table B.4 should be considered as upper limits. That is, for example, KIC 201438515 has a Kp=17.981 and variability $\sim 0.8\%$ over several different time scales largely due to the photometric precision degradation for faint targets. It does not necessary mean KIC 201438515 is varying at the 0.8% level. One can also calculate the Poisson error for a median flux of 913 (e^-/s) with a 30-minute integration time is down to the $\sim 0.08\%$ level, which is insignificant even for faint target like this one. A clear trend of increasing variability can be seen when targets are fainter. This is consistent with the fact that systematic error increases for fainter targets and it results in poorer photometric precision.

I again performed Fourier Transforms on all the WDs in this extended sample. Among the 4 WDs in the *Kepler* field within this sample, I recovered the period reported by Maoz et al. (2015) for KIC 11337598 with a period of 0.09 days and KIC 11604781 with a period of 4.87 days. However, I did not recover the 8.32 days period for KIC 5769827. KIC 11337598 and KIC 11604781 are fairly bright among the extended sample. I folded the light curves using the periods found and calculated the peak to peak amplitudes on the smoothed folded light curves.

KIC 11337598 has a ~ 2 hour period with 0.06% peak to peak amplitude, which is consistent with the finding in Maoz et al. (2015). This very short period modulation might be explained by UV-fluorescence or re-radiation from a hot planet. Even so, the variability of KIC 11337598 can still be constrained to 0.1% level on variety of timescales.

KIC 11604781 exhibits a 4.87 days period with 0.35% peak to peak amplitude, a little smaller than the number quoted (semi-amplitude of 0.2%) in Maoz et al. (2015). They concluded that WD rotation through spots induced by convection or accretion might be the

best cause for the observed variability. However, I noted that a three sigma contour based on the effective temperature and log g values presented in Table B.3 can make this WD encounter the cool side of the instability strip plotted in Figure B.4. Thus, the possibility of being a DAV candidate might need to be considered in the discussion for its observed modulation. Again, the variability of KIC 11604781 on different time scales does not exceed too much above 0.1%.

The only WD with detected period in my K2 samples is KIC 206197016. The light curve of KIC 206197016 (see Figure B.5) shows an obvious variation and the power spectrum picked out the significant period of ~ 0.83 days, the same you would judge by eye. The peak-to-peak amplitude is 6.88%. It is also the hottest DA WDs in my samples with an effective temperature of 87,805K. The time scale for its 1-2% variation is normally too large for a single WD. This could be due to an unresolved companion like a planet or another WD. The SED of this object showed no infrared excess and resembled a single white dwarf. Variation on this time scale might not be recognized by a telescope other than *Kepler* and if it is used as local standard, it will introduce systematic errors in calibration.

B.3.3 Summary

I selected out 15 spectroscopically confirmed DA WDs that were observed in the *Kepler* mission and its extended two-wheel mission K2. For these 15 brighter than the $K_p=16$, away from the instability strip and not in known binary or multiple system DA WDs, I have tested that DA WDs can truly be stable at 0.1% level or better on both long (several days) and short (several hours) time scales. Thus, calibration needs for better supernova cosmology (better than 1%) can be met using DA WDs. However, for a total of 31 randomly selected DA WDs (brighter than 18 Kep. Mag., single and not in the instability strip), 1 out of 31 (KIC 206197016) has a variability way above 1% at several different time scale and a high 6.88% peak to peak amplitude, while the rest of the WDs in my samples vary less than 1%. This very large variation like the one I found in KIC 206197016 can be potentially

unrecognized by teams aiming to calibrate supernova cosmology photometry, such an object could jeopardize any calibration process if being used. However, repeatedly monitoring the DA WDs used in any calibration program is recommended, as variation as high as the one I am finding can be easily spotted and excluded. To summarize, single DA WDs not in the instability strip can be stable at 0.1% level or better (as low as 0.02%). So supernova cosmology is fine and using DA WDs as local standards can push the systematic error in the calibration better than 1%. For small number statistics, there is a $\sim 3\%$ chance that a DA WD can vary $> 1\%$ and completely fail as a standard.

B.4 References

- Armstrong D. J., Kirk J., Lam K. W. F., et al. 2015, *A&A*, 579, A19
Bell, K. J., Hermes, J. J., Bischoff-Kim, A., et al. 2015, *ApJ*, 809, 14
Bell, K. J., Hermes, J. J., Montgomery, J. J., et al. 2016, arXiv:1609.09097
Bergeron P., Fontaine G., Billères M., Boudreault S., & Green E. M., 2004, *ApJ*, 600, 404
Bohlin, R. C., Gordon, K. D., & Tremblay, P. E. 2014, *PASP*. 126, 711
Bohlin, R. C. & Landolt, A. U. 2015, *AJ* 149, 122
Deming, D., Knutson, H., Kammer, J., et al. 2015, *ApJ*, 805, 132
Doyle, T. F., Howell, S. B., Petit V. et al. 2016, *MNRAS*, in press, arXiv1610.04895
Fontaine, G., Bergeron, P., Billères M., & Charpinet S., 2003, *ApJ*, 591, 1184
Gianninas, A., Bergeron, P., & Fontaine, G., 2005, *ApJ*, 631, 1100
Gianninas, A., Bergeron, P., & Ruiz, M. T., 2011, *ApJ*, 743, 138
Hermes, J. J., Montgomery, M. H., Bell, K. J., et al. 2015, *ApJ*, 810, L5
Holberg, J. B. 1982, *ApJ*, 257, 656
Holberg, J. B., Ali, B., Carone, T. E., et al. 1991, *ApJ*, 375, 716
Holberg, J. B. & Bergeron, P. 2006, *AJ*, 132, 1221
Howell, S. B., Sobek, C., Haas, M., et al. 2014, *PASP*, 126, 398
Kawka A. & Vennes S., 2006, *ApJ*, 643, 402
Kleinman S. J., Kepler, S. O., Koester, D. et al., 2013, *ApJS*, 204, 5
Koester, D., Provencal, J., & Shipman, H. L. 1997, *A&A*, 320, L57

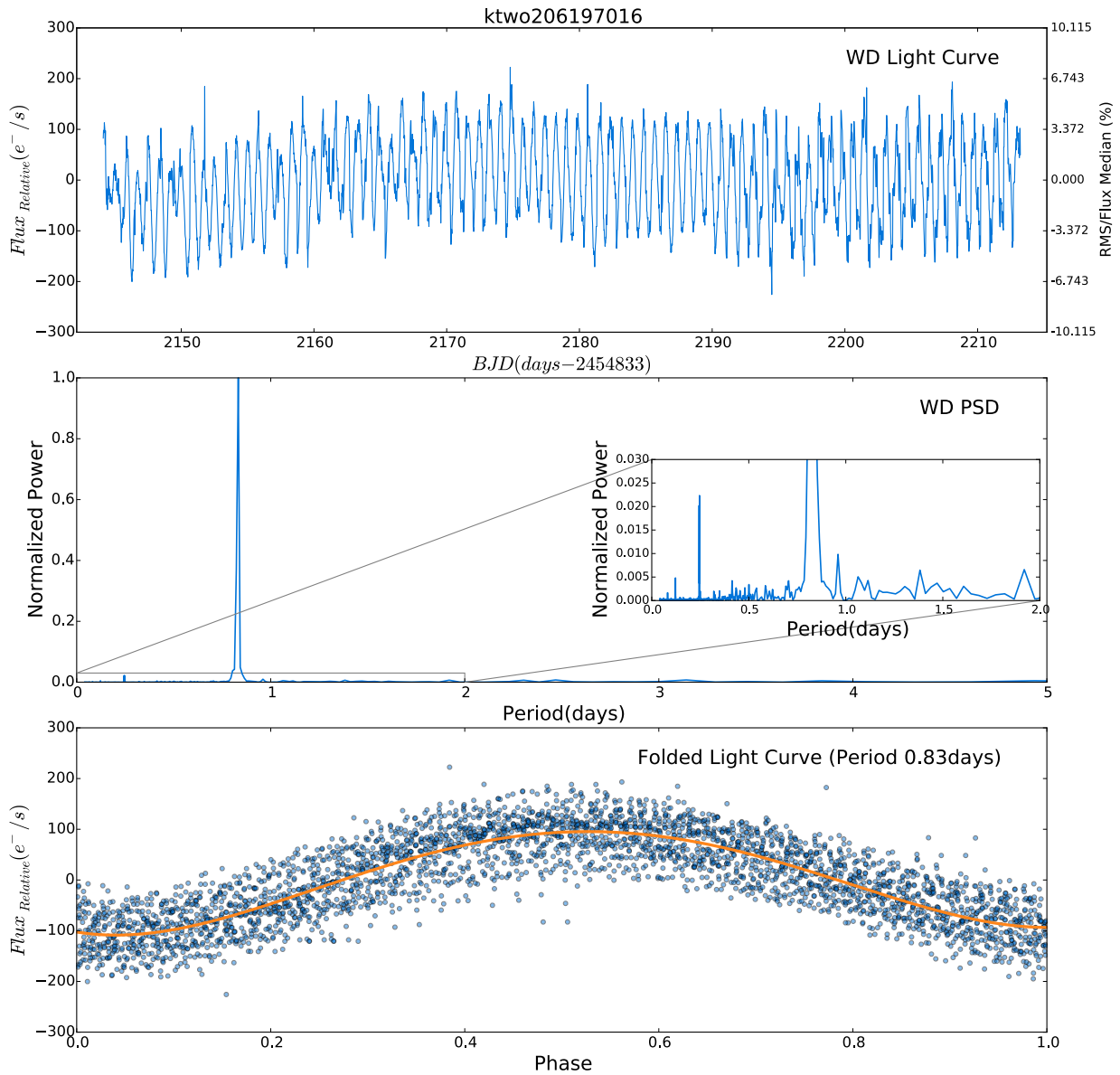


Figure B.5: KIC 206197016 is a DA WD in K2 Campaign 3 with Kep Mag of 16.5. Top two panels are the de-trended light curve and the power spectrum for this WD. Both judging by eye and the power spectrum picked out a period of 0.83 days. The blow-up plot inside the second panel shows a power spectrum peak at 6 hour (0.25 day), which corresponds to the not fully corrected effect due to the spacecraft thruster firing every 6 hours (to correct the telescope pointing). The bottom panel shows the folded light curve using the 0.83 day period with the orange line showing the smoothed light curve, via which I calculated a peak to peak amplitude of 6.88%. Such high amplitude will certainly fail KIC 206197016 as a photometry standard star.

Koester D., Napiwotzki R., Christlieb N. et al. 2001, A&A, 378, 556
Koester, D., Voss, B., Napiwotzki, R., et al. 2009, A&A, 505, 441
Landolt, A. U., 1983, AJ, 88, 439
Landolt, A. U., 1992, AJ, 104, 340
Limoges, M.-M., Lépine, S., & Bergeron, P. 2013, AJ, 145, 136
Luger, R., Agol, E., Kruse, E., 2016, AJ., 152, 4
Maoz, D., Mazeh, T., McQuillan, A., 2015, MNRAS, 447, 1749
Mukadam A. S., Mullally, F., Nather, R. E., et al., 2004, ApJ, 607, 982
Østensen, R., Silvotti, R., Charpinet, S., et al. 2011, MNRAS, 414, 2860
Perlmutter, S., Aldering, G., Goldhaber, G., et al. 1999, ApJ, 517, 565
Riess, A., Filippenko, A. V., Challis, P., et al. 1998, AJ, 116, 1009
Savitzky, A. & Golay, M. J. E. 1964, Analytical Chemistry, 36, 1627
Smith J. C., Stumpe M. C., Van Cleve J. E., et al. 2012, PASP, 124, 1000
Stumpe M. C., Smith J. C., Catanzarite J. H., et al. 2014, PASP, 126, 100
Stumpe M. C., Smith J. C., Van Cleve J. E., et al. 2012, PASP, 124, 985
Stubbs, Christopher W. & Brown, Yorke J. 2015, Modern Physics Letters A, 30, 40
Tremblay, P.-E., Bergeron, P., & Gianninas, A. 2011, ApJ, 730,128
Van Cleve J. E., Howell S. B., Smith J. C. et al. 2015, PASP, in press, arXiv:1512.06162
Vanderburg A., & Johnson J. A., 2014, PASP, 126, 948
Vogt, F.P.A., Dopita, M.A., Kewley, L.J., et al., 2014, ApJ, 793, 127
Winget, D. E., van Horn, H. M., Tassoul, M., et al. 1982, ApJ, 252, L65

Vita

Zhichao Xue was born June 1990 in Zhenjiang, P. R. China. He graduated from the Zhenjiang No.1 High School, P. R. China in June 2008 and then enrolled at Shandong University, P. R. China in August of the same year. He received his Bachelor of Science in Applied Physics from Shandong University, P. R. China in May 2012. After graduation (June 2012), he enrolled in the graduate school at Louisiana State University in August of the same year, where he started to collaborate with Dr. Bradley Schaefer who later became his thesis advisor. He is expecting his doctoral degree in August 2017.